



UNIVERSITÀ DEGLI STUDI DI MILANO

Scuola di Dottorato in Fisica, Astrofisica e Fisica Applicata
Dipartimento di Fisica

Corso di Dottorato in Fisica, Astrofisica e Fisica Applicata
Ciclo XXVII

Stabilization of Bloch Oscillations of Ultracold Atoms in a Ring Cavity

Settore Scientifico Disciplinare FIS/03

Supervisore: Dr. Nicola Piovella

Coordinatore: Prof. Marco Bersanelli

Tesi di Dottorato di:

Marina Samoylova

Anno Accademico 2014/2015

Commission of the final examination:

External Referee:
Ass.Prof. Leonardo Fallani

External Member:
Prof. Luca Salasnich

External Member:
Prof. Gian-Luca Oppo

Final examination:

Date 11/05/2015

Università degli Studi di Milano, Dipartimento di Fisica, Milano, Italy

PACS:

37.10.Jk, 32.80.Qk, 03.75.-b, 42.50.Nn

Keywords:

Bloch oscillations, ring cavity, mode-locking

Contents

Abstract	5
1 Introduction	7
1.1 Bloch oscillations in solids	7
1.2 Bloch oscillations in optical lattices	12
1.3 Atomic Bloch oscillations with ring cavities	16
2 Model	21
2.1 Gravitational CARL system	22
2.2 Bloch oscillations dynamics without cavity	26
2.2.1 Adiabatic rapid passage sequence	27
2.2.2 Two-state model	29
2.2.3 Average atomic momentum	31
2.2.4 Momentum states population	35
2.2.5 Variable optical potential depth	37
3 Mode-locking with ring cavity	41
3.1 Mode-locking mechanism	42
3.1.1 Comparison with ARP approximation	45
3.1.2 Population of momentum states	47
3.1.3 Reduced potential depth	49
3.2 Non-destructive monitoring	50
4 Transition to synchronized regime of Bloch oscillations	53
4.1 Collective atomic recoil lasing (CARL)	54
4.2 CARL-BEC model	61
4.3 CARL dynamics vs Bloch oscillations	64

5	Robustness of Bloch oscillations of a BEC in a ring cavity	73
5.1	Radiation pressure force effect	74
5.1.1	Analytical description of the effect	74
5.1.2	The impact of the radiation pressure force	76
5.2	Impact of fluctuations	83
5.2.1	Phase fluctuations	83
5.2.2	Amplitude fluctuations	88
5.3	Clearance of excited Bloch bands	92
5.4	Impact of collisions	95
6	Conclusion	99
	Appendices	103
A	Derivation of angle β	105
B	Origin of transient	107
	Acknowledgements	111
	Bibliography	113

Abstract

The work presented in this thesis is dedicated to studies of stabilization of Bloch oscillations of ultracold atoms in a one-dimensional vertical optical lattice under the influence of the gravitational force. The atoms simultaneously interact with both the lattice potential and a unidirectionally pumped optical ring cavity whose vertical arm is collinear with the optical lattice. In the proposed scheme, the atoms not only exchange photons between the optical lattice laser beams, but also collectively scatter light from the pump into the reverse cavity mode.

The initial investigation of the system without the cavity allows understanding of the importance of the perfectly adiabatic atomic motion in the observation of stable Bloch oscillations and how easily the adiabaticity can be broken due to a very fast switch-on of the lattice or its amplitude and phase modulation. Under certain parameter regimes, adding the ring cavity to the system provides a surprisingly positive feedback on the atomic dynamics. It is found that, while acting back on the atoms, the cavity field establishes a mode-locking mechanism which assists adiabatic rapid passages between adjacent momentum states. Thus, the cavity-induced feedback mechanism enforces the adiabaticity of the process and reveals a regime where the Bloch oscillations are self-synchronized for long times. This stabilization technique is shown to steer the atoms to the lowest Bloch band preventing the problem of interband tunneling. A demonstration is also made of the ability of the system to stabilize the atomic Bloch oscillations against technical amplitude or phase noise and even suppress dephasing due to the atom-atom interactions.

Furthermore, the response of the system to the atomic motion is generated in the form of perfectly detectable periodic bursts of light emitted into the counter-propagating cavity mode. Thus, the system offers a continuous and reliable non-destructive method to monitor the Bloch oscillations dynamics without perturbing their periodicity by detecting the scattered light transmitted through the cavity. All features studied in this work may be crucial for future improvements of the design of atomic gravimeters based on recording Bloch oscillations.

Contents

Chapter 1

Introduction

1.1 Bloch oscillations in solids

The phenomenon of Bloch oscillations was first predicted theoretically by F. Bloch while studying the electrical properties of crystals [1]. In particular, the problem of an electron confined in a general periodic potential under the action of a constant electric field has been considered [2], and the motion of the electron is proven to be oscillatory instead of uniform. Here is a revision of the main concepts of the semiclassical model describing how, in the absence of collisions, the position \mathbf{r} and wave vector \mathbf{k} of each electron evolve in the presence of an externally applied electric field.

The Schrödinger equation for an electron with mass m in a full periodic potential of ions $V(\mathbf{r}) = V(\mathbf{r} + \mathbf{R})$ valid for all Bravais lattice vectors \mathbf{R} ,

$$H\psi(\mathbf{r}) = \left[-\frac{\hbar}{2m}\nabla^2 + V(\mathbf{r}) \right] \psi(\mathbf{r}) = \varepsilon\psi(\mathbf{r}), \quad (1.1)$$

is expected to have many stationary solutions $\psi_{n\mathbf{k}}$ called Bloch levels. Indeed, according to the Bloch's theorem [3], the solutions of the Schrödinger equation are found in the Bloch form

$$\psi_{n\mathbf{k}}(\mathbf{r}) = e^{i\mathbf{k}\mathbf{r}} U_{n\mathbf{k}}(\mathbf{r}), \quad (1.2)$$

where plane waves $e^{i\mathbf{k}\mathbf{r}}$ are modulated by the function $U_{n\mathbf{k}}$ which is determined by the periodic boundary condition $U_{n\mathbf{k}}(\mathbf{r}) = U_{n\mathbf{k}}(\mathbf{r} + \mathbf{R})$, but has no simple

explicit form. Thus, for a given wave vector \mathbf{k} there is an infinite number of solutions with energies $\varepsilon_n(\mathbf{k})$ labeled with band index n . The set of functions $\varepsilon_n(\mathbf{k})$ has an upper and lower bounds forming an energy band. The electronic band structure successfully used to explain many physical properties of solids describes such energy bands, i.e., those energy intervals that an electron may belong to within a solid, together with the ranges of energy the electron is not allowed to have, called band gaps. The semiclassical model takes $\varepsilon_n(\mathbf{k})$ as given functions, so the description is based entirely on the knowledge of the band structure of a solid, while the explicit information about the periodic potential of the ions is not provided. For a fixed band n , both $\psi_{n\mathbf{k}}$ and their energies $\varepsilon_n(\mathbf{k})$ vary continuously with \mathbf{k} , and the relations

$$\psi_{n,\mathbf{k}+\mathbf{K}} = \psi_{n\mathbf{k}}, \quad (1.3)$$

$$\varepsilon_n(\mathbf{k} + \mathbf{K}) = \varepsilon_n(\mathbf{k}) \quad (1.4)$$

are valid for any reciprocal lattice vector \mathbf{K} . Therefore, the solutions can be fully characterized by their behavior in a single uniquely defined primitive cell of the reciprocal k -space, called Brillouin zone.

The wave function $\psi_n(\mathbf{r}, t)$ constructed similarly to the free electron wave packet [3] is taken as a wave packet of Bloch levels $\psi_{n\mathbf{k}}$ from a given band:

$$\psi_n(\mathbf{r}, t) = \sum_{\mathbf{k}'} g(\mathbf{k}') \psi_{n\mathbf{k}'}(\mathbf{r}) \exp \left[-\frac{i}{\hbar} \varepsilon_n(\mathbf{k}') t \right], \quad (1.5)$$

where $g(\mathbf{k}') \approx 0$ for $|\mathbf{k}' - \mathbf{k}| > \Delta k$ with Δk being the spread in wave vector, which is assumed to be small compared to the Brillouin zone dimensions, so that the energy $\varepsilon_n(\mathbf{k})$ does not vary much over the Bloch levels present in the wave packet. In order to evaluate the spread of the wave packet (1.5), the points $\mathbf{r} = \mathbf{r}_0 + \mathbf{R}$ separated by a Bravais lattice vector \mathbf{R} are considered. Then, according to the basic rules for wave packets, the function $\psi_n(\mathbf{r}_0 + \mathbf{R})$ becomes notable in the region $\Delta R \approx 1/\Delta k$ which is much larger than the lattice constant d ($\Delta R \gg d$), since the wave vector is well defined on the scale of the Brillouin zone of the order of $1/d$ ($\Delta k \ll 1/d$). This result is totally independent of the value of \mathbf{r}_0 , so the semiclassical model deals with a wave packet spread over a large number of primitive cells, which is schematically demonstrated in Fig.1.1. Therefore, the semiclassical model is characterized by the fact that the periodic potential of the ions must be treated quantum mechanically, since it varies over the regions essentially smaller compared to the dimensions of the wave packet, while the applied electric field is assumed to change slowly on the scale of the considered lattice and can be described classically (see Fig.1.1).

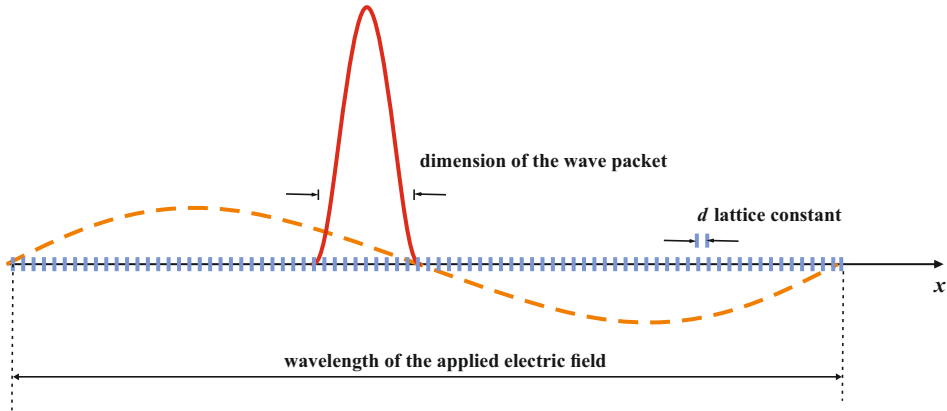


Figure 1.1: Schematic representation of the semiclassical model. The wave packet is spread over many primitive cells of the lattice, so the classical description of the periodic potential is no longer suitable, while the applied electric field varies over the regions much greater than the dimensions of the wave packet and can be treated classically.

The semiclassical model is also based on the assumption that the externally applied electric field is weak enough to induce the interband transitions and it affects only the position and wave vector of an electron, while the energy spectrum of the system remains unmodified. The time evolution of an electron with charge e , position \mathbf{r} , wave vector \mathbf{k} and band index n in the presence of an external electric field $\mathbf{E}(\mathbf{r}, t)$ is described by the following equations of motion:

$$\dot{\mathbf{r}} = \mathbf{v}_n(\mathbf{k}) = \frac{1}{\hbar} \frac{\partial \varepsilon_n(\mathbf{k})}{\partial \mathbf{k}}, \quad (1.6)$$

$$\hbar \dot{\mathbf{k}} = -e\mathbf{E}(\mathbf{r}, t), \quad (1.7)$$

where $\mathbf{v}_n(\mathbf{k})$ is the velocity of the electron, and the functions $\varepsilon_n(\mathbf{k})$ periodic in k -space are assumed to be known in the frame of the semiclassical model. Eq.(1.7) has the solution

$$\mathbf{k}(t) = \mathbf{k}(0) - \frac{e\mathbf{E}t}{\hbar} \quad (1.8)$$

which demonstrates that in time t the wave vector of each electron is shifted by the same amount. However, it is impossible to obtain a current with a configu-

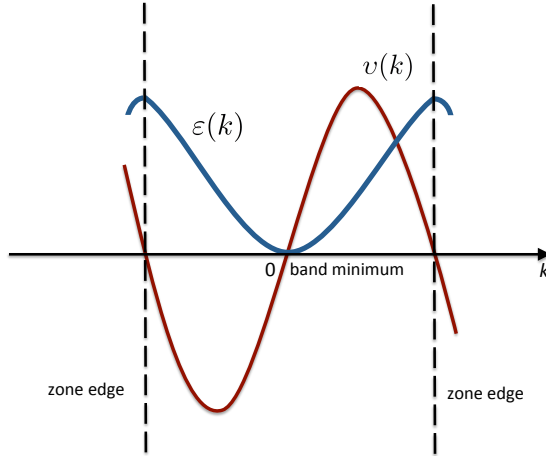


Figure 1.2: The energy ε and velocity v of an electron within a single energy band as functions of \mathbf{k} in one dimension. The direct dependence on time can be found using the expression $\mathbf{k}(t) = \mathbf{k}(0) - e\mathbf{E}t/\hbar$. The velocity is increasing linearly with k in the vicinity of the band minimum and gets its maximum value as the right edge of the zone is approached, thereafter it is decreased significantly and turns to zero at the zone boundary. This unusual dynamics is due to an extra force acting on the electron, which is created by the periodic potential.

ration similar to the case of free electrons, in which the velocity is proportional to \mathbf{k} and grows linearly in time. In the semiclassical model, the current is proportional to the velocity of the electron

$$\mathbf{v}(\mathbf{k}(t)) = \mathbf{v}\left(\mathbf{k}(0) - \frac{e\mathbf{E}t}{\hbar}\right), \quad (1.9)$$

but this velocity is clearly not proportional to \mathbf{k} unlike the free electrons case. Since the function $\mathbf{v}(\mathbf{k})$ is periodic in the reciprocal lattice, it is a bounded function of time, and its behavior is oscillatory when the field \mathbf{E} is parallel to a

reciprocal lattice vector. This phenomenon is illustrated in Fig.1.2 where, for a certain energy band, both functions $\varepsilon(k)$ and $v(k)$ are given in one dimension. Even though the velocity is linearly increasing near the band minimum and reaches its maximum value as the zone boundary is approached, it drops down significantly and vanishes at the zone edge with increasing k . Therefore, in the region of k between the maximum of the velocity and the right zone edge, the electron is accelerated in the direction opposite to the externally applied electric field. Such peculiar behavior is caused by an additional force produced by the periodic potential. In the semiclassical model, the explicit form of the potential is not provided, but the information about it is stored in the functional form of $\varepsilon(\mathbf{k})$. Thus, if an electron is represented by a wave packet confined into a single energy band, the applied electric field forces the electron to move in the direction of the field towards the levels in which the electron is most likely to be reflected back in the opposite direction by the lattice until it is stopped by the field, whereupon the oscillatory motion is repeated.

This fundamental description explains how electrons execute Bloch oscillations within a solid under the action of a constant external electric field. This remarkable feature of electrons, however, has never been observed experimentally because of the scattering of electrons by the lattice defects or impurities in natural crystals. However, this effect has been recently seen in semiconductor superlattices [4–6], where shorter oscillation periods have been obtained by taking longer spacing of the structures. Furthermore, due to development of techniques in laser cooling of atoms [7, 8], new systems which use ultracold atomic clouds in optical lattices instead of electrons in periodic crystalline potentials have recently appeared, allowing study of Bloch oscillations [9–11]. Such systems, as discussed in Sec.1.3, may serve as useful tools for high precision measurements due to extremely long coherence times and absence of defects in optical lattices.

1.2 Bloch oscillations in optical lattices

The behavior of ultracold atoms in optical lattices is very similar to the physics of an electron gas in an ideal crystalline solid [12], since both an atom moving in an optical lattice and an electron in a solid can be described as quantum particles interacting with a periodic potential, as it is done, for example, in the previous section using the semiclassical description. Here is an alternative representation of the origin of Bloch oscillations.

In the one-dimensional case, if a constant external force F is suddenly applied to a particle with mass m and momentum p in a periodic potential of particular choice $V(x) = V_0 \cos^2(kx)$ with $k = \pi/d$ related to the lattice spacing d and V_0 representing the strength of the sinusoidal potential, the resulting Schrödinger equation can be written as:

$$i\hbar \frac{\partial}{\partial t} \psi = (H_0 - Fx)\psi, \quad (1.10)$$

where

$$H_0 = \frac{p^2}{2m} + V_0 \cos^2(kx). \quad (1.11)$$

According to the standard theory of Bloch oscillations [13–18], the eigenfunctions $\chi_{n,q}(x)$ of H_0 are Bloch waves

$$\chi_{n,q}(x) = e^{iqx} U_{n,q}(x) \quad (1.12)$$

that generally depend on the position x , band index n and the quantum number q called *quasimomentum* restricted to the first Brillouin zone $-\pi/d \leq q \leq \pi/d$. Functions $U_{n,q}(x) = U_{n,q}(x+d)$ have the same periodicity of the lattice potential and satisfy the Schrödinger equation

$$\left[\frac{(p + \hbar q)^2}{2m} + V_0 \cos^2(kx) \right] U_{n,q}(x) = \varepsilon_{n,q} U_{n,q}(x), \quad (1.13)$$

where the eigenenergies $\varepsilon_{n,q}$ of the Hamiltonian H_0 are periodic functions of the quasimomentum q with period $2\pi/d$.

For the full Hamiltonian $H_0 - Fx$ the following gauge transformation can be made:

$$\psi(x, t) = \exp(iFtx/\hbar) \tilde{\psi}(x, t), \quad (1.14)$$

yielding the Schrödinger equation

$$i\hbar \frac{\partial}{\partial t} \tilde{\psi}(x, t) = \left[\frac{(p + Ft)^2}{2m} + V_0 \cos^2(kx) \right] \tilde{\psi}(x, t). \quad (1.15)$$

Comparing this equation with Eq.(1.13) it can be seen that the effect of the applied external force F is to evolve the quasimomentum according to the Bloch's acceleration theorem [1]:

$$q(t) = q(0) + \frac{Ft}{\hbar}, \quad (1.16)$$

where $q(0)$ is the quasimomentum at $t = 0$. Setting $q(0) = 0$, the corresponding Bloch wave within the adiabatic approximation that the rate of change \dot{U}/U is too small to excite higher bands, i.e., when F is weak enough, has the following form [19]:

$$\tilde{\psi}(x, t) = U_{n,q(t)}(x) \exp\left(-\frac{i}{\hbar} \int^{t'} \varepsilon_{n,q(t')} dt'\right) \quad (1.17)$$

with $U_{n,q(t)}(x)$ being the instantaneous solution of Eq.(1.13).

The phenomenon of Bloch oscillations performed under the action of the constant force F is explained in Fig.1.3 in terms of quasimomentum q given in the reduced-zone scheme. When $q(t)$ reaches the edge of the Brillouin zone at π/d is is mapped to the identical point $q = -\pi/d$, giving rise to the oscillatory behavior. After one Bloch period $\tau_B = \hbar/(Fd)$ the quasimomentum fully scans the first Brillouin zone and returns to the same starting value of $q(0)$. Since the external force induces a uniform motion in quasimomentum space, the wave function $\tilde{\psi}(x, t)$ is also periodic in time with period τ_B , which corresponds to oscillations in real space.

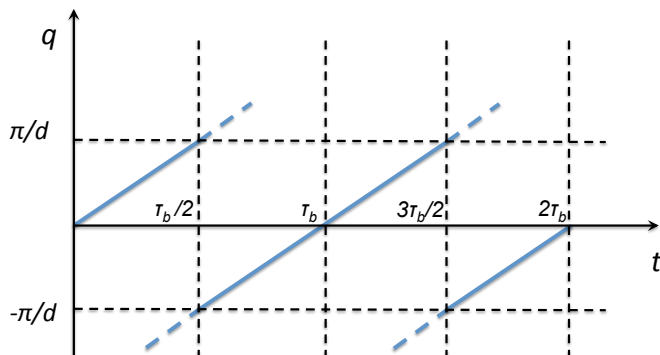


Figure 1.3: Time-dependent quasimomentum $q(t)$ given by Eq.(1.16) in the first Brillouin zone restricted to $-\pi/d \leq q \leq \pi/d$.

A constant external force driving the Bloch dynamics in systems of ultracold atoms in optical lattices can be provided by either a constant acceleration of the confining potential or by a real force, e.g., gravity. The former possibility was used in the first experiment on Bloch oscillations with cold atoms [9]. A cloud of cold cesium atoms was trapped in an optical lattice that was then accelerated by linearly increasing the frequency difference between the two counter-propagating lattice beams. In the moving reference frame, the effect of the acceleration a was indeed replaced by an inertial constant force $F = -ma$. Fig.1.4 shows the momentum distribution of the Bloch states in the accelerated frame between $t = 0$ and $t = \tau_B$. It is seen that as the force drives the Bloch dynamics, the peak at zero velocity starts moving towards higher velocities until the atomic cloud experiences a Bragg reflection at time $\tau_B/2$ at the edge of the first Brillouin zone $\hbar k$, after which the atoms are accelerated again starting from the other edge $-\hbar k$. This provided the first direct demonstration of the atomic Bloch oscillations that could be observed for several cycles with no signal decay.

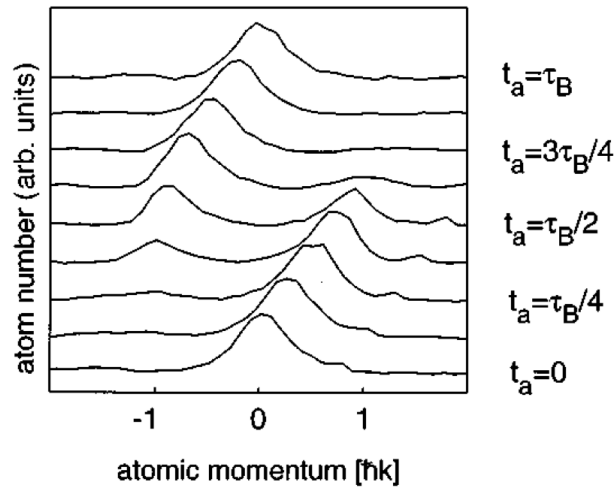


Figure 1.4: Demonstration of the Bloch dynamics in the fundamental band in the first experiment on Bloch oscillations with cold atoms in a periodic potential. Adapted from Ben Dahan *et al.* (1996) [9].

A precise determination of the Bloch oscillation period τ_B may provide an accurate measurement of the h/m ratio which is remarkably important in metrology, since it allows to define the fine structure constant [20, 21]. If the optical lattice moves with the acceleration a , the Bloch oscillation period can be defined as

$$\tau_B = \left(\frac{h}{m}\right) \frac{1}{ad}. \quad (1.18)$$

The lattice spacing d and the acceleration a are known with very high precision, thus, the value of h/m can be determined accurately.

The effect of Bloch oscillations can be used not only for high-precision measurements of fundamental constants. Ultracold atoms undergoing Bloch oscillations may serve as very accurate sensors of forces as well. The force F making the atoms execute Bloch oscillations is given by

$$F = \frac{h}{\tau_B d}, \quad (1.19)$$

i.e., there is no dependence on the potential depth, only the lattice spacing d which can be very accurately determined is entering this expression. Therefore, with this approach, the measurement of the force is reduced to the determination of the frequency $1/\tau_B$ which can be measured with high precision.

The precision of the described above measurements is literally given by the uncertainty in the Bloch period τ_B . Several thousands of Bloch oscillations have been observed in existing experiments, hence, the Bloch oscillation period can be defined more precisely. Recent experiments with phase or amplitude modulated optical lattices [22, 23] have allowed to determine even the local gravity acceleration with the relative uncertainty in the range of 10^{-7} [24]. The application of Bloch oscillations of ultracold atoms in optical lattices to high-precision gravity measurements is discussed in detail in the next section.

1.3 Atomic Bloch oscillations with ring cavities

The research project of this thesis originates from the idea to verify whether Bloch oscillations of ultracold atoms confined in a vertical standing light wave created by light fields inside a laser-pumped optical ring cavity can be monitored non-destructively. This result is relevant for the development of a new generation of gravity sensors based on atomic interferometry. The impressive precision of state-of-the-art gravity sensors makes them a useful tool in a wide range of applications in industry, such as worldwide gravity surveys along seismic lines, oil and gas fields prospection [25–27], geophysical research [28–30], and inertial navigation [31,32]. They are equally important in fundamental research, where they are used for measurements of fundamental constants [20,33–38], tests of general relativity [39–45] and the precise measurements of Casimir forces [46–50]. Gravity measurements based on atom interferometry with sensitivities in the order of $2 \times 10^{-8} \text{ m/s}^2$ in 1s integration time and accuracies in the order of $4 \times 10^{-9} \text{ m/s}^2$ have been demonstrated [51–54]. A higher precision could be achieved within longer integration times that are, however, limited by slow repetition rates due to the fact that the test mass must be raised before being dropped in the field of gravity, which takes a finite amount of time. This drawback motivated ideas on how to recycle the test mass in a continuous fashion. An important step to solve this problem is to use Bloch oscillations.

With the realization of cold [9] and ultracold atoms in optical lattices [55–57], it became possible to produce Bloch oscillations with much longer coherence times than with electrons in superconducting superlattices, characterized by rapid dephasing due to impurities. While initially the force acting on the atoms and inducing oscillations was simulated by accelerating the optical lattice, in subsequent experiments the acceleration was replaced by the force arising from gravity. The frequency of Bloch oscillations, $\nu_b = mg/2\hbar k_l$, is proportional to the test mass m , the gravitational acceleration g and the periodicity $\lambda_l/2 = \pi/k_l$ of the standing wave. Very low damping rates have allowed to record 10000 Bloch oscillation cycles in more than 20s [58]. With such long coherence times Bloch oscillations of cold atoms are suitable for high accuracy measurements. Recently, new gravimeters have been developed based on the detection of Bloch oscillations of atoms confined in a far-detuned vertical standing light wave potential, yielding resolutions in the range of 10^{-7} [24,58,59]. In these experiments, the detection of the gravitational acceleration with a falling atomic cloud is done by absorption imaging techniques or precise mapping of the atomic velocity distribution along the vertical axis using Doppler-sensitive Raman transitions. However, for each measurement a new atomic sample must be prepared,

cooled, loaded into the optical lattice and finally accelerated. Varying the evolution time, Bloch oscillations are reconstructed, from which the acceleration force can be extracted based on a large number of performed measurements. This process is laborious and suffers from uncertainties and fluctuations in the initial state in which the atomic cloud is prepared. To overcome the destructive nature of the measurements in atomic gravimeters a new technique that allows monitoring of the Bloch oscillations *in vivo* has been proposed [60, 61].

The measurement process can be dramatically accelerated if instead of making successive images of the atomic motion, the impact of the atomic displacement on the confining standing light wave is monitored. Indeed, recent experiments have shown that atoms moving in a stationary light wave can modify its amplitude or phase, assuming that the wave is sufficiently decoupled from the driving laser beams [62–64]. A way to satisfy this requirement is to let the standing wave form inside an optical ring cavity, like schematically shown in Fig.1.5. The role of the cavity is to amplify interaction between the atoms and laser light. Due to the atomic motion inside the ring cavity, the phase



Figure 1.5: Schematic representation of a three-mirror ring cavity designed for continuous detection of Bloch oscillations of atoms falling inside a vertical light wave sustained by the cavity.

and intensity of the light transmitted through one of the cavity mirrors become modulated. Remarkably, the Bloch oscillation period becomes unaffected during the evolution, so that the transmitted light provides an opportunity to continuously observe the Bloch oscillations dynamics. Thus, the cavity fields themselves carry signatures of the Bloch oscillations that can be monitored in a non-destructive way.

The first proposal on such continuous monitoring of Bloch oscillations avoiding the need for numerous measurements of the atomic velocity after given evolution times [60], however, suffers from the assumption that the probe field is very weak so that the continuous measurement is performed without affecting the atomic dynamics. The neglected backaction of the probe field on the atoms is surely the main drawback of that proposal, since the cavity field is shown to act back on the atomic motion [65], establishing a mode-locking mechanism that causes the synchronization of the Bloch oscillations for a long time [66]. The mode-locking mechanism and stabilization of Bloch oscillations even in the presence of unfavorable effects are subjects of discussion in this thesis. The installation of the corresponding experiment oriented on a non-destructive observation of Bloch oscillations of ultracold atoms in a ring cavity is expected to be accomplished soon by the Optics Group at the Institute of Physics of São Carlos, University of São Paulo, Brazil. It is important to emphasize that the goal of that experiment is *not* to construct a better gravimeter, but to provide the proof of principle that continuous operation of an atomic gravimeter is technically feasible and could be a realistic way to improve its performance.

^{88}Sr ultracold atoms are planned to be used in the actual experiment for a number of reasons. The coherence time of the system may be reduced due to technical imperfections, interatomic collisions and perturbations by electromagnetic fields, and the usage of strontium allows to eliminate some of these problems. Its extremely small collisional scattering length entails a negligible collision rate, and the absence of any angular momentum in the ground state reduces coupling to electric and magnetic stray fields [67, 68]. However, for the theoretical investigation of the phenomenon of interest the choice of the atomic species is not crucial. Thus, the theoretical model admits also alkali atoms which are most commonly employed in experiments involving optical cooling. A careful selection of parameters for the chosen atomic species is required though.

The design of already made vertical ring-shaped cavity and magneto-optical trap (MOT) is presented in Fig.1.6. The location of the MOT is slightly shifted from that of the cavity mode, so that the trapping and cooling processes are not perturbed by the presence of the ring cavity. By adjusting the magnetic fields of the MOT the atomic cloud can be moved inside the cavity. Then, the laser

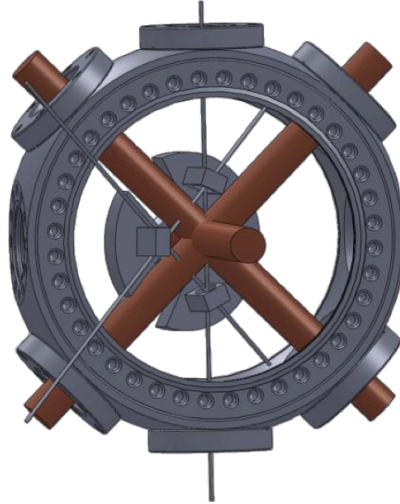


Figure 1.6: Design of the three-mirrors ring cavity located in an ultrahigh vacuum chamber. Also shown are the MOT beams (big cylinders) and the narrow laser beams passing through the ring cavity.

beams pumping the two counter-propagating cavity modes are switched on at an intensity calculated such that the atoms perform Bloch oscillations. The light fields leaking out of the cavity modes are phase-matched on a photodetector, and the beat signal is searched for signatures revealing the Bloch oscillations. Once the experimental apparatus is completed, the objective is to make the atoms perform Bloch oscillations in the natural gravitational field of the earth, leaving visible fingerprints in the dynamics of the intensity and phase of the ring cavity fields. Then the major goal is to make sure that the proposed non-destructive technique of monitoring the atomic Bloch oscillations via their backaction on the cavity fields allows to gather information on the periodicity of the Bloch oscillations faster than other conventional techniques [24, 58, 59]. If this process can be sped up considerably, a better signal-to-noise ratio can be obtained in shorter integration times. In other words, in a given time higher precision can be reached for the determination of the gravitational acceleration.

Theoretical investigation of Bloch oscillations of ultracold atoms inside a unidirectionally pumped vertical optical ring cavity under the action of gravity and the described above non-destructive technique to continuously monitor their dynamics are subjects of this work. In Chapter 2 the studied system is introduced by the coupled atom-ring cavity equations which serve as the basis for the numerical simulations presented in the thesis. It is important to consider the system without the cavity first, since it allows to understand that perfectly adiabatic atomic motion is essential to observe stable Bloch oscillations. The given adiabaticity criteria can be easily broken, which leads to interband tunneling problem and atomic momentum drifts. The system without the cavity is thus unreliable.

Chapter 3 considers the case when the ring cavity is added to the system. The scattered field in the reverse cavity mode is shown to provide a positive feedback on the atomic dynamics. This feedback mechanism enforces the adiabaticity even in the cases when the process is no longer adiabatic in the absence of the cavity. As a result, the tunneling to the next higher Bloch band is self-suppressed and the Bloch oscillations become stabilized for long times. Moreover, a detectable burst of light is emitted into the counter-propagating cavity mode every time a Bloch oscillation happens. This provides a reliable non-destructive monitor of the atomic Bloch oscillations without perturbing their periodicity.

However, the system with the ring cavity is still sensitive to the choice of parameters. It is demonstrated in Chapter 4 that there are two distinct regimes in which the atom-cavity interaction are qualitatively different. For a strong collective coupling, the Bloch oscillations are completely overruled by the collective atomic recoil lasing instability, and the radiation field experiences multiple light bursts per Bloch oscillation period. Therefore, this regime is not acceptable as a reliable monitor of the atomic motion. However, if the collective coupling is weak, the Bloch oscillations dynamics stay dominant and develop the synchronized regime of interest.

Chapter 5 is dedicated to a detailed analysis of the weak collective coupling regime. The cavity-induced feedback mechanism turns out to be capable of refocusing the whole atomic population in the fundamental Bloch band after some accidental excitation of higher bands, for example, by technical amplitude or phase noise or a non-adiabatic switch-on of the confining lattice potential. Thus, this regime demonstrates robustness against atomic momentum drifts, certain fluctuations and even dephasing due to interatomic collisions. Consequently, the considered system shows its potential for application as an optical monitor of Bloch oscillations.

Chapter 2

Model

As mentioned in the introductory chapter, the theoretical work presented in this thesis has been conducted in close relation to the experiment that is currently under construction at the Institute of Physics of São Carlos, University of São Paulo, Brazil. Thus, the system under investigation corresponds to the experimental setup and the selected parameters tend to satisfy real experimental conditions. This chapter is dedicated to a detailed description of a theoretical model on interaction of a Bose-Einstein condensate (BEC) with laser light as an application for non-destructive monitoring of the atomic motion and possible future improvements of the design of atomic gravimeters based on recording Bloch oscillations [60,69]. The novel scheme described in Sec.2.1 allows also the analysis of a synchronization phenomenon in the motion of many atoms in the framework of the studied model. This effect is known as collective atomic recoil lasing (CARL) [62,70–72]. On top of that, it is worth studying the simplified system first (Sec.2.2) before turning to the investigation of the features of the complex CARL-BEC model, covered in the next chapter. After an acceleration frame is implemented to the system, some of the conditions necessary to select experimental parameters are clarified in Sec.2.2. If those conditions are for some reason violated, the dynamics of the system experiences some undesirable deviations in the simplified case.

2.1 Gravitational CARL system

The examined model is given by a cloud of ultracold atoms confined in a vertical optical standing wave, as depicted in Fig.2.1. This standing wave with the lattice constant π/k_l can, for instance, be generated by two external laser beams detuned sufficiently far from the atomic resonance and intersecting at the location of the atoms under the angle β defined by $K \sin(\beta/2) = k_l$, where K is the wavenumber of the laser beams. A derivation of the angle β for some specific parameters is provided in Appendix A. The externally imposed optical lattice traps the atoms in a one-dimensional potential $(\hbar W_0/2) \sin(2k_l x)$ along the x axis, where the potential depth is denoted by $\hbar W_0$. In addition to the effect of the periodic potential, the atoms are exposed to the gravitational potential

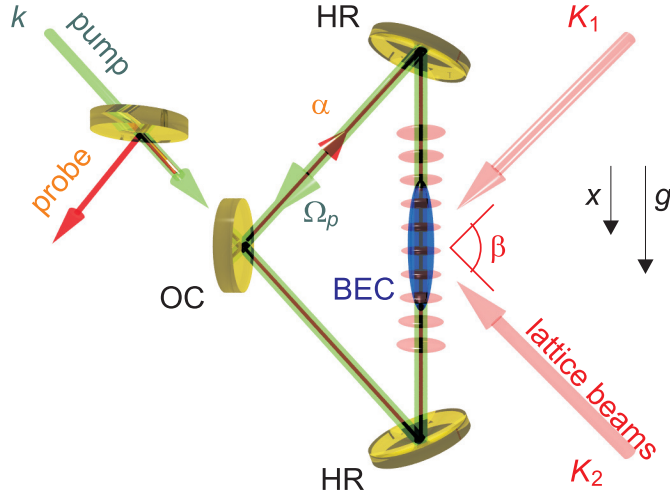


Figure 2.1: Scheme of a ring cavity consisting of two high-reflecting mirrors (HR) and one output coupler (OC) interacting with a Bose-Einstein condensate (BEC) stored in one arm of the ring cavity. Only one cavity mode is pumped (Ω_p, k), the counterpropagating probe mode (α) is populated by backscattering from the atoms. Two lasers ($K_{1,2}$) crossing the cavity mode at the location of the BEC under angles $\pm\beta/2$ generate an optical lattice whose periodicity is commensurate with the standing wave created by the pump and probe modes. The atoms are also subject to an external accelerating force mg .

mgx , where m is the atomic mass and g is the gravitational acceleration. As a result, the atoms undergo Bloch oscillations with frequency $\nu_b = mg/2\hbar k_l$ [9] under the influence of the applied gravitational force.

Then, an optical ring cavity is added to the system, letting the atoms simultaneously interact with its two counter-propagating cavity modes. The cavity is unidirectionally pumped in the upwards direction, oppositely to the gravitational force, by a laser beam with the wavenumber k (see Fig.2.1). The atomic motion in such environment in the absence of the external optical lattice and gravity, i.e., in the horizontal plane, has been experimentally shown [62,71,73,74] to act back onto the intracavity light fields and modulate their phases and amplitudes detectable signatures. This backaction, called collective atomic recoil lasing (CARL), in certain parameter regimes, evolves into a spontaneous formation of a standing wave optical potential. It is thus reasonable to expect observable signatures of the atomic Bloch oscillations when the externally imposed standing wave is commensurate with the one formed by the intracavity fields, i.e., $k = k_l$. The role of the cavity in the vertical gravitational configuration in Fig.2.1 with the external optical lattice, as it is explained in the next chapter, is to provide a positive feedback on the Bloch oscillations which become stabilized via a mode-locking mechanism [65]. Remarkably, the Bloch oscillation period remains unaffected by this feedback throughout the evolution. Therefore, the cavity light field transmitted through the output coupler (OC) provides a way to continuously observe the Bloch oscillations *in vivo*. This allows for high precision force measurements with small atomic clouds in a cavity [61].

A symmetric three-mirror ring cavity with one right angle and the round trip length $L = 3.8$ cm has been designed for the corresponding experiment. Consequently, the free spectral range is $\delta_{fsr} = c/L = 7.76$ GHz, where c is the speed of light in vacuum. The two curved high reflecting mirrors (HR) have radius $\rho = 50$ mm of the curvature, while the input coupler is plane. Using the defined above parameters it is possible to obtain the free space waist at the location of the atoms $w_0 = 70\mu\text{m}$ and the cavity mode volume $V = \pi \int_0^L w(z)^2 dz = 0.5$ mm³. The size of the thermal atomic cloud depends on the temperature, but can be made to fit into the waist. The spectral features of the ring cavity are determined by the reflection capability of the high reflector $R_{hr} = 99.9\%$ and the input coupler $R_{ic} = 99.7\%$, which allow to calculate the cavity finesse $F = \frac{\pi(R_{hr}^2 R_{ic})^{1/6}}{1 - (R_{hr}^2 R_{ic})^{1/3}} \simeq 2000$. Hence, the cavity linewidth is $\kappa = \delta_{fsr}/F = 160\omega_r$, where the recoil frequency is defined as $\omega_r = \hbar k^2/2m$.

The Bloch oscillations dynamics in this work is discussed at the example of an ultracold cloud of ^{87}Rb atoms interacting with the light fields via their D2-line ($5^2S_{1/2} \rightarrow 5^2P_{3/2}$) with the transition wavelength $\lambda = 780\text{nm}$, for which the recoil frequency is $\omega_r = (2\pi)3.75\text{ kHz}$, the Bloch oscillation frequency is $\nu_b = 0.035\omega_r$ and the transition linewidth is $\Gamma = 1600\omega_r$. With $d = \sqrt{3\pi\epsilon_0\hbar\Gamma/k^3}$ being the electric dipole moment of the atomic transition and $E_1 = \sqrt{\hbar kc/(2\epsilon_0 V)}$ the electric field generated by a single photon in the cavity mode, where ϵ_0 is the permittivity of free space, the atom-field coupling strength is $\Omega_1 = dE_1/\hbar = 54\omega_r$. The Rabi frequency generated by the incident pump light of intensity $I_p = 50\text{mW/cm}^2$ is

$$\Omega_p = \frac{dE_p}{\hbar} = \frac{d}{\hbar} \sqrt{\frac{2I_p}{c\epsilon_0}} = 6240\omega_r, \quad (2.1)$$

and Δ (taken positive for convenience) is the detuning of the laser frequency ω from the atomic resonance. Thus, the atom-mediated pump-probe coupling strength is $U_0 = \Omega_1\Omega_p/4\Delta$. In the performed numerical simulations, $U_0 = 0.04\omega_r$ is taken, and the cavity is loaded with $N = 2 \cdot 10^4$ atoms. All these parameters can be realized in state-of-the-art experiments without any particular difficulty.

Indicating the probe mode with frequency ω_s by the complex amplitude α , where $|\alpha|^2$ is the average photon number, the interference between the pump and probe modes generates a dipolar potential with the depth $\hbar\alpha U_0$ along the x axis of the optical ring cavity. Starting from the basic equations describing the CARL-BEC model [75, 76] and disregarding for the moment the atomic interaction in sufficiently dilute atomic clouds, the self-consistent equations of motion for the probe mode $\alpha(t)$ and the atomic wave function $\psi(x, t)$ can be written in the following form:

$$i\hbar \frac{\partial \psi(x, t)}{\partial t} = -\frac{\hbar^2}{2m} \frac{\partial^2 \psi(x, t)}{\partial x^2} - i\hbar U_0 [\alpha(t)e^{2ikx} - \alpha^*(t)e^{-2ikx}] \psi(x, t) - mgx\psi(x, t) + \hbar \frac{W_0}{2} \sin(2kx)\psi(x, t), \quad (2.2)$$

$$\frac{d\alpha(t)}{dt} = NU_0 \int |\psi(x, t)|^2 e^{-2ikx} d(2kx) + (i\delta - \kappa)\alpha(t), \quad (2.3)$$

where $\delta = \omega - \omega_s$ is the pump-probe detuning.

The evolution of the system can be conveniently described in the accelerated frame moving with the velocity gt along the positive direction of the x axis pointing downwards as in Fig.2.1. In this frame, the wave function is transformed

according to $\psi = \tilde{\psi} \exp(imgxt/\hbar)$. Substituting $\alpha = \tilde{\alpha} - \alpha_0$ with $\alpha_0 = W_0/4U_0$ ($W_0 = 3.2\omega_r$, which corresponds to $|\alpha_0|^2 = 400$ photons in the pump mode), into Eq.(2.2) and Eq.(2.3), the corresponding equations of motions become:

$$\frac{\partial \tilde{\psi}}{\partial t} = \frac{i\hbar}{2m} \left(\frac{\partial}{\partial x} + \frac{imgt}{\hbar} \right)^2 \tilde{\psi} - U_0 (\tilde{\alpha} e^{2ikx} - \tilde{\alpha}^* e^{-2ikx}) \tilde{\psi}, \quad (2.4)$$

$$\frac{d\tilde{\alpha}}{dt} = NU_0 \int |\tilde{\psi}|^2 e^{-2ikx} d(2kx) + (i\delta - \kappa)(\tilde{\alpha} - \alpha_0). \quad (2.5)$$

It should be noted that Eq.(2.5) shows that the impact of the externally imposed standing wave can be accounted for as an additional laser beam pumping the probe mode at the rate $\alpha_0\kappa$.

If the size of the atomic sample is much larger than the radiation wavelength, and its density is uniform, the atomic wave function $\tilde{\psi}(x, t)$ may be expanded into plane waves with periodicity $2kx$,

$$\tilde{\psi}(x, t) = \frac{1}{\sqrt{2\pi}} \sum_n C_n(t) e^{2inkx}, \quad (2.6)$$

where $|C_n|^2$ is the probability of finding the atoms in the n th momentum state $p_n = n(2\hbar k)$. Note that the atomic wave function is expanded in the momentum states $|p_n\rangle$ [77], rather than the often-used Bloch states $|n_b, q\rangle$ with quasimomentum q and the band index n_b [78], discussed in the introduction. Using the definitions of the Bloch oscillation frequency $\nu_b = mg/(2\hbar k)$ and the single-photon recoil frequency $\omega_r = \hbar k^2/2m$, Eqs.(2.4) and (2.5) are transformed into:

$$\frac{dC_n}{dt} = -4i\omega_r(n + \nu_b t)^2 C_n + U_0 (\tilde{\alpha}^* C_{n+1} - \tilde{\alpha} C_{n-1}), \quad (2.7)$$

$$\frac{d\tilde{\alpha}}{dt} = U_0 N \sum_n C_{n-1}^* C_n + (i\delta - \kappa)(\tilde{\alpha} - \alpha_0). \quad (2.8)$$

These equations describing the coupled atom-ring cavity dynamics represent the basis of the numerical simulations of this work.

2.2 Bloch oscillations dynamics without cavity

Without the cavity, the system under investigation is reduced to an ultracold atomic cloud confined into a vertical periodic optical potential created by two counter-propagating laser waves and subjected to a constant external force. In this case, the atomic behavior in the light field of the two laser beams is examined under the action of the gravitational acceleration g , and the revealed dynamics can be interpreted in the usual Bloch oscillation picture. The initial momentum $p \simeq 0$ of the atomic plane wave accelerated by gravity increases linearly until it reaches a critical value at which the atomic wave is reflected and the momentum is reversed. The ulterior dynamics is nothing but a continuous repetition of the same process, i.e., the acceleration of the matter wave by the gravitational force is followed by its Bragg reflection. The atomic Bloch oscillations can be viewed as reflections at Brillouin zones [10] as, for example, shown in Fig.2.2 where the energy spectrum of an atom in a periodic potential is given in the reduced zone scheme limited to the first Brillouin zone as a function of quasimomentum q . In the fundamental Bloch band the atom is forced to move in the direction of the applied gravitational force until the zone edge is approached and the atom is reflected back by the lattice till it is stopped again by gravity, after which the

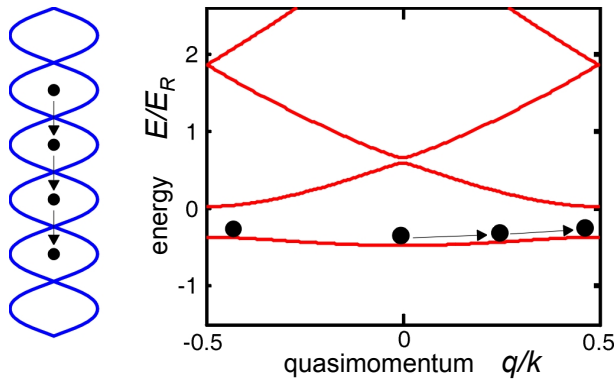


Figure 2.2: Left: Schematic representation of atoms dropping from node to node inside a vertical optical standing wave under the action of gravity. Right: Atoms accelerated within the lowest Bloch band being reflected at the edges of the first Brillouin zone. The energies are expressed in recoil energy units $E_R = (\hbar k)^2/2m$.

oscillatory behavior is repeated.

An accelerated frame is commonly used to describe such a system [77]. In this frame, the system is uniformly accelerated by gravity along the x axis, which leads to a Doppler shift of the frequencies of the two counter-propagating light fields. If the frequency difference is time-dependent, the lattice potential in the accelerated frame is no longer a standing wave, and the effect of gravity acting on the atoms in the laboratory frame manifests itself as a linear chirp in the first term on the right-hand side of Eq.(2.7). In this section, the dynamics revealed by the system in the absence of the ring cavity is studied in both laboratory and accelerated frames. In particular, the cases of adiabatic and non-adiabatic switch-on of the optical lattice are investigated as well as the variable lattice potential depth. The system without the cavity appear to be very sensitive to the choice of parameters and the way in which the lattice is turned on. Thus, some specific conditions must be satisfied to observe regular Bloch oscillations in this case.

2.2.1 Adiabatic rapid passage sequence

The atomic motion in a periodic potential is based on the photon redistribution between the two counter-propagating laser beams creating the standing wave. Due to the atom-field interaction, the atoms that are initially prepared in their ground state with a momentum spread much smaller than $2\hbar k$ ($\delta p \ll 2\hbar k$) populate excited momentum states during the evolution of the system. Assuming that spontaneous emission is negligible, the atomic momentum in the accelerated frame can only change by $2\hbar k$ every time a photon is absorbed from one beam of the optical lattice and re-emitted into the other one in a stimulated way. This momentum transfer results in an upward force that in the laboratory frame compensates for gravity. Note that in the considered case there are many sequential resonance crossings happening at $t = -n\tau_b$, where $\tau_b = 1/\nu_b$ is the Bloch period. At every crossing repeated periodically for $n = -1, -2, -3, \dots$, the atoms change their momentum by $2\hbar k$ and transfer to the negative n -mode states. The frequency difference changing in time produces a sequence of such transitions between momentum states. As a result, the atoms happen to be coherently accelerated in the direction of the laser wave with higher frequency from which the photons are absorbed and emitted into the other with lower frequency.

The way the momentum transfer is performed via scanning through the resonance is known as the *adiabatic rapid passage* (ARP) method [79]. The system prepared in an eigenstate at $t = 0$, when the frequency difference is increased, adiabatically follows the evolution of the eigenstate, leading to a series of momentum changes. If the initial frequency difference is zero, the atomic momentum is periodically increased by $2\hbar k$ at each resonance crossing, which is a signature of Bloch oscillations in the fundamental band in the accelerated frame [77]. The ARP method has been used extensively to create beam splitters and mirrors for atomic interferometry [80, 81], for instance, accelerate atoms trapped in optical potentials [10, 82] and observe adiabatic population inversion with light pulses [83, 84]. However, a number of features distinguish the studied system from previous ARP applications. Firstly, a non-dissipative regime is considered since the internal atomic states are not involved into the dynamics of the system. Secondly, it is possible to successfully produce a large number of momentum transfers because the amount of states is unlimited. Lastly, the momentum states are connected by a two-photon transition in the examined model, while a one-photon transition is generally used [85].

To produce an efficient momentum transfer using the ARP method, some adiabatic conditions must be satisfied for all sequential crossings. First of all, the frequency difference $\Delta\omega$ should vary slowly, so that the atoms can adiabatically follow the eigenstates of the system, and hence the atomic transition from one momentum state to another is complete. To make this happen, the rate at which the eigenstates change must be small in comparison to the coupling rate, i.e., $\Delta\dot{\omega} \ll (W_0/2)^2$. The adiabaticity may be easily violated by an increasing chirp rate, and the non-adiabatic couplings causing a small amount of atoms to remain in lower momentum states play an important role in this case. Thus, to fulfill the adiabatic conditions and be able to have a full momentum transfer, the chirp rate should not be too large.

The ARP conditions have been derived for a system with a time-dependent frequency difference of the two counter-propagating optical fields interacting with free atoms, which is analogous to the gravitational acceleration involved in the considered system [77]. Those conditions can be tailored to fit the system under investigation:

$$\frac{\nu_b}{8\omega_r} \ll \left(\frac{W_0}{16\omega_r} \right)^2 \ll 1. \quad (2.9)$$

Therefore, a properly chosen set of parameters needs to be used to make sure the inequalities above are satisfied. In order to understand the interpretation of these two conditions it is necessary to return to the laboratory frame. It

is clear that the dynamics of the Bloch oscillations associated with the atoms being accelerated by the gravitational force in the laboratory frame is equivalent to a sequence of adiabatic rapid passages between momentum states in the accelerated frame. The first condition can then be read as the force driving the atoms to perform Bloch oscillations should be weak enough to prevent interband transitions, $mg \ll (m/2k)(W_0/2)^2$. This crucial criteria necessary to observe stable Bloch oscillations ensures the adiabaticity of the process. The other condition requires the optical lattice to be sufficiently weak, $W_0 \ll 16\omega_r$, so that the dynamics involves only two adjacent momentum states at a time and the transfers are successive. This condition represents the so called weak binding limit [86]. In the weak binding approximation, the periodic potential is assumed to be quite shallow, and the atoms behave almost as if they were free. Indeed, the atoms in deeper lattices are not allowed to be considered as free particles coupled only at the edge of the Brillouin zone. More details about the time evolution of the system for different values of the lattice depth are provided in Sec.2.2.5. It can therefore be seen that satisfying the ARP conditions mentioned above is crucial for a successful population transient, and the non-adiabatic transition probability is required to be insignificantly small.

2.2.2 Two-state model

A mathematical description of the Bloch oscillations has been carried out extensively in the literature [17]. However, it is worth to demonstrate how the considered model, adopting the momentum state picture (not to be confused with the quasimomentum picture), describes the Bloch oscillations in the adiabatic rapid passage (ARP) approximation.

For sufficiently weak optical lattices, $W_0/\omega_r \ll 16$, the dynamics involves only two adjacent momentum states [77], say n and $n - 1$, so that $|C_n|^2 + |C_{n-1}|^2 = 1$. In this limit, Eqs.(2.7) and (2.8) can be reduced to a simple set of Maxwell-Bloch equations:

$$\frac{dS}{dt} = -i\Lambda_n S + U_0 \tilde{\alpha} W , \quad (2.10)$$

$$\frac{dW}{dt} = -2U_0 (\tilde{\alpha} S^* + \tilde{\alpha}^* S) , \quad (2.11)$$

$$\frac{d\tilde{\alpha}}{dt} = U_0 N S + (i\delta - \kappa)(\tilde{\alpha} - \alpha_0) , \quad (2.12)$$

where $\Lambda_n = (\omega_r/4)(2n - 1 + 2\nu_b t)$ is the time-dependent detuning, $S = C_{n-1}^* C_n$ is the interference term, and $W = |C_n|^2 - |C_{n-1}|^2$ is the population difference. These equations admit the constant of motion

$$4|S|^2 + W^2 = 1. \quad (2.13)$$

In the bad cavity regime, $\kappa \gg \alpha_0 U_0$ and for $\delta = 0$, the probe field from Eq.(2.12) is approximated by

$$\tilde{\alpha} \approx \alpha_0 + \frac{U_0 N S}{\kappa}. \quad (2.14)$$

Then, the adiabatic following assumption that both S and W vary slowly in time is made. The condition $|dS/dt| \ll |\Lambda_n S|$ and the assumption $\tilde{\alpha} \approx \alpha_0$ (i.e., neglecting the cavity entirely) allow S to be expressed in terms of the population difference W as $S = -iU_0\alpha_0 W/\Lambda_n$. Then, using the constant of motion $4|S|^2 + W^2 = 1$, one finds:

$$W = \frac{\Lambda_n}{\sqrt{4U_0^2\alpha_0^2 + \Lambda_n^2}}, \quad S = -i\frac{U_0\alpha_0}{\sqrt{4U_0^2\alpha_0^2 + \Lambda_n^2}}. \quad (2.15)$$

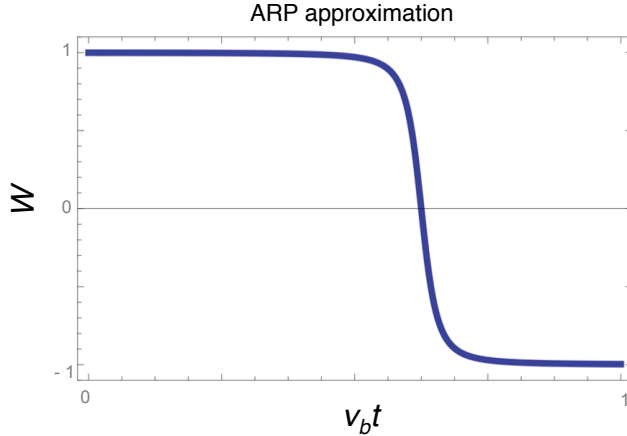


Figure 2.3: Evolution of the population difference W based on the expression (2.15). Full atomic transfer from the momentum state n to $n - 1$ is achieved.

Initially, the population difference $W = 1$ since all the atoms reside in the n th momentum state. However, there is a point where $\Lambda_n \rightarrow 0$, thereby $W \rightarrow 0$. As time passes, the population difference becomes negative (see Fig.2.3), which is equivalent to a transfer of the atoms to the state $n-1$. This confirms the validity of the ARP assumption and provides an analytical proof of why the Bloch oscillations are initiated. The ability of the ARP approximation to describe the evolution of the system in the presence of the ring cavity will be considered in the next chapter.

2.2.3 Average atomic momentum

Let us now turn to numerical studies of the system in the case when the optical ring cavity is absent. By keeping $\tilde{\alpha} = \alpha_0$ constant the atomic backaction on the cavity field is eliminated, and the influence of the cavity on the evolution of the system is generally disregarded. This situation corresponds to the standard case of a constant optical lattice. Eqs.(2.7) and (2.8) then reflect the usual Bloch oscillation picture or equivalently, a sequence of adiabatic rapid passages discussed above. This self-consistent set of equations represents the basis of the numerical simulations.

The behavior of the average atomic momentum in the laboratory frame, which is given by

$$\langle p \rangle_{lab} = \langle p \rangle + \nu_b t, \quad (2.16)$$

is investigated first, where the average atomic momentum $\langle p \rangle$ in the accelerated frame is determined by

$$\langle p \rangle = \sum_n n |C_n|^2. \quad (2.17)$$

Neglecting the contribution from the cavity field, Eq.(2.7) is integrated and the obtained results are shown in Fig.2.4. In the standing reference frame, the average atomic momentum $\langle p \rangle_{lab}$ given in $2\hbar k$ units is plotted as a function of rescaled time $\nu_b t$. One can immediately notice that the way in which the optical potential is turned on has a great impact on the dynamics of the system. The optical lattice can be optionally switched on abruptly, so that a constant light field is imposed even at the very beginning of the evolution, or switched on adiabatically as it is done in general experimentally. Both these cases are studied, and the results are provided below.

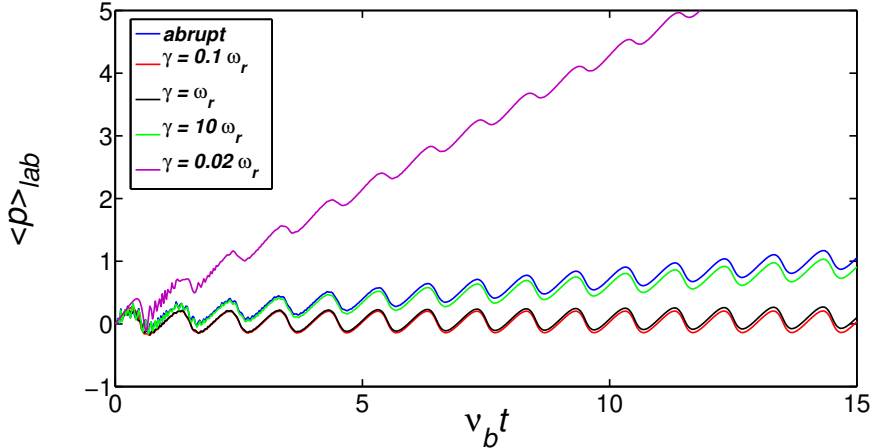


Figure 2.4: Average atomic momentum in the laboratory frame in $2\hbar k$ units in the absence of the cavity as a function of rescaled time $\nu_b t$. Different methods of the lattice switch-on are investigated: $\alpha_0 = 20$ corresponds to a sudden switching of the optical potential (blue curve), while an adiabatic switch-on is performed via $\alpha_0 = \tilde{\alpha}_0 (1 - \exp(-\gamma t))$ with $\tilde{\alpha}_0 = 20$ and various values of the amplitude rising rate γ . The evolution of the system for critical values of $\gamma = 0.02\omega_r$ and $\gamma = 10\omega_r$, for which the adiabaticity of the process is already broken, is given by purple and green curves, respectively. Another two values, $\gamma = 0.1\omega_r$ (red) and $\gamma = \omega_r$ (black), are shown to satisfy the ARP conditions well. The other rubidium parameters used in the simulations are: $\nu_b = 0.035\omega_r$, $\kappa = 160\omega_r$, $\delta = 0$ and $U_0 = 0.04\omega_r$.

For an abrupt switch-on of the optical lattice the evolution of the average atomic momentum in the laboratory frame is shown by the blue curve in Fig.2.4. In this case, an atomic drift associated with a coherent directed transport of the Bloch oscillating atoms [87] is observed. If a sudden switch-on is performed, the atomic population is initially distributed over several momentum states, not all of which participate in the Bloch oscillations. Consequently, the change in average atomic momentum in the accelerated frame at each step is slightly less than $2\hbar k$, which can be seen in Fig.2.5, and the upward force caused by the momentum transfer does not fully compensate for gravity. As the result, the

center-of-mass momentum of the atomic cloud steadily increases in time. Thus, it is demonstrated that in the absence of the ring cavity, an abrupt switch-on of the optical potential leads to a sustained drift of the atomic momentum in the laboratory frame.

On the other hand, instead of a sudden switch-on of the lattice with $\alpha_0 = \text{const}$, it can be turned on in an adiabatic fashion via

$$\alpha_0 = \tilde{\alpha}_0 (1 - e^{-\gamma t}), \quad (2.18)$$

where $\tilde{\alpha}_0$ is a constant corresponding to a saturation value of the light field amplitude eventually achieved as time goes on, and γ is the rate at which the amplitude of the optical potential is increased. An important criteria for selection of a proper value of γ is given by the fact that the raising time of the potential $\tau_r = 1/\gamma$ should be much shorter than the first Bloch period τ_b ($\tau_r \ll \tau_b$), i.e., the optical lattice is assumed to be created already before the actual evolution of the system starts. In other words, a typical value of the lattice amplitude rising rate γ should be much larger than the Bloch oscillation frequency ($\gamma \gg \nu_b$) in order to provide an adiabatic switch-on of the optical potential. Indeed, if a value smaller than the Bloch frequency is taken, for example, $\gamma = 0.02\omega_r$ (purple) in the performed simulations (see Fig.2.4 and Fig.2.5), the lattice is turned on so slowly that it is actually not created by the time the first momentum transfer occurs. Consequently, the matter wave diffuses quickly over various bands, and the oscillations remain degraded. Thus, it is seen that the amplitude of the lattice potential should not arise too slowly, otherwise the adiabaticity of the process is no longer reliable. It is also not valid for a very fast switch-on of the potential, which is demonstrated for $\gamma = 10\omega_r$ (green) in Fig.2.4 and Fig.2.5. The behavior of the system in this case is similar to an abrupt switching of the lattice: the chosen value of the amplitude rate is so high that the saturation is reached almost immediately, and the efficiency of the momentum transfer is visibly reduced.

A suitable value of the amplitude rising rate γ should clearly belong to a certain interval to secure the adiabaticity of the process. In practice, it is relatively easy to realize an adiabatic switch-on of the lattice with respect to the interband excitation. A typical time period of a few hundred microseconds is generally used as a rising time of the optical potential. For the selected values of $\gamma = 0.1\omega_r$ (red) and $\gamma = \omega_r$ (black) the ARP conditions (2.9) seem to be fulfilled well. Consequently, the momentum transfer at each Bloch period is efficient and no atomic drift is observed.

This section clearly demonstrates that the evolution of the system without the cavity appears to be highly sensitive to the manner in which the optical

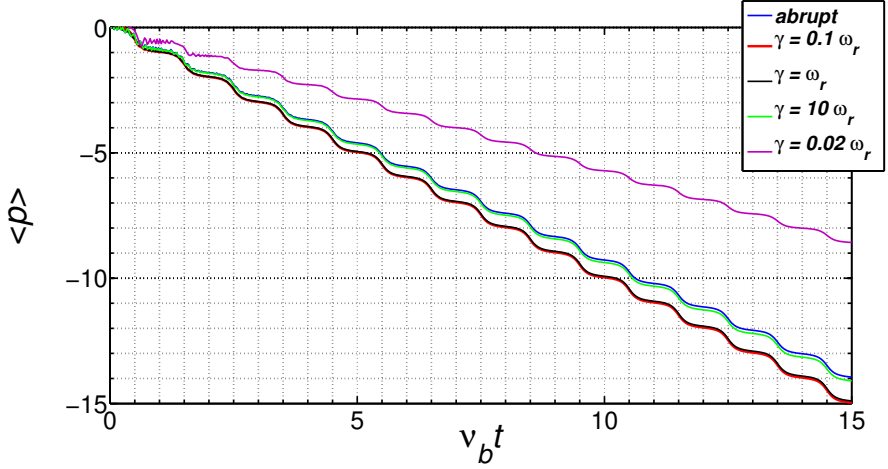


Figure 2.5: Dynamics of the average atomic momentum in $2\hbar k$ units in the accelerated frame without the cavity as a function of scaled time $\nu_b t$. The same parameters as in Fig.2.4 are used.

potential containing the atoms is switched on. The reason for the observed atomic drift is that any non-adiabatic process violates the first ARP assumption $32\nu_b/\omega_r \ll (W_0/\omega_r)^2$. If the process is not perfectly adiabatic, the applied force may cause a part of the matter wave to tunnel into the neighboring Bloch band where it continues being accelerated. In this case, there is always a fraction of the atomic population that remains in the lower states during the sequential transitions between momentum states, and as a result the momentum transfer at each step is rather less than $2\hbar k$, i.e., is incomplete. Thus, the selection of the suitable parameters must be done carefully, since it is essential for the observation of regular Bloch oscillations.

2.2.4 Momentum states population

This subsection is dedicated to a visual demonstration of the consecutive population transfer between adjacent momentum states happening every Bloch period τ_b . In order to confirm the fact that the way the optical potential is created notably influences the behavior of the system, the time evolution of the population of every momentum state involved in the dynamics for both sudden and adiabatic switch-on of the lattice is studied. For these cases, the results of the numerical simulations of Eqs.(2.7) and (2.8) with $n_{max} = 15$ and typical rubidium parameters are provided in Fig.2.6(a) and Fig.2.6(b), respectively. To ease the visual distinction between the population dynamics of each momentum state $|C_n|^2$, various colors are used. It should be noted that the atoms are prevented to leak out of the system as seen also in Fig.2.6, where the total momentum states population shown by the green line on the top of each picture is verified to be equal to unity and remains unchanged during the evolution in both cases.

For the case of an abrupt switching of the potential, the atoms end up being initially dispersed over several momentum states with the majority of the atoms residing in the n th state. Fig.2.6(a) shows that the atoms from the states other than n stay in those momentum states throughout the evolution and remain excluded from the Bloch oscillations dynamics. As it is seen in Fig.2.6(a), an atomic transition to the next negative momentum state happens every Bloch period. However, only the atoms found in the state n at the beginning of the evolution execute Bloch oscillations, the rest of the atomic population is considered to be lost for the dynamics. Due to this issue, the efficiency of the momentum transfers is reduced and the previously discussed steady atomic drifts occur.

If the optical lattice is created in an adiabatic fashion, and all the atoms are assumed to be located in a single momentum state initially, the atomic population transfer taking place every τ_b is shown to be fully complete. Unlike the case of a sudden rise of the lattice, all atoms now participate in the dynamics. Fig.2.6(b) demonstrates that at each step all atomic matter is successfully transferred to the next adjacent momentum state. No atomic drift is present in this case, and the Bloch oscillations appear to be stable and regular.

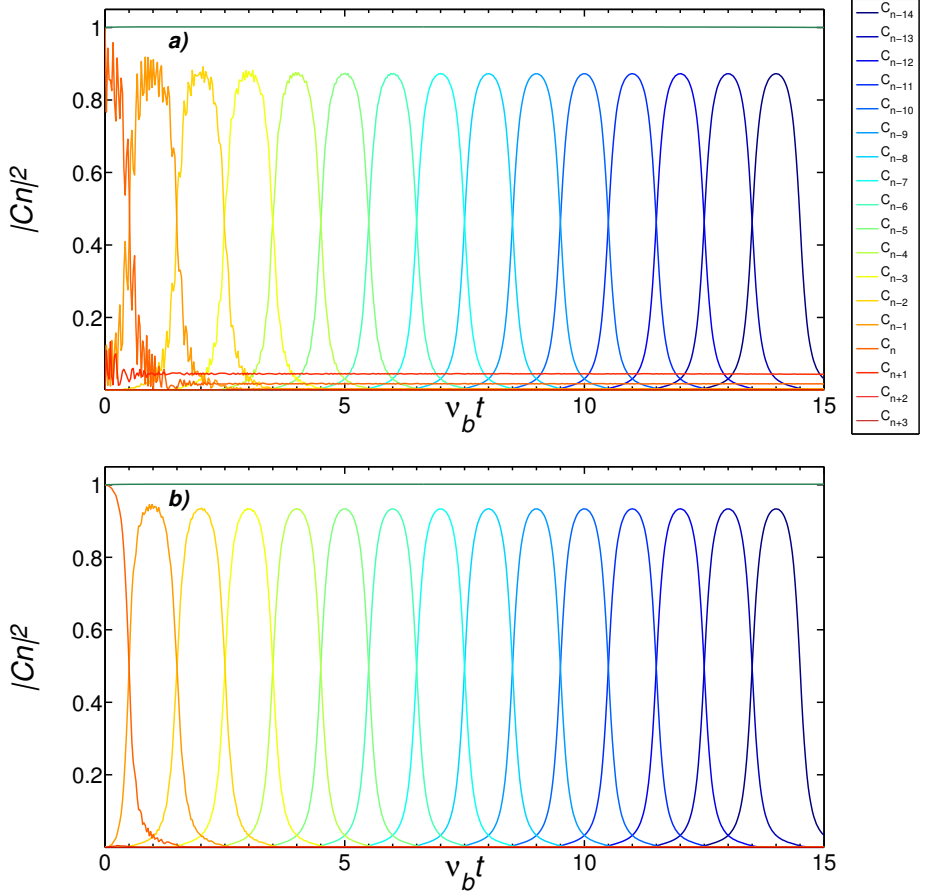


Figure 2.6: Evolution of the momentum states populations $|C_n|^2$ with $n_{max} = 15$ in the absence of the cavity for a) abrupt switch-on of the lattice potential with $\alpha_0 = 20$ and b) adiabatic switching with $\gamma = 0.1\omega_r$ and $\tilde{\alpha}_0 = 20$. The other chosen parameters are $\nu_b = 0.035\omega_r$, $\kappa = 160\omega_r$, $\delta = 0$ and $U_0 = 0.04\omega_r$. The population dynamics of each momentum state is given by a different color to enable visual distinction between the curves.

2.2.5 Variable optical potential depth

In the previous subsections it has been shown that the way in which the lattice potential is switched on significantly influences the dynamics of the system without the cavity. An adiabatic switching of the lattice is required for detection of stable Bloch oscillations, since if the lattice is turned on adiabatically, in this case only the non-excited momentum state is initially populated and all the atoms undergo Bloch oscillations. However, even if all atoms reside initially in a single momentum state, atomic drifts may occur.

This might happen, for instance, when the optical lattice is too shallow. Such a situation is illustrated in Fig.2.7 showing the dynamics of the average atomic momentum in $2\hbar k$ units in both laboratory and accelerated frames for a slightly reduced lattice potential depth of $W_0 = 1.6\omega_r$. As it has already been

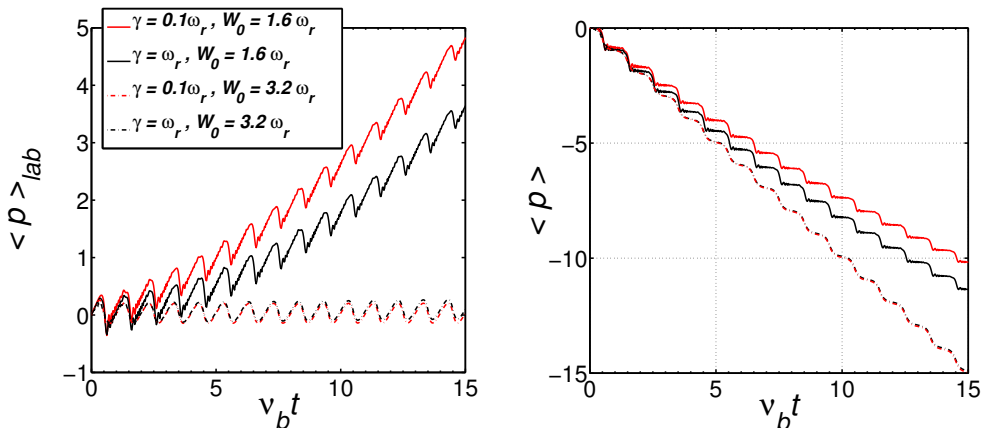


Figure 2.7: Evolution of the average atomic momentum in $2\hbar k$ units in the laboratory (left) and accelerated (right) frames without the cavity for a reduced lattice depth of $W_0 = 1.6\omega_r$. The other parameters remain the same: $\nu_b = 0.035\omega_r$, $\kappa = 160\omega_r$, $\delta = 0$ and $U_0 = 0.04\omega_r$. The adiabatic switch-on of the optical potential via $\alpha_0 = \tilde{\alpha}_0 (1 - \exp(-\gamma t))$ with $\tilde{\alpha}_0 = 20$ (dashed curves) is compared to the case when the value of $\tilde{\alpha}_0 = 10$ is taken instead (solid curves). Both values $\gamma = 0.1\omega_r$ (red) and $\gamma = \omega_r$ (black) fulfill the ARP conditions for the lattice depth of $W_0 = 3.2\omega_r$, whereas for a potential depth twice as small the adiabaticity is broken, and a prominent atomic drift is observed.

demonstrated, both values $\gamma = 0.1\omega_r$ and $\gamma = \omega_r$ of the amplitude rising rate certainly fulfill the ARP conditions (2.9) for the lattice depth of $W_0 = 3.2\omega_r$. In Fig.2.7 the evolution of the system corresponding to this case for $\gamma = 0.1\omega_r$ and $\gamma = \omega_r$ is given by dashed red and black curves, respectively, and regular Bloch oscillations as well as full momentum transfers are detected. However, if the depth of the optical potential is twice as small the previous value (solid curves in Fig.2.7), the adiabaticity of the process is obviously destroyed, and a prominent atomic drift is observed as the result of the non-efficient population transitions between momentum states.

This particular case of a slightly reduced optical potential depth in the case without the ring cavity points out once again that the selected parameters must be appropriate to satisfy the ARP conditions, otherwise the atomic population participating in the Bloch oscillations is reduced due to redistribution over several momentum states, and an atomic drift is observed instead of synchronous Bloch oscillations.

To sum up so far, the principal model of interest has been derived and the system without the ring cavity has been investigated in detail. Since the adiabatic sequential transfer between adjacent momentum states corresponds to the Bloch oscillations in the lowest Bloch band, the ARP conditions are applied to the system in order to obtain regular Bloch oscillations. The evolution of the system is demonstrated to be strongly dependent on a chosen method of the lattice switch-on. If a non-adiabatic switching of the optical potential is performed, an atomic drift may occur since one of the ARP conditions, $32\nu_b\omega_r \ll W_0^2$, is violated, and as a result the momentum transfer is inefficient. To prevent the atoms from tunneling to the next higher Bloch band and avoid a drift of the atomic momentum, the atomic motion is required to be perfectly adiabatic. For an adiabatic switch-on of the lattice potential a certain set of parameters can be selected to satisfy the ARP conditions; consequently, the momentum transfer becomes fully successful. This adiabaticity can be easily broken by small changes of the parameters. Therefore, a careful selection of the parameters is absolutely necessary in the case without the cavity. The next chapters, however, reveal multiple benefits of the presence of the ring cavity such as the interband tunneling suppression and the Bloch oscillations stabilization via the enforced adiabaticity.

Note that there are no collective effects in the absence of the cavity. Thus, it is possible to observe stable Bloch oscillations for any reasonable amount of

atoms N contained in the system without the cavity, assuming that the other parameters are close to fulfill the ARP conditions. However, as it will be seen later, this is definitely not the case when the cavity is present. The fact that the coupling parameter NU_0/κ may become critically large with increasing N plays an important role in the evolution of the system in the presence of the cavity. As the coupling parameter is enhanced, the backscattering of the pump light into the probe mode gets stronger. Here, the collective CARL effect may impose its dynamics to the atoms, leading to a competition with the Bloch oscillations dynamics. For a significantly large coupling parameter the Bloch oscillations dynamics may be even overruled. A more detailed explanation of this phenomenon is provided in Sec.4.3 where the presence of the cavity is taken into consideration.

Chapter 3

Mode-locking with ring cavity

The situation changes considerably in the presence of a unidirectionally pumped optical ring cavity. The system, as before, consists of ultracold atoms undergoing Bloch oscillations in a vertical optical potential under the action of the gravitational force (see Fig.2.1). However, if the cavity is present, the reverse cavity mode α becomes available, which obviously imposes an additional effect. The atoms now not only exchange photons between the optical lattice laser beams, but also collectively scatter light from the pumped cavity mode into the counter-propagating one. The intracavity pump and probe fields form a standing wave optical potential, and it is reasonable to expect the observable signatures of the atomic Bloch oscillations when the standing wave created inside the cavity is commensurate with the externally imposed one, i.e., $k = k_l$. The photons emitted into the reverse cavity mode happen to be added to the mode α_0 of the external optical lattice. Even though in the regime of interest the contribution of this scattered field to the optical lattice strength remains negligibly small, it provides a feedback on the atomic motion, such that the momentum transfer at each Bloch period τ_b becomes complete, and the Bloch oscillations are stabilized. This effect can be interpreted as a mode-locking of the Bloch oscillations induced by the cavity field. A detailed investigation of this phenomenon is provided in the next sections. In particular, Sec.3.1 compares the behavior of the system in the presence of the ring cavity with the dynamics revealed in the case without the cavity, studied in the previous chap-

ter, including the ARP approximation which describes the long-term dynamics perfectly well and only fails to reproduce a few rapid oscillations at the very beginning of the evolution. The feedback generated by the cavity is demonstrated to provide a number of advantages among which are, for example, the long-term persistence of the Bloch oscillations, even if the lattice potential is turned on non-adiabatically, and the opportunity to monitor the atomic motion in a non-destructive fashion via the light scattered into the probe mode of the ring cavity, discussed in Sec.3.2.

3.1 Mode-locking mechanism

Since the ring cavity is now added to the system, the atoms scatter cooperatively the pump photons into the reverse cavity mode, and the time evolution of the cavity field must be taken into account. In this case, the numerical simulations are performed letting the field $\tilde{\alpha}$ evolve dynamically according to Eq.(2.8). The evolution of the average atomic momentum shown in Fig.3.1 exhibits the first example of a positive impact of the atom-field coupling in the cavity on the dynamics of the system.

Fig.3.1 represents a comparison of the constant optical lattice solution without the cavity shown by the dashed curves with the dynamics given by the case when the contribution of the scattered cavity field is included (solid curves), obtained by solving Eqs.(2.7) and (2.8) with the parameters $N = 2 \cdot 10^4$, $\nu_b = 0.035\omega_r$, $\kappa = 160\omega_r$, $\delta = 0$ and $U_0 = 0.04\omega_r$. First, both sudden switch-on of the optical lattice with $\alpha_0 = 20$ (blue) and adiabatic switching via $\alpha_0 = \tilde{\alpha}_0(1 - \exp(-\gamma t))$ with $\tilde{\alpha}_0 = 20$ and $\gamma = 0.1\omega_r$ (red) are considered in the laboratory (left) and accelerated (right) frames in Fig.3.1(a). Then, very fast (green) and very slow (purple) lattice switchings are examined with $\gamma = 10\omega_r$ and $\gamma = 0.02\omega_r$, respectively, and the results are presented in Fig.3.1(b).

From the previous chapter it is known that if the contribution from the cavity field is neglected, after the optical potential is turned on non-adiabatically, the population transfer between adjacent momentum states is not complete, and as a result the change of the average atomic momentum at each step is slightly less than $2\hbar k$. Consequently, the Bloch oscillations are not preserved, and the average momentum drifts steadily after each period, which is clearly demonstrated by the dashed blue curves in Fig.3.1(a). Unlike the case without

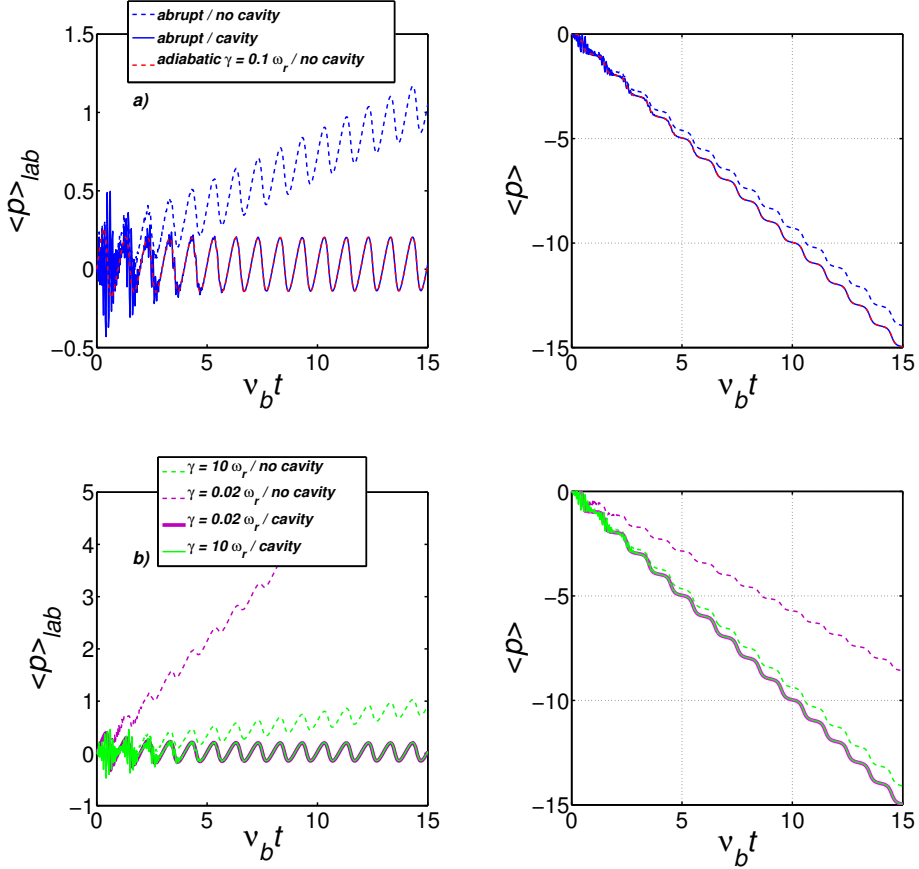


Figure 3.1: Average atomic momentum in the laboratory (left column) and accelerated (right column) frames in units of $2\hbar k$ as a function of normalized time $\nu_b t$ for an abrupt (blue), adiabatic (red) with $\gamma = 0.1\omega_r$, very slow (purple) with $\gamma = 0.02\omega_r$ and very fast (green) with $\gamma = 10\omega_r$ switch-on of the optical potential. The dashed curves correspond to a constant optical lattice, i.e., the case without the cavity, while the solid ones represent the case when the radiation field evolves according to Eq.(2.8) in the presence of the cavity. The simulations are performed for $N = 2 \cdot 10^4$, $\nu_b = 0.035\omega_r$, $\kappa = 160\omega_r$, $\delta = 0$, $U_0 = 0.04\omega_r$, and $\alpha_0 = 20$ for a sudden switch-on of the lattice and $\tilde{\alpha}_0 = 20$ for an adiabatic one.

the cavity, the solid blue curves show that after a transient of approximately three Bloch periods the population is efficiently restored into the first Brillouin zone in the presence of the cavity, even if an abrupt switch-on of the lattice potential is performed. Thus, the momentum drift is obviously canceled, and the Bloch oscillations persist for long times. A similar behavior of the system apart from the transient is shown by the dashed red curves in Fig.3.1(a) for the case when an adiabatic switching of the lattice takes place in the absence of the cavity, for which the ARP conditions (2.9) are fully satisfied. This proves that if the lattice is turned on abruptly, the feedback provided by the cavity field onto the atomic motion also tends to assist the adiabatic rapid passages between momentum states helping to complete the momentum transfer each Bloch period τ_b . Fig.3.1(b) manifests that the same effect occurs also when the optical lattice is turned on very fast or very slowly in the presence of the cavity. While both these ways to perform the lattice switching without the cavity lead to the violation of the ARP conditions and unsuccessful momentum transfer, the cavity is proven to bring back the stability of the Bloch oscillations lasting for indefinite times.

The reason of the observed cavity-induced stabilization is the positive feedback of the cavity field on the atomic evolution. The cavity seems to force the atoms to execute synchronous Bloch oscillations since its presence is shown to contribute to the transitions between adjacent momentum states, resulting in a fully efficient momentum transfer. The mechanism of stabilization is organized in such a way that the Bloch oscillations become persistent through a process analogous to the mode-locking in Q-switched lasers [88–90], representing the operation regime of mode-locked lasers with fluctuations in the pulse energy. As it will be seen later in the section, every Bloch oscillation is accompanied by a detectable burst of light in the reverse cavity mode. Thus, the dynamics of the studied system can be associated with a regular pulse train similar to the one emitted by a mode-locked laser together with a low-level background noise. For this reason, the process behind the displayed Bloch oscillations stabilization is termed *mode-locking mechanism* in this work.

3.1.1 Comparison with ARP approximation

As it is demonstrated in Sec.2.2.2, if the dynamics involves only two adjacent momentum states, Eqs.(2.7) and (2.8) can be substituted by the set of Maxwell-Bloch equations (2.10)-(2.12) for the populations difference W , interference term S and time-dependent detuning Λ_n , admitting the constant of motion $4|S|^2 + W^2 = 1$. According to the ARP approximation

$$W = \frac{\Lambda_n}{\sqrt{4U_0^2\alpha_0^2 + \Lambda_n^2}}, \quad S = -i \frac{U_0\alpha_0}{\sqrt{4U_0^2\alpha_0^2 + \Lambda_n^2}}. \quad (3.1)$$

From these, one can express the average atomic momentum in $2\hbar k$ units in the accelerated frame as

$$\langle p \rangle = n + \frac{(W - 1)}{2}. \quad (3.2)$$

The results obtained using the ARP approximation correspond to the dashed red curves in Fig.3.2, where the average atomic momentum is given in both the

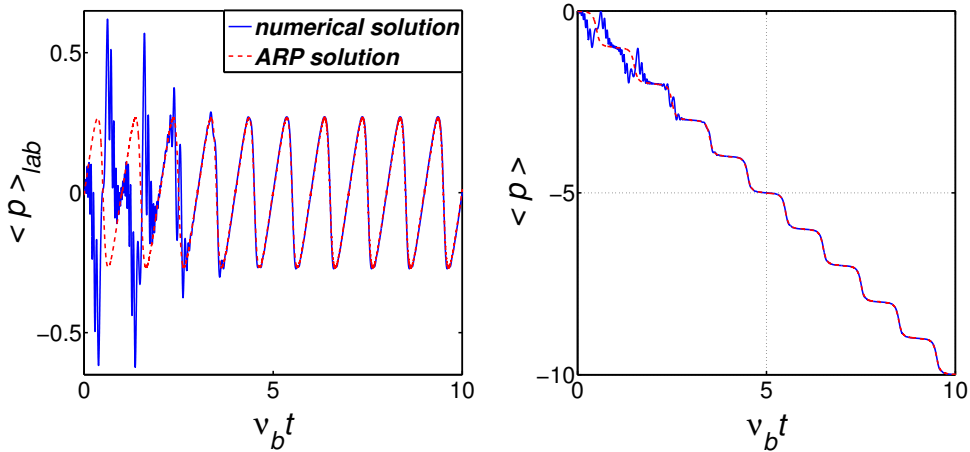


Figure 3.2: Comparison of the average atomic momentum given in units of $2\hbar k$ in the laboratory (left) and accelerated (right) frames, obtained from the ARP solution (dashed red) of Eq.(3.1) and numerical solution (solid blue) of Eqs.(2.7) and (2.8). The used parameters are $N = 2 \cdot 10^4$, $\nu_b = 0.035\omega_r$, $\kappa = 160\omega_r$, $\delta = 0$ and $U_0 = 0.04\omega_r$.

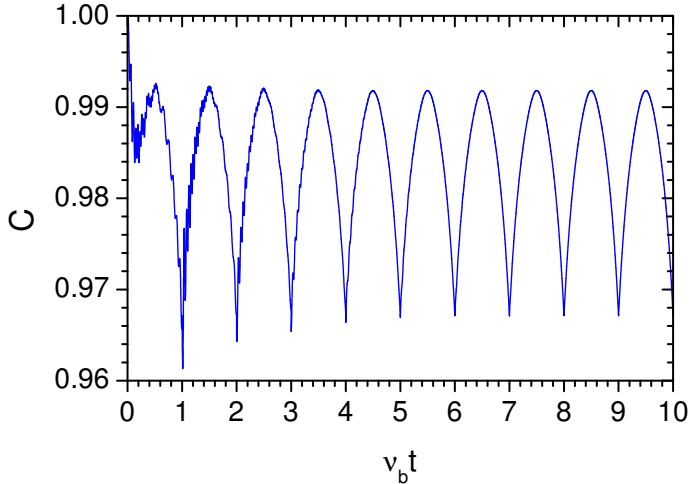


Figure 3.3: Constant of motion $C = W^2 + 4|S|^2$ as the result of the numerical solution of Eqs.(2.7) and (2.8). The same parameters as in Fig.3.2 are used.

laboratory and accelerated frames in $2\hbar k$ units, while the results of the numerical solution of Eqs.(2.7) and (2.8) are shown in blue. It is seen that ARP describes the behavior of the system well after a transient of a few Bloch periods, and it allows to interpret Bloch oscillations as a succession of transitions between two adjacent momentum states [77]. Fig.3.3 representing the constant of motion $C = W^2 + 4|S|^2$ calculated numerically from the exact solution of Eqs.(2.7) and (2.8) reveals an insignificant deviation from unity expected in the made approximation. Thus, the results obtained from the ARP solution are in good agreement with the numeral simulations, which confirms that ARP is sufficient to characterize the long-term evolution of the system. However, a more complete description is required to explain the wild transient at the very beginning of the evolution. Since the mode-locking mechanism actually involves more than just two momentum states at each transition, the presence of which is shown to be responsible for the transient in Appendix B, the full description turns out to be very challenging. For this reason, a more precise study of the Bloch oscillations in this work has to rely on the numerical integration of Eqs.(2.7) and (2.8).

3.1.2 Population of momentum states

Sec.2.2 of the previous chapter considers how the turning on of the optical lattice affects the behavior of the system in the absence of the ring cavity. Only if an adiabatic switch-on is performed, the displayed evolution reveals no atomic momentum drifts because the ARP conditions are completely satisfied and all the atoms participate in the Bloch oscillations dynamics. In contrast to the case without the cavity, it does not matter if the lattice potential is switched on adiabatically or non-adiabatically in the presence of the cavity, since the mode-locking mechanism secures the stabilization of the Bloch oscillations via assistance of sequential adiabatic rapid passages between momentum states. This can also be observed in the time evolution of the momentum states populations $|C_n|^2$ showing each state's dynamics by a different color to distinguish the separate curves. Comparing Fig.2.6(a) produced for an abrupt switch-on of the optical lattice without the cavity with Fig.3.4 representing the case when the cavity is added to the system and the same non-adiabatic way of the lattice switching, one can realize that the cavity-induced feedback makes all the atoms

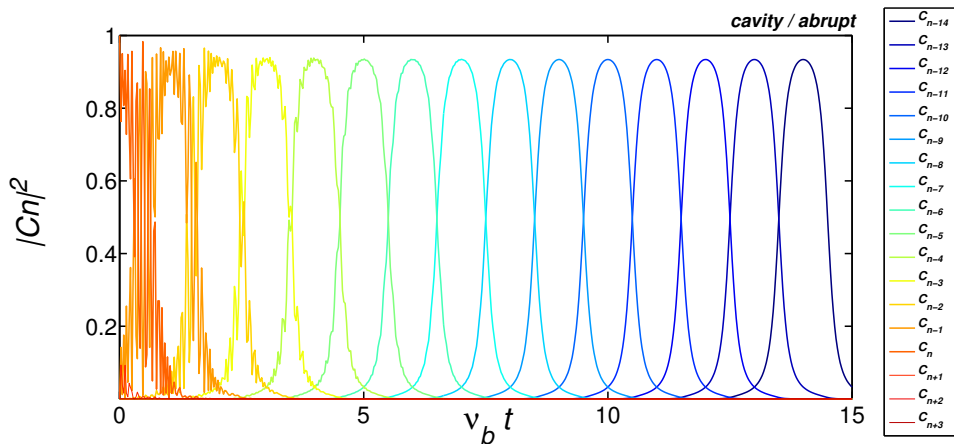


Figure 3.4: Time evolution of the momentum states populations $|C_n|^2$ in the case of an abrupt switch-on of the optical lattice in the presence of the cavity. The parameters used to perform the simulations are $N = 2 \cdot 10^4$, $\nu_b = 0.035\omega_r$, $\kappa = 160\omega_r$, $\delta = 0$ and $U_0 = 0.04\omega_r$. To be compared with Fig.2.6(a) realized for an abrupt lattice switching without the cavity.

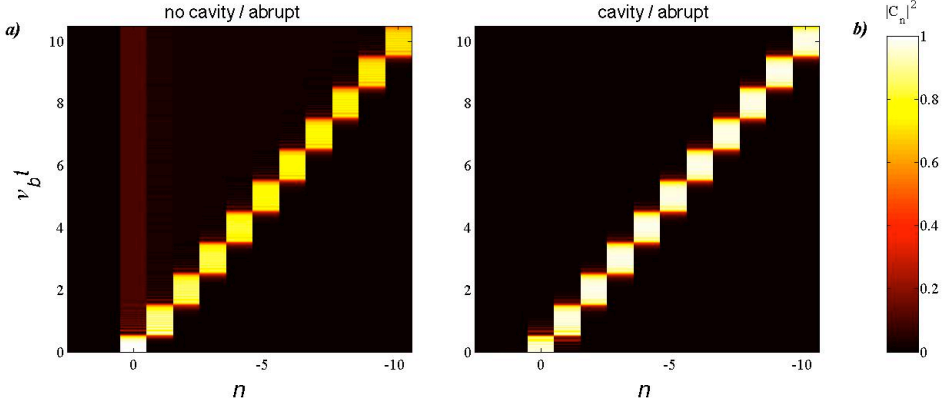


Figure 3.5: Momentum states population diagram for the case of an abrupt switch-on of the optical potential a) without the cavity and b) with the cavity. Diagram a) is an alternative representation of Fig.2.6(a), while diagram b) corresponds to Fig.3.4. The same parameters as in Fig.3.4 are used.

undergo the synchronous Bloch oscillations despite the initially imposed non-adiabaticity. These dynamics are alternatively represented in Fig.3.5(a) and (b), respectively, which may help understanding of the role of the ring cavity even better. Each square in Fig.3.5 corresponds to a momentum state n whose population is shown by the color diagram. The difference between the two cases is evident. In the absence of the ring cavity a fraction of the atoms is lost from the Bloch oscillation dynamics since the atoms remain in the starting momentum state given by the brown line in Fig.3.5(a), and accordingly the momentum transfer each Bloch period cannot be complete. In the case with the cavity, the feedback provided by the cavity field on the atoms restores the effective dynamics by forcing full $2\hbar k$ transitions between the momentum states. Thus, again thanks to the mode-locking scheme with the ring cavity, the Bloch oscillations remain stable for long times.

3.1.3 Reduced potential depth

In Sec.2.2.5 it is demonstrated that even if the confining lattice potential is turned on in an adiabatic fashion, a drift of the cloud's center-of-mass momentum may still occur. The fact that only the $p = 0$ momentum state is initially populated may not guarantee that all the atoms undergo the Bloch oscillations. If, for example, the lattice potential is too shallow (i.e., the chirping rate is too fast), the matter wave in the absence of the ring cavity diffuses over various momentum states, which eventually degrades the Bloch oscillations (see Fig.2.7). Here, a lower lattice potential depth of $W_0 = 1.6\omega_r$ is taken as an example to compare the dynamics of the system with and without the cavity. The optical lattice is switched on adiabatically via $\alpha_0 = \tilde{\alpha}_0(1 - \exp(-\gamma t))$ with $\tilde{\alpha}_0 = 10$ and two values of the amplitude rising rate $\gamma = 0.1\omega_r$ (red) and $\gamma = \omega_r$ (black). The time evolution of the average atomic momentum in the laboratory ($\langle p \rangle_{lab} = \langle p \rangle + \nu_b t$) and accelerated frames is shown in Fig.3.6 in the pres-

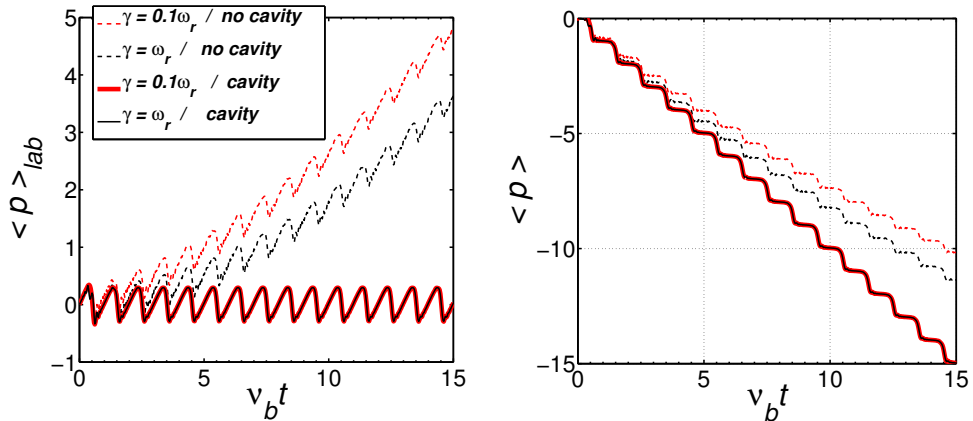


Figure 3.6: Comparison of the average atomic momentum in the laboratory (left) and accelerated (right) frames for the cases with (solid curves) and without (dashed curves) the cavity for a reduced optical potential depth of $W_0 = 1.6\omega_r$. The lattice is realized in an adiabatic fashion with $\tilde{\alpha}_0 = 10$ for $\gamma = 0.1\omega_r$ (red) and $\gamma = \omega_r$ (black). The rest of the parameters used to perform the simulations are $N = 2 \cdot 10^4$, $\nu_b = 0.035\omega_r$, $\kappa = 160\omega_r$, $\delta = 0$ and $U_0 = 0.04\omega_r$.

ence of the cavity (solid curves) and without the cavity (dashed curves). Unlike, the latter case with no cavity, where an immediate drift in the average atomic momentum for both values of γ is observed despite the adiabatic switch-on of the lattice potential, the cavity brings back the stability of the system even with the reduced lattice potential depth. This is another advantage of the feedback provided by the cavity which assists full momentum transfers between neighboring momentum states and stabilizes the Bloch oscillations via the mode-locking mechanism, whereas the system without the cavity fails to do so.

3.2 Non-destructive monitoring

The mode-locking mechanism in the unidirectionally pumped optical ring cavity can be shown to provide direct signatures of the atomic Bloch oscillations in the defined parameter regime. In particular, the radiation field reaches a stationary regime characterized by periodic bursts of light at each Bloch oscillation. Even though it takes slightly more time for the Bloch oscillations to self-synchronize, if the confining lattice potential is turned on abruptly rather than adiabatically, the stationary regime is achieved within the first few Bloch periods. This can be seen in Fig.3.7(a), where the intracavity photon number evolution $|\alpha|^2$ of the probe mode α is given for the cases of adiabatic (solid red) and sudden (dashed blue) switch-on of the optical lattice. The phase ϕ of the field $\alpha = \tilde{\alpha} - \alpha_0$ of the probe mode, shown in Fig.3.7(b), also stabilizes after the transients to a constant value only slightly perturbed at each Bloch oscillation. The average number of photons in the cavity field throughout the evolution is $|\alpha|^2 \simeq 5$. To estimate the count rate on an external photodetector the intracavity power is introduced as $P_{cav} = \hbar\omega|\alpha|^2\delta_{fsr}$, where $\delta_{fsr} = \kappa F$ is the free spectral range and F is the cavity finesse. It is linked to the power leaking through the input coupling mirror via $P_{out} = TP_{cav}$, where $T = \kappa/\delta_{fsr}$. This gives a photon flux rate of $P_{out}/\hbar\omega = \kappa|\alpha|^2$. For the chosen cavity decay rate $\kappa = 160\omega_r$ and the Bloch oscillation frequency $\nu_b = 0.035\omega_r$, the expected photon flux is $\sim 4600 \text{ s}^{-1}$ outside the cavity or approximately 35 photons per Bloch oscillation, which can be easily detected through a photon counter. Thus, after a transient of a few Bloch periods, the radiation field develops a constant phase and becomes periodic with perfectly detectable signatures of the Bloch oscillations, thereby providing a reliable and non-destructive monitor of the atomic motion. Such

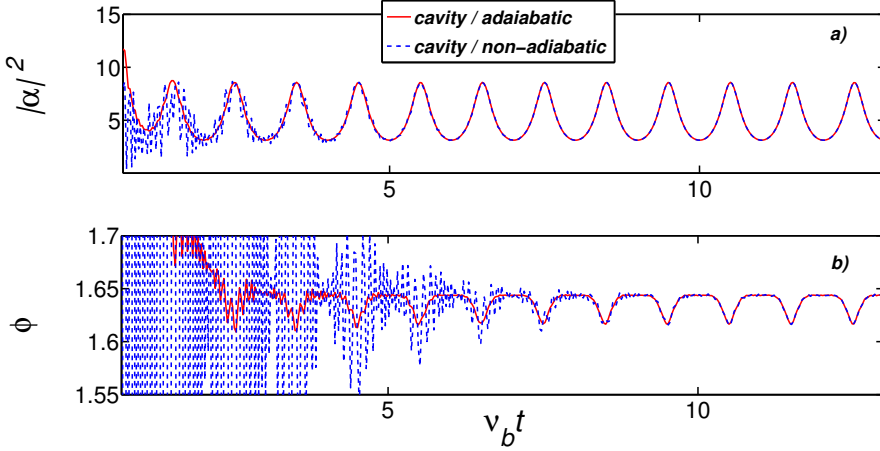


Figure 3.7: a) Average number of photons $|\alpha|^2$ in the radiation field and b) phase ϕ of the cavity mode α as functions of scaled time $\nu_b t$ for a sudden (dashed blue) and adiabatic (solid red) switch-on of the lattice potential in the presence of the cavity. The used parameters are $N = 2 \cdot 10^4$, $\nu_b = 0.035\omega_r$, $\kappa = 160\omega_r$, $\delta = 0$, $U_0 = 0.04\omega_r$. The lattice is turned on either abruptly with $\alpha_0 = 20$ or adiabatically with $\tilde{\alpha}_0 = 20$ and $\gamma = 0.1\omega_r$.

regime may be very useful for experimental studies since the detection of the signal coming out of the cavity seems to be very convenient. Furthermore, in contrast to the previous proposals on continuous monitoring of the Bloch oscillations [60, 69], the studied scheme does not require heterodyne detection. Generally, in heterodyne detection, a signal of interest at some frequency is non-linearly mixed with a reference signal that is set at a close-by frequency. The desired outcome is the frequency difference which carries the information on the amplitude, phase and frequency modulation of the original higher frequency signal, but is oscillating at a lower and more easily processed carrier frequency. However, the considered model allows to avoid the non-linear mixing, since the light pulses are emitted directly into the reverse cavity mode, from where they are detected straight away.

To summarize, the presence of the optical ring cavity in the considered configuration is certainly beneficial. While an adiabatic switch-on of the confining lattice potential is essentially important in the initial phase in the case without the cavity, the system with the cavity does not require any specific method for the lattice to be turned on, i.e., both adiabatic and non-adiabatic ways are acceptable. The ring cavity induces a positive feedback on the atomic motion by efficiently restoring the whole atomic population in the first Brillouin zone within a few Bloch periods and preventing the atomic momentum drifts. Due to the cavity-induced feedback the atomic Bloch oscillations become synchronized through the mode-locking mechanism enforcing adiabaticity and remain stable even in the presence of adverse effects considered in Chapter 5. Besides, the periodic bursts of light in the reverse cavity mode provide reliable signatures of the Bloch oscillations without perturbing their periodicity, which may serve as an improvement of current systems that aim to measure gravity with high precision through Bloch oscillations of ultracold atoms.

Moreover, the regime where the radiation field evolves with time can be considered as collective since the revealed dynamics strongly depends on the total number of atoms N present in the system, but the synchronization due to the mode-locking is still the key mechanism. However, it should be noted that if the number of atoms contained in the system is increased by a fairly large amount in the presence of the cavity, the system exhibits a dynamics different from the one described in this chapter. If the coupling parameter NU_0/κ happens to be exceedingly large, resulting in a much stronger backscattering of the pump light into the probe mode, the collective CARL effect interferes the regular Bloch oscillations dynamics and may even become dominant. The next chapter shows that such phenomenon has a negative impact on the system's evolution and the non-destructive monitoring of the atomic motion is no longer reliable since the Bloch oscillations are distorted. Nevertheless, if the parameters are selected correctly, the two dynamics collaborate in order to establish the regime of persistent for infinite times Bloch oscillations.

Chapter 4

Transition to synchronized regime of Bloch oscillations

The effect of collective atomic recoil lasing (CARL) plays a significant role in the studied model. Therefore, this whole chapter is dedicated to the detailed description of the CARL operating principles and emphasizes its most crucial characteristic features as well as considering a possible competition between the CARL dynamics and the Bloch oscillations in the given configuration. Originally proposed as a new source of tunable coherent light [70, 91, 92], the CARL mechanism is a hybrid between a free electron laser (FEL) [93, 94] and a traditional laser with physical properties common to both. The CARL effect arises in an optical ring cavity filled with cold atoms interacting with an intense far off-resonant pump laser and a counter-propagating probe field with respect to the pump. The effect manifests itself as a collective phenomenon accompanied by atomic bunching and exponential enhancement of the emitted radiation. What CARL system has in common with an original laser is the active medium with no population inversion, which is characterized by internal degrees of freedom that are responsible for the amplification process. As in the FEL, instead, the light enhancement is the result of cooperative scattering from the density grating structure generated within the active medium, and it comes at the expense of the momentum partially transformed into the radiation similarly to the case of individual electrons in the FEL. The classical FEL-CARL model is revised in Sec.4.1, followed by the quantum description of the CARL dynamical evolution within the framework of the semiclassical approximation as an extension

to the ultracold atoms regime [95–98] revealed in Sec.4.2. The work presented in Sec.4.3 is based on the paper [M. Samoylova et al., Laser Phys. Lett. **11**, 126005 (2014)], where the regimes in which either CARL or Bloch oscillations dynamics dominate over one another are investigated as well as the intermediate case. It turns out that, even though the CARL effect may strongly modify the Bloch oscillation frequency, the two dynamics may collaborate and synchronize giving rise to regular and stable Bloch oscillations.

4.1 Collective atomic recoil lasing (CARL)

While interacting with a coherent laser light, atoms may experience both scattering and dipole forces. The *scattering force* originates from absorption of a photon from the laser beam and its spontaneous emission in any direction. Since this force pushes an atom forward in the direction of the beam propagation, in the case of two counter-propagating laser beams the applied forces will tend to cancel each other in average, assuming that fluctuations in both absorption and spontaneous emission processes are disregarded. There is another type of force called *dipole force* that is schematically illustrated in Fig.4.1 at the example of a macroscopic particle approximated by a dielectric sphere deflecting the focused laser beam. As a result, the direction of the light momentum changes, which induces the reaction dipole force acting on the particle itself. If the particle is away from the beam focus, this force pulls the particle towards the region of high intensity, i.e. back to the focus. Macroscopically, the dipole force arises from the refraction of the incident light by the particle that is considered as a dispersive medium with the refractive index higher than the one of the surrounding area. However, from our microscopic point of view, the origin of the dipole force relies in the existence of a nonzero atomic polarizability.

During the CARL process a cold atomic cloud in a ring cavity interacts with a constant intense pump laser beam of frequency ω_p and Rabi frequency Ω_p and a weak probe field, fed by the back-scattered pump photons, of frequency ω_s and Rabi frequency $\Omega_s = |\Omega_s| \exp(i\phi)$ variable in time, where ϕ is the phase difference between the two light fields. If the pump detuning from the atomic resonance is much larger than the atomic natural linewidth ($\Delta \gg \Gamma$), the scattering force can be neglected and the dipole force is approximated by

$$F_{dip} \approx \frac{\hbar k}{2\Delta} \Omega_p |\Omega_s| \sin(2kx + (\omega_p - \omega_s)t + \phi). \quad (4.1)$$

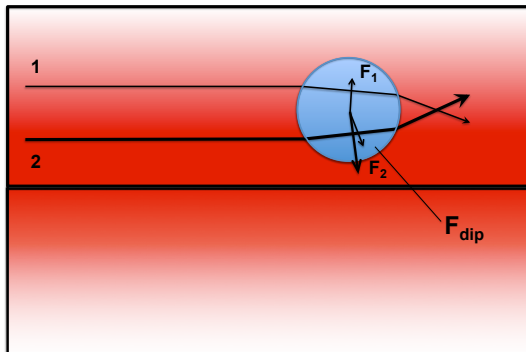


Figure 4.1: Schematic demonstration of the dipole force. The macroscopic particle off the beam focus is pulled back into it by the dipole force.

The phase $\theta_j = 2kx_j$ and momentum $p_j = mv_j$ are defined for each atom $j = 1, 2, \dots, N$ to derive the following atomic equations of motion:

$$\frac{d\theta_j}{dt} = \frac{2k}{m}p_j, \quad (4.2)$$

$$\frac{dp_j}{dt} = \frac{\hbar k}{2\Delta}\Omega_p|\Omega_s|\sin(\theta_j + \delta t + \phi), \quad (4.3)$$

where for simplicity the atoms driven by the laser pump are assumed to radiate at the same frequency ($\omega_p \approx \omega_s$), therefore, the corresponding wave numbers k_p and k_s of the pump and probe fields are nearly equal too, i.e., $k_p \approx k_s \equiv k$.

The third equation completing the classical CARL model is given by the complex scattered field written in the mean-field approximation under the assumption that the pump laser beam is very strong ($\Omega_p \gg \Omega_s$):

$$\frac{d\Omega_s}{dt} \approx -i\frac{\Omega_p}{2\Delta}\omega_{pl}^2 \langle e^{-i(\theta+\delta t)} \rangle - \kappa\Omega_s, \quad (4.4)$$

where $\omega_{pl} = \sqrt{e^2 n_e / \epsilon_0 m_e}$ is the plasma frequency (e is the electric charge, n_e is the plasma density, m_e is the electron mass, ϵ_0 is the permittivity of free space), $\delta = \omega_p - \omega_s$ is the pump-probe detuning and κ is the cavity damping. In this last equation the average is taken over all N atoms of the ensemble, so that

$$\langle e^{-i\theta} \rangle = \left| \frac{1}{N} \sum_{j=1}^N e^{-i\theta_j} \right| \equiv b, \quad (4.5)$$

where b is the coherence factor of emission called *bunching parameter*. At the beginning of the evolution the phases θ_j of the uniform atomic cloud are randomly distributed and initially there is no macroscopic field source, since $\sum_{j=1}^N \exp(-i\theta_j(0)) = 0$. However, when the atomic phases become correlated during the CARL dynamics, the bunching parameter approaches unity, so that the atomic cloud spontaneously creates a spatial structure and due to the exponential instability the macroscopic field is immensely enhanced upon the emission process.

Eqs.(4.2)-(4.4), representing the simplified *classical CARL model*, can be written in dimensionless units following the universal scaling used in the theory of FEL [93]. The new collective CARL parameter ρ is defined as

$$\rho = \frac{1}{2} \left(\frac{\Omega_p}{2\Delta} \right)^{2/3} \left(\frac{\omega}{4\omega_r} \right)^{2/3}, \quad (4.6)$$

where $\omega_r = \hbar k^2/2m$ is the single photon recoil frequency. Thus, the other parameters are redefined as follows: $\tau = 8\omega_r \rho t$ is the scaled time, the momentum variable is

$$\tilde{p}_j = \frac{p_j}{2\hbar k \rho} = \frac{k v_j}{4\omega_r \rho}, \quad (4.7)$$

the pump-probe detuning and the cavity decay width are $\tilde{\delta} = \delta/(8\omega_r \rho)$ and $\tilde{\kappa} = \kappa/(8\omega_r \rho)$, respectively, $C_1 = \Omega_p/(32\omega_r \Delta)$ and $C_2 = \Omega_s \omega^2/(16\omega_r \Delta)$ with $C_1 C_2 = \rho^3$. Eqs.(4.2)-(4.4) then take the following form:

$$\frac{d\theta_j}{d\tau} = \tilde{p}_j, \quad (4.8)$$

$$\frac{d\tilde{p}_j}{d\tau} = 2 \frac{C_1}{\rho^2} |\Omega_s| \sin(\theta_j + \tilde{\delta}\tau + \phi), \quad (4.9)$$

$$\frac{d\Omega_s}{d\tau} = -i \frac{C_2}{\rho} \langle e^{-i(\theta + \tilde{\delta}\tau)} \rangle - \tilde{\kappa} \Omega_s. \quad (4.10)$$

Finally, using the subsequent definitions

$$\frac{iC_1 \Omega_s}{\rho^2} \equiv A e^{-i\tilde{\delta}\tau}, \quad \frac{i\rho \Omega_s}{C_2} \equiv A e^{i\tilde{\delta}\tau} \quad (4.11)$$

in Eqs.(4.9) and (4.10), respectively, the coefficients can be eliminated:

$$\frac{d\theta_j}{d\tau} = \tilde{p}_j, \quad (4.12)$$

$$\frac{d\tilde{p}_j}{d\tau} = -(Ae^{i\theta_j} + A^*e^{-i\theta_j}), \quad (4.13)$$

$$\frac{dA}{d\tau} = \langle e^{-i\theta} \rangle + (i\tilde{\delta} - \tilde{\kappa})A. \quad (4.14)$$

This self-consistent set of equations describing the collective CARL effect classically is formally identical to the traditional FEL model with the only difference in the definitions of the variables, which clearly demonstrates that CARL and FEL share common physical features [70]. The CARL phenomenon is basically the atomic realization of FEL that works instead with relativistic electrons and intense magnetic field, while the analogy with the original laser is only qualitative.

The typical signature of the CARL phenomenon is the development of the exponential growth of both the probe field intensity $|A|^2$ and the atomic bunching b for sufficiently long interaction times ($\tau \gg 1$), and Eqs.(4.12)-(4.14) are able to predict it. To demonstrate this effect, the exact CARL equations are solved numerically, for example, with $N = 10^5$ atoms for the resonance case ($\tilde{\delta} = 0$) in the good-cavity limit ($\tilde{\kappa} \ll 1$), for which the maximum amplification is observed. As can be seen in Fig.4.2, the maximum probe field intensity is

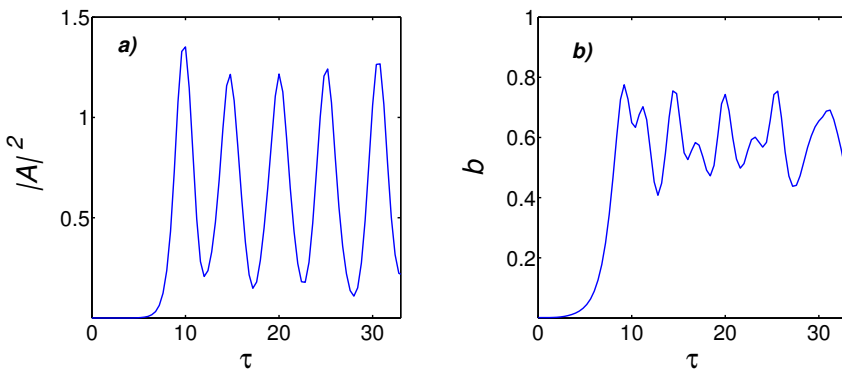


Figure 4.2: a) The intensity of the probe field $|A|^2$ and b) the atomic bunching parameter b as functions of scaled time τ as the result of the numerical simulation of Eqs.(4.12)-(4.14) with $N = 10^5$ atoms in the good-cavity limit $\tilde{\kappa} \ll 1$ on resonance $\tilde{\delta} = 0$.

1.4, while the maximum bunching reached is about 0.8, after which both the scattered field and the atomic bunching display undamped nonlinear oscillations revealing the unstable behavior.

The CARL mechanism can be described qualitatively as follows. The cold atomic cloud exposed to a strong pump laser serves as an active medium in an optical ring cavity that supports a counter-propagating probe field. Due to either the spontaneous light emission or the density fluctuations in the active medium which backscatters the pump photons, the probe field is initiated and interferes with the pump. The resulting field forms a periodic optical potential, so that the uniformly distributed atoms acquire a density modulation (see Fig.4.3). The back-scattered radiation amplifies the magnitude of the standing wave and generates more bunching, which in turn gives rise to the further stimulated backscattering etc. This collective feedback mechanism transforms the initially stable system of the atomic cloud driven by the strong pump beam in the presence of the ring cavity into the unstable one where the probe field intensity and the atomic bunching are characterized by the exponential growth.

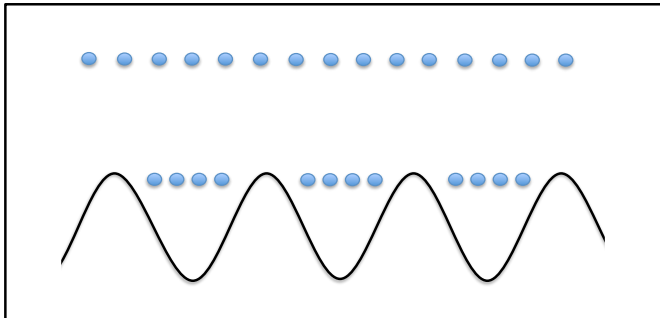


Figure 4.3: The effect of bunching: due to the superposition of the pump and probe fields the uniformly distributed atoms (above) experience the density grating (below).

The first attempts to experimentally observe the striking features of the CARL dynamics were realized with various hot atomic vapors [99–101]. In these experiments, the detected recoil induced probe gain turned out to have the CARL expected characteristics. The macroscopic polarization created by the incident pump laser in the active medium due to the internal structure of the atoms was considered as the source of the probe field. However, the coherent scattering from the induced polarization grating is not the only possible way for the probe gain to arise. Both the atomic bunching and the probe gain may have other sources not related to the atomic recoil [102]. For example, the gain observed in the reverse field can emerge spontaneously from fluctuations [92]. Moreover, these experiments do not take into consideration the probe feedback mechanism that is absolutely necessary to observe the CARL instabilities on the long time scale. Also, the long-term dynamics yields the inclusion of dissipation to the CARL equations due to the effect of atomic collisions [103–106].

As it was foreseen [107], a cold atomic cloud is a better environment for the CARL effect to emerge more clearly. To observe the CARL action, the used lasers are preferred to be detuned far from the atomic resonance, so that in this regime the atomic polarization grating effects are avoided. It is also desirable not to seed the probe to emphasize the role of the exponential gain responsible for the atomic self-bunching. Then, the observation of a probe beam is a distinct indication for the CARL effect.

The first nonambiguous experimental proof of the CARL phenomenon was realized in a system of non-interacting ^{85}Rb cold atoms [74, 108]. In this experiment, a unidirectionally pumped high-finesse optical ring cavity served as a dipole trap for the atomic cloud. Based on the experimental observations, it was deduced that the reverse field grew due to the recoil effect even with no seed probe field, which constituted the evidence for the atomic self-bunching. The backaction of the atomic motion on the light fields in such configuration can be observed directly as a frequency shift between the pump and reverse modes. In the experiment, this frequency shift was provided by a beat signal between the pump and probe beams, which was recorded using the light leaking out the cavity through one of its mirrors. Since all atoms interacted with the same pump laser, the net frequency shift could only arise if the atoms exhibited collective behavior. Moreover, the increasing in time detuning between the pump and probe led to a displacement of the standing wave and its acceleration by the atoms. The atoms in turn were dragged by the moving standing wave and thus experienced a constant accelerating light force coming from the light scattering process into the reverse mode accompanied by the photonic momentum transfer. These first reliable observations of the CARL feedback mechanism gave rise to

other experiments with CARL as the key effect, for example, [71, 72, 109–112], and further theoretical investigation of the phenomenon [113–120].

The CARL process also turns out to have a common root with superradiant Rayleigh scattering (SRyS), since they both share the same gain mechanism [121]. Several experiments have been dedicated to the observation of this close analogy [71, 110]. Generally, in SRyS experiments [122–125] a Bose-Einstein condensed atomic cloud of ellipsoidal shape is exposed to a short pump laser pulse moderately detuned from the atomic resonance. The atoms scatter the pump light into the long axis of the condensate, and simultaneously a matter wave grating is formed because of the photonic momentum transfer. While SRyS usually requires temperatures lower than $1 \mu\text{K}$ and can be hardly observed with thermal clouds [126] due to fast decoherence of the system, the CARL phenomenon is seen with several $100 \mu\text{K}$ atoms [74]. Despite different experimental circumstances and parameter regimes, both SRyS and CARL became accessible in a single experiment [71] by operating the ring cavity at either low or high finesse. This experiment also represented the first realization of a BEC in a macroscopic optical cavity. It was demonstrated that SRyS, as the low-finesse regime of CARL, is also possible at a high temperature, and the presence of a high-finesse ring cavity preserves the system's coherence against diffusion in the momentum space. The detailed analysis of the CARL behavior as a function of temperature from $1 \mu\text{K}$ to several tens of μK with $N = 10^6$ atoms reveals that the effect is not observable at $40 \mu\text{K}$, whereas CARL was realized with $N = 10^7$ atoms as hot as several $100 \mu\text{K}$ in the former experiments. With increasing temperature, the atomic momentum distribution becomes spread, which leads to a reduced effective atom number. Thus, the reason lies in the difference of the number of atoms N participating in the CARL dynamics. The fact that the CARL effect can be observed at temperatures far above $1 \mu\text{K}$ proves that the gain process linking SRyS and CARL is not based on the quantum state of the atoms, but on their cooperative behavior [127].

4.2 CARL-BEC model

In the case of an ultracold atomic cloud (BEC) with the temperature below the recoil limit $T_{rec} = \hbar^2 k^2 / 2mk_B$, where k_B is the Boltzmann constant, the atoms behave as quantum waves instead of classical particles. Thus, in this case the atomic motion in the CARL process can no longer be described by the classical equations and must be quantized. In the following description the semiclassical model is adopted, which treats the atoms as quantum particles, while the radiation field remains classical. With the newly defined atomic momentum variable

$$p_{\theta_j} = \frac{p_j}{2\hbar k} = \rho \tilde{p}_j \quad (4.15)$$

Eqs.(4.12)-(4.14) become:

$$\frac{d\theta_j}{d\tau} = \frac{p_{\theta_j}}{\rho}, \quad (4.16)$$

$$\frac{dp_{\theta_j}}{d\tau} = -\rho (Ae^{i\theta_j} + A^*e^{-i\theta_j}), \quad (4.17)$$

$$\frac{dA}{d\tau} = \frac{1}{N} \sum_{j=1}^N e^{-i\theta_j} + (i\tilde{\delta} - \tilde{\kappa})A. \quad (4.18)$$

Eqs.(4.16) and (4.17) can be easily derived from the Hamiltonian of the system

$$H = \sum_{j=1}^N \left[\frac{p_{\theta_j}^2}{2\rho} - i\rho (Ae^{i\theta_j} - A^*e^{-i\theta_j}) \right] = \sum_{j=1}^N H_j \quad (4.19)$$

using the canonical equations

$$\frac{d\theta_j}{d\tau} = \frac{\partial H}{\partial p_{\theta_j}}, \quad \frac{dp_{\theta_j}}{d\tau} = -\frac{\partial H}{\partial \theta_j}. \quad (4.20)$$

To be able to describe the quantum motion of the atoms, the atomic phase θ_j and momentum p_{θ_j} must be considered as quantum canonical operators with the commutation relation $[\theta_j, p_{\theta_j}] = i\delta_{jj}$. Note that the N atoms are independent in the periodic potential depending on the self-consistent probe field A that is assumed to be classical. Therefore, instead of solving N Heisenberg equations for the time-dependent functions $\theta_j(\tau)$ and $p_{\theta_j}(\tau)$, the Schrödinger equation for

the atomic wave function $\Psi(\theta, \tau)$, with the normalization condition

$$\int_0^{2\pi} |\Psi(\theta, \tau)|^2 = 1, \quad (4.21)$$

should be considered. Since $p_\theta \rightarrow -i\partial/\partial\theta$, the Schrödinger equation takes the following form:

$$i\frac{\partial\Psi(\theta, \tau)}{\partial\tau} = H_1\Psi(\theta, \tau) = -\frac{1}{2\rho}\frac{\partial^2\Psi}{\partial\theta^2} - i\rho(Ae^{i\theta_j} - A^*e^{-i\theta_j})\Psi, \quad (4.22)$$

where H_1 is the single-particle Hamiltonian. The equation equivalent to Eq.(4.14) for the radiation field A in the semiclassical model can be obtained replacing the sum over all atoms in the bunching parameter (4.5) by the ensemble average $\int |\Psi|^2 \exp(-i\theta)d\theta$, where $|\Psi|^2$ is interpreted as the probability density. In this way, Eq.(4.18) becomes:

$$\frac{dA}{d\tau} = \int_0^{2\pi} |\Psi(\theta, \tau)|^2 e^{-i\theta} d\theta + (i\tilde{\delta} - \tilde{\kappa})A. \quad (4.23)$$

Eqs.(4.22) and (4.23) represent the simplest *quantum model* describing semi-classically the behavior of an ultracold atomic cloud in the CARL dynamics.

Since the density of the atomic cloud is assumed to be uniform, the homogeneous atomic wave function Ψ with periodicity θ can be expanded into Fourier series according to

$$\Psi(\theta, \tau) = \frac{1}{\sqrt{2\pi}} \sum_{m=-\infty}^{+\infty} C_m(\tau) e^{im\theta}, \quad (4.24)$$

where $|C_m(\tau)|^2$ is the probability of finding the atoms in the momentum state m . While backscattering the photons from the pump beam into the reverse mode, the atoms change their momentum only by discrete steps of $2\hbar k$ and move to the adjacent momentum states. The potential $V(\theta) = -i\rho(A \exp(i\theta) - A^* \exp(-i\theta))$ is actually responsible for the transition from the m th momentum state to the state $m \pm 1$. In fact,

$$V(\theta)\Psi(\theta) = -i\rho \left(\frac{A}{\sqrt{2\pi}} \sum_m C_m e^{i(m+1)\theta} - \frac{A^*}{\sqrt{2\pi}} \sum_m C_m e^{i(m-1)\theta} \right) \quad (4.25)$$

or, equivalently, in the Dirac notation with $|\Psi\rangle = \sum_m C_m |m\rangle$

$$V(\theta)|\Psi(\theta)\rangle = -i\rho \left(A \sum_m C_m |m+1\rangle - A^* \sum_m C_m |m-1\rangle \right). \quad (4.26)$$

Since $\langle n|m\rangle = \delta_{nm}$, then $\langle n|V|\Psi\rangle = -i\rho(AC_{n-1} - A^*C_{n+1})$. Hence, substituting $|\Psi\rangle = \sum_m C_m|m\rangle$ into Eqs.(4.22) and (4.23) and projecting to the state $|n\rangle$, the equations take the following form:

$$\frac{dC_n}{d\tau} = -i\frac{n^2}{2\rho}C_n + \rho(A^*C_{n+1} - AC_{n-1}), \quad (4.27)$$

$$\frac{dA}{d\tau} = \sum_{n=-\infty}^{+\infty} C_{n-1}^*C_n + (i\tilde{\delta} - \tilde{\kappa})A, \quad (4.28)$$

and it is seen that the effect of bunching occurs when the neighboring momentum states overlap since the bunching parameter becomes defined as

$$\begin{aligned} b &= \int_0^{2\pi} |\Psi|^2 e^{-i\theta} d\theta = \sum_{m,n} C_m^* C_n \int_0^{2\pi} e^{-i(n-m-1)\theta} d\theta = \\ &= \sum_{m,n} C_m^* C_n \delta_{n,m+1} = \sum_n C_{n-1}^* C_n. \end{aligned} \quad (4.29)$$

The obtained Eqs.(4.27) and (4.28) is a generalization of the CARL-BEC model [75,76] for the case of infinite momentum states. One can easily employ this set of equations to derive Eqs.(2.7) and (2.8) describing the studied model, which first make an appearance in Chapter 2.

4.3 CARL dynamics vs Bloch oscillations

In this section, the CARL dynamics of an ultracold atomic cloud is analyzed in close relation to the examined model described in Chapter 2. The atoms of the condensate placed in a unidirectionally laser-pumped ring cavity in the presence of an externally imposed one-dimensional optical lattice aligned along the cavity axis are additionally exposed to a constant force accelerating the atoms along the same axis. In this particular work, the system is subject to the gravitational force (see Fig.2.1), although the model presented originally in [65] is effective for any constant external force. While gravity incites the atoms to undergo Bloch oscillations in the imposed lattice, the CARL mechanism coherently scatters the pump light into the reverse mode in a self-amplified way accompanied by an atomic redistribution in a self-determined optical lattice that competes with the external one. In the following, the interplay between the CARL dynamics and the Bloch oscillations is illustrated by numerical simulations, and the way the CARL mechanism may operate to stabilize and monitor the Bloch oscillations of the ultracold atoms is discussed.

Using the generalized BEC-CARL model presented in the previous section, one can derive Eqs.(2.7) and (2.8) describing the system under investigation. Under the assumptions that the cavity decay is much faster than the Bloch or CARL dynamics, so that $\kappa\tilde{\alpha} \gg d\tilde{\alpha}/dt$, and the detuning is small on the scale of the cavity linewidth, i.e., $\delta \ll \kappa$, the cavity can be adiabatically eliminated. This results in the light field being slaved to the collective atomic motion, and the equations of motion in this regime take the following form:

$$\frac{dC_n}{dt} = -4i\omega_r(n + \nu_b t)^2 C_n + U_0 (\tilde{\alpha}^* C_{n+1} - \tilde{\alpha} C_{n-1}), \quad (4.30)$$

$$\tilde{\alpha} \approx \alpha_0 + \frac{NU_0}{\kappa} \sum_n C_{n-1}^* C_n. \quad (4.31)$$

Indeed, the last term in Eq.(4.31) represents the backaction of the atoms onto the cavity field, which defines the dynamics of the light in the reverse mode. The type of dynamics described by Eq.(4.30) and (4.31) depends critically on the cooperative coupling NU_0/κ of the atoms to the cavity fields, which can be controlled via the number of atoms N .

For $NU_0/\kappa \ll \alpha_0$, the cooperative coupling is very weak, so that the atomic backaction onto the cavity fields may be disregarded. The cavity field decouples from the atoms and quickly evolves into a steady state given by $\tilde{\alpha} = \alpha_0$. In this case, the usual Bloch oscillations picture in which the motion of the atoms

is governed by Eq.(4.30) can be recovered. For larger cooperative coupling, the ring cavity comes into play. Now, the matter wave may not only scatters light between the optical lattice beams, but it also cooperatively scatters photons from the pumped cavity mode into the reverse one, which exerts influence on the atomic dynamics. If $NU_0/\kappa \gg \alpha_0$, the CARL mechanism dominates over the Bloch oscillations dynamics. In this regime, the mechanism responsible for transferring momentum to the atoms is no longer scanning through the resonance like in the ARP method [79], but the backscattering of the pump light by the self-generated atomic density grating [91]. As a consequence, the population transfer between adjacent momentum states does not occur at the regular Bloch periods, but may vary in time. Only for moderate cooperative coupling ($NU_0/\kappa \approx \alpha_0$), a parameter range where both the CARL and Bloch dynamics cooperate to set up a synchronized regime with regular and stable Bloch oscillations is found. However, at some point, when the backscattering of the pump light into the probe mode becomes stronger, the depth of the potential formed in the cavity by interference of the pump and the counterpropagating probe light may exceed the depth of the optical lattice generated by the external beams. In this case, the CARL mechanism takes over and imposes its dynamics on the atoms [62, 71, 91], dominating the Bloch oscillations.

Figs.4.4-4.6 illustrate the intricate dynamics in the regimes dominated by either the Bloch oscillations or by the CARL dynamics, as well as an intermediate regime where both dynamics compete. Again, an ultracold cloud of ^{87}Rb atoms is chosen as an example to perform the numerical simulations. The atoms interact with the light fields via their D2-line at $\lambda_0 = 780$ nm, for which the recoil frequency is $\omega_r = (2\pi) 3.75$ kHz and the Bloch oscillation frequency is $\nu_b = 0.035\omega_r$ in the case when the accelerating force is given by gravity. The other parameters are also assumed to be the same as in Chapter 3: the cavity decay width $\kappa = 160\omega_r$, the pump-probe detuning $\delta = 0$, the atom-mediated coupling strength between the pump and probe fields $U_0 = 0.04\omega_r$, and the external optical potential depth $W_0 = 3.2\omega_r$, which corresponds to $|\alpha_0|^2 = 400$ photons in the pump laser beam. The control over the collective coupling is done by varying the atom number between $N = 4 \cdot 10^4$ and $12 \cdot 10^4$. These parameters are perfectly realizable in state-of-the-art experiments. Besides, the constant radiation pressure force that may be exerted on the atoms the by the pump is assumed to be negligible and has no impact on the considered dynamics, if the pump laser is detuned far from the atomic resonance ($\Delta \geq 1.5 \cdot 10^7 \omega_r$). However, if it is not the case and the pump laser is tuned close to the atomic resonance, the Bloch oscillation frequency may be altered, as it will be seen in the next chapter.

Fig.4.4 represents the regime dominated by the Bloch oscillations dynamics. Fig.4.4(a) shows a typical evolution of the momentum state populations $|C_n|^2$ as a function of scaled time $\nu_b t$ for the case of pure Bloch oscillations. The population of each momentum state is put in evidence by a different color in order to facilitate their visual distinction during the temporal evolution. As can be seen, all atoms initially prepared in a single momentum state participate in the dynamics. This is explained by the fact that throughout the evolution the momentum transfer between adjacent momentum states remains fully efficient. As a consequence, the Bloch oscillations persist for long times, as seen in Fig.4.4(b) showing the evolution of the average atomic momentum in the laboratory frame, $\langle p \rangle_{\text{lab}} = \langle p \rangle + \nu_b t$ with $\langle p \rangle = \sum_n n |C_n|^2$. After a transient of approximately three Bloch oscillations, the population is efficiently restored into the first Bloch band and the feedback provided by the cavity field onto the atomic motion tends to assist the adiabatic rapid passages between momentum states helping to complete the momentum transfer each Bloch period τ_b .

Moreover, the atomic Bloch oscillations dynamics is accompanied by the radiation field reaching, after a transient, a stationary regime characterized by periodic bursts of light emitted into the probe mode α at each oscillation. The evolution of the intracavity photon number $|\alpha|^2$ in the probe mode is demonstrated in Fig.4.4(c). The average photon number $|\alpha|^2 \simeq 20$ corresponds, for the chosen value of κ , to a photon flux of $\sim 18400 \text{ s}^{-1}$ outside the cavity behind the output coupler, i.e., ~ 140 photons/Bloch oscillation. Hence, the light bursts appear to be perfectly detectable via a photon counter and provide a reliable and stable monitor of the atomic motion.

In the intermediate regime, when both dynamics are present, only a fraction of the atoms perform the Bloch oscillations, whereas the remaining atoms fail to synchronize. This case is illustrated in Fig.4.5(a). The competition between the CARL dynamics and the Bloch oscillations leads to irregular oscillation frequencies, and the dispersion of the atoms over different momentum states induces average atomic momentum drifts (see Fig.4.5(b)). Moreover, the bursts of light in the radiation field shown in Fig.4.5(c) are no longer periodic and cannot be used as a reliable signature of the atomic dynamics.

In contrast to the previous cases, in the regime dominated by the CARL dynamics, the atoms quickly jump from one momentum state to the next one in a superradiant fashion. This can be seen in Fig.4.6(a). The backscattering of the pump light and the amplification of the coherent wave in the probe mode of the ring cavity is accompanied by a rapidly increasing drift of the average atomic momentum (see Fig.4.6(b)). At longer times the increase slows down because the Doppler shift associated with the atomic motion drives the scattered light

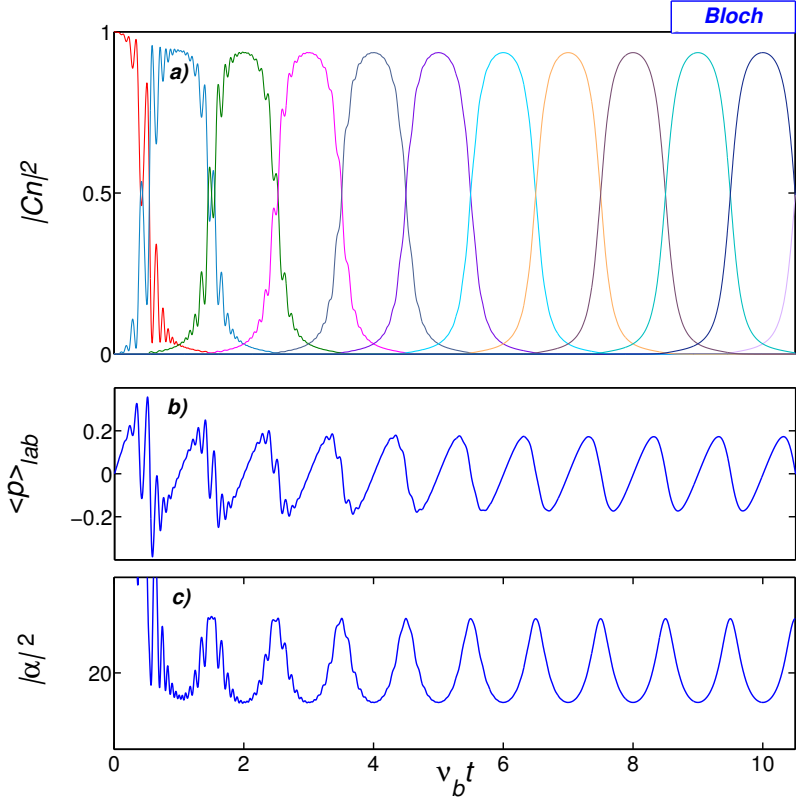


Figure 4.4: Time evolution of (a) the populations $|C_n|^2$ of the momentum states, (b) the average atomic momentum $\langle p \rangle_{lab}$ in the laboratory frame with $N = 4 \cdot 10^4$ atoms, and (c) the average number of photons $|\alpha|^2$ in the probe field in the regime dominated by Bloch dynamics. The parameters used to perform the simulations are: $\alpha_0 = 20$, $\nu_b = 0.035\omega_r$, $\kappa = 160\omega_r$, $\delta = 0$ and $U_0 = 0.04\omega_r$.

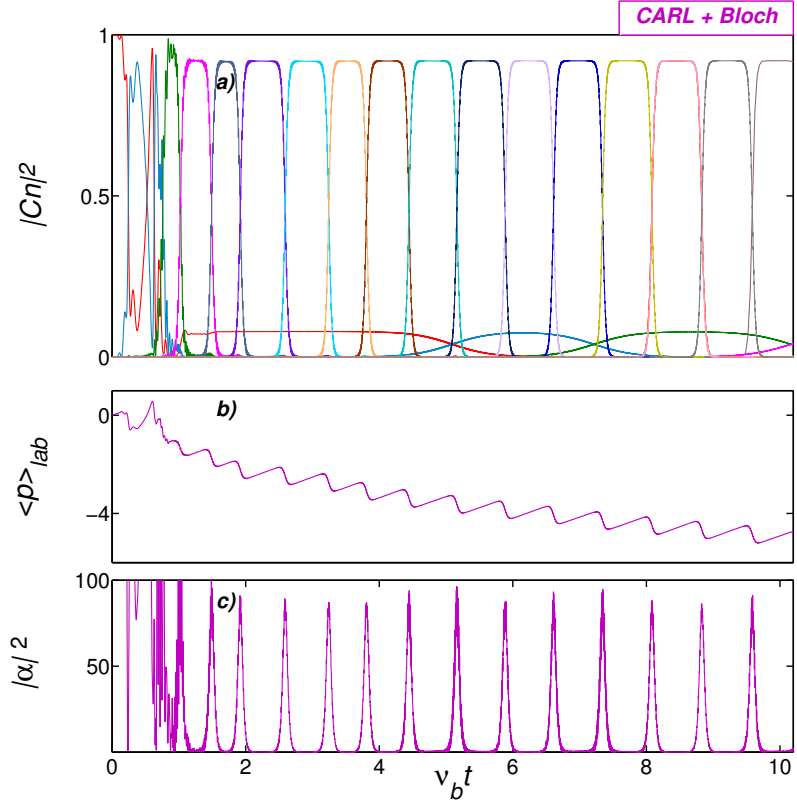


Figure 4.5: Dynamics of (a) the momentum states populations, (b) the average atomic momentum in the laboratory frame, and (c) the average photon number as functions of normalized time $\nu_b t$ in the regime where CARL and Bloch dynamics compete. The number of atoms used is $N = 8 \cdot 10^4$, the other parameters are the same as in Fig.4.4.

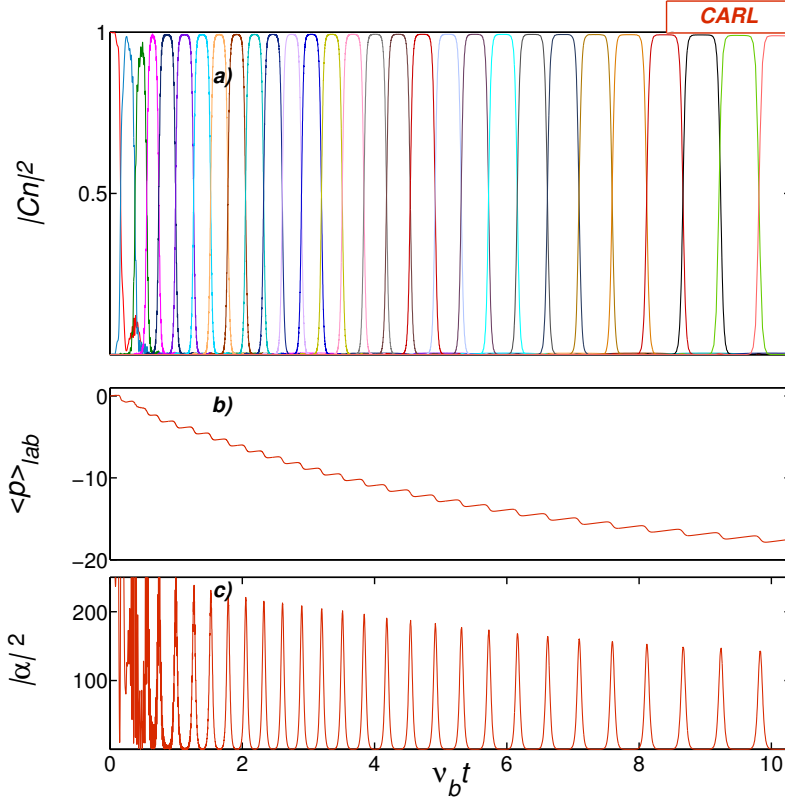


Figure 4.6: Evolution of (a) the momentum states populations $|C_n|^2$, (b) the average atomic momentum $\langle p \rangle_{lab}$ in the laboratory frame, and (c) the average number of photons $|\alpha|^2$ in the radiation field in the regime dominated by CARL dynamics. $N = 12 \cdot 10^4$ atoms, the rest of the parameters are the same as in Fig.4.4.

out of the cavity resonance, and as a result the CARL force decreases. In this regime, the radiation field experiences multiple light bursts per Bloch oscillation period (see Fig.4.6(c)) and, consequently, its dynamics cannot be considered as a reliable monitor of the atomic motion.

The transition between the discussed regimes is illustrated in Fig.4.7 that shows the time evolution of the phase ϕ of the probe field α in the regime of pure Bloch oscillations (blue), as well as in the intermediate case (purple) and the regime dominated by CARL (red). Being absolutely unstable in the case of the CARL dynamics, the phase fluctuations gradually decrease in the intermediate regime, when the Bloch dynamics becomes stronger. And they totally disappear when the Bloch oscillations dominate. Then the feedback provided by the cavity stabilizes the Bloch oscillations, and after some transient rapid oscillations, the phase remains locked to $\pi/2$ with only slight perturbations at each Bloch oscillation.

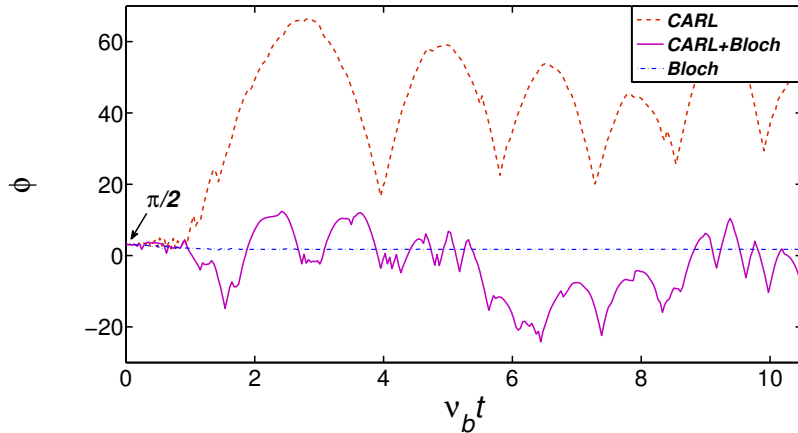


Figure 4.7: Phase ϕ of the probe field α in the CARL regime with $N = 12 \cdot 10^4$ atoms (red), the intermediate regime with $N = 8 \cdot 10^4$ (purple), and the regime of pure Bloch oscillations with $N = 4 \cdot 10^4$ (blue) as a function of scaled time $\nu_b t$. The remaining parameters are the same as in Fig.4.4.

It is possible to conclude that the feedback mechanism of the atomic motion onto the amplitude and phase of the counterpropagating light field, provided by the atom-field coupling in the unidirectionally pumped optical ring cavity, can be turned into an advantage. Whether the CARL and the Bloch oscillations dynamics perturb each other or cooperate, depends on the collective atom-field coupling strength. A certain range of parameters for which both dynamics set up a synchronized regime is found. Indeed, for moderate collective coupling the CARL feedback mechanism is suitable to get stabilized Bloch oscillations and monitor non-destructively the dynamics of the ultracold atoms in the optical lattice over long times.

Chapter 5

Robustness of Bloch oscillations of a BEC in a ring cavity

In this chapter some specific properties of the investigated system, which may occur under real experimental circumstances, are specified. Sec.5.1, for example, demonstrates the importance of taking into account the radiation pressure force in the considered unidirectionally pumped ring cavity setup and confirms that the selected parameters are suitable to disregard the effect. The same set of parameters is used to analyze the following features of the system, assuming the impact of the radiation pressure force on the studied dynamics is negligibly small. In Sec.5.2 and Sec.5.3 adverse effects such as dephasing mechanism due to amplitude or phase fluctuations and accidental excitation of higher Bloch bands are discussed, respectively. The mode-locking of the Bloch oscillations generated by the cavity is accompanied by not only a significantly suppressed interband tunneling, but also by a depopulation of the excited bands. Finally, Sec.5.4 accounts for the atom-atom interactions, as they lead to a strong collisional dephasing of the Bloch oscillations and rapid broadening of the average momentum of the atomic system. However, even in the case of an interacting BEC, the cavity has a control over the interaction induced dephasing and guarantees a large number of regular and stable Bloch oscillations.

5.1 Radiation pressure force effect

This section is devoted to a detailed analysis of the effect that the radiation pressure force (RPF) has on the considered system. While transferring the energy absorbed from the incoming pump laser beam into the form of scattered light, the atoms of the condensate experience the RPF exerted by the pump light. Generally, if the pump laser is tuned far from the atomic resonance ($\Omega_p \ll \Delta$) which in turn is much larger than the natural atomic linewidth ($\Delta \gg \Gamma$), the RPF is negligibly small to be taken into consideration. However, as it will be seen below, the RPF may significantly affect the examined dynamics.

5.1.1 Analytical description of the effect

In the presence of the radiation pressure force defined under the assumption $\Delta \gg \Gamma$ as

$$F_{RP}(t) = -\frac{\hbar k \Gamma}{4\Delta^2} (\Omega_p^2 - \Omega_1^2 |\alpha(t)|^2) \quad (5.1)$$

and imposing the potential $F_{RP}(t)x$, the initial equations of motion for the atomic wave function ψ and the probe mode α gain the following form :

$$i\hbar \frac{\partial \psi}{\partial t} = -\frac{\hbar^2}{2m} \frac{\partial^2 \psi}{\partial x^2} - i\hbar U_0 (\alpha e^{2ikx} - \alpha^* e^{-2ikx}) \psi \quad (5.2)$$

$$- mgx\psi - F_{RP}(t)x\psi + \hbar \frac{W_0}{2} \sin(2kx)\psi,$$

$$\frac{d\alpha}{dt} = NU_0 \int |\psi|^2 e^{-2ikx} d(2kx) + (i\delta - \kappa)\alpha. \quad (5.3)$$

Here $\Gamma = 1600\omega_r$ is the single-atom spontaneous decay rate, $\Omega_1 = 54\omega_r$ is the atom-field coupling strength, $\Omega_p = 6240\omega_r$ is the Rabi frequency of the incident pump light of intensity $I_p = 50\text{mW/cm}^2$, and its detuning from the atomic resonance is defined as $\Delta = \Omega_1\Omega_p/4U_0$. Thereafter the procedure describing the derivation of the studied model is repeated, see Chapter 2, with only one difference: the RPF is now taken into account.

After moving into the accelerated frame of reference for the sake of convenience, the atomic wave function is modified according to

$$\psi = \tilde{\psi} \exp\left(\frac{imgxt}{\hbar} + \frac{i}{\hbar}x \int_0^t F_{RP}(t')dt'\right). \quad (5.4)$$

Note that due to the scattered field instability the RPF is no longer a constant but a function of time, therefore, it appears as a time integral in the moving reference frame. Thus, Eqs.(5.2) and (5.3) result in the following set of equations:

$$\begin{aligned} \frac{\partial \tilde{\psi}}{\partial t} &= \frac{i\hbar}{2m} \left[\frac{\partial}{\partial x} + \frac{imgt}{\hbar} + \frac{i}{\hbar} \int_0^t F_{RPF}(t') dt' \right]^2 \tilde{\psi} \\ &- U_0 (\tilde{\alpha} e^{2ikx} - \tilde{\alpha}^* e^{-2ikx}) \psi, \end{aligned} \quad (5.5)$$

$$\frac{d\tilde{\alpha}}{dt} = NU_0 \int |\tilde{\psi}|^2 e^{-2ikx} d(2kx) + (i\delta - \kappa)(\tilde{\alpha} - \alpha_0), \quad (5.6)$$

where $\alpha = \tilde{\alpha} - \alpha_0$ with $\alpha_0 = W_0/4U_0$. Then the atomic wave function $\tilde{\psi}$ is expanded into plane waves

$$\tilde{\psi} = \frac{1}{\sqrt{2\pi}} \sum_n C_n(t) e^{2inkx} \quad (5.7)$$

with $|C_n|^2$ being the probability of finding the atoms in the n th momentum state, and the definitions of the single-photon recoil frequency $\omega_r = \hbar k^2/2m$ and the Bloch oscillation frequency $\nu_b = mg/2\hbar k$ are used. Eqs.(5.5) and (5.6) then result in

$$\frac{\partial C_n}{\partial t} = -4i\omega_r \left[n + \nu_b t - \frac{\Gamma}{8\Delta^2} \left(\Omega_p^2 t - \Omega_1^2 \int_0^t |\alpha(t')|^2 dt' \right) \right]^2 C_n \quad (5.8)$$

$$\begin{aligned} &+ U_0 (\tilde{\alpha}^* C_{n+1} - \tilde{\alpha} C_{n-1}), \\ \frac{d\tilde{\alpha}}{dt} &= U_0 N \sum_n C_{n-1}^* C_n + (i\delta - \kappa)(\tilde{\alpha} - \alpha_0). \end{aligned} \quad (5.9)$$

In comparison to the prior system where the RPF action is disregarded, in this case an additional term appears in Eq.(5.8). This term corresponds to the RPF occurring in the description and it certainly affects the Bloch oscillation frequency. As a result, the expression for the average atomic momentum in the laboratory frame is also modified according to

$$\langle p \rangle_{lab} = \langle p \rangle + mgt - \frac{2\hbar k \Gamma}{8\Delta^2} \left(\Omega_p^2 t - \Omega_1^2 \int_0^t |\alpha(t')|^2 dt' \right), \quad (5.10)$$

or equivalently, in terms of $2\hbar k$ units:

$$\langle p \rangle_{lab} = \sum_n n |C_n|^2 + \nu_b t - \frac{\Gamma}{8\Delta^2} \left(\Omega_p^2 t - \Omega_1^2 \int_0^t |\alpha(t')|^2 dt' \right). \quad (5.11)$$

5.1.2 The impact of the radiation pressure force

Indeed, the RPF may have a great impact on the dynamics of the system. This assertion can be demonstrated, for example, taking the parameters used in the previous chapters, where the RPF is neglected. In particular, the average atomic momentum given in both accelerated and laboratory frames in the presence of the optical ring cavity is considered for the following set of parameters: $\nu_b = 0.035\omega_r$, $\kappa = 160\omega_r$, $\delta = 0$, $N = 2 \cdot 10^4$, $U_0 = 0.04\omega_r$ and $\alpha_0 = 20$. For these parameters, the RPF constant term $\Gamma\Omega_p^2/8\Delta^2 = 0.05\nu_b$ induces the greatest modification of 5% of the Bloch oscillation frequency, which is quite large to be neglected.

Fig.5.1 shows the negative impact of such Bloch frequency variation on the evolution of the system. For the case when the lattice potential is turned on abruptly (Fig.5.1(a)), instead of the expected regular oscillations with the Bloch frequency ν_b in the laboratory frame without the RPF (solid black curve), the system dynamics in the presence of the RPF (dashed red curve) display an average atomic momentum modification caused by the frequency alteration. This effect remains even if an adiabatic switch-on of the optical lattice is performed, see Fig.5.1(b).

In addition to this observation, the evolution of the average atomic momentum $\langle p \rangle$ represented in the moving reference frame reveals a slight change in the slope of the corresponding dynamics for both adiabatic (Fig.5.1(c)) and non-adiabatic (Fig.5.1(d)) switch-on of the optical lattice when the RPF is applied. The momentum transfer between adjacent momentum states is, however, still complete and the ARP conditions are not violated. These may be seen, for example, in Fig.(5.2), where the case of an adiabatic switch-on of the lattice is selected for investigation and the time evolution of each momentum state population $|C_n|^2$ in the presence of the RPF is given by a different color. Fig.(5.2) makes it evident that at each Bloch oscillation cycle all atoms are successfully transferred to the next nearest momentum state. Thus, the RPF effect that seriously affects the system for the chosen set of parameters is accompanied only by the frequency modification, while the momentum transfer remains effective.

Another way to show the importance of including the RPF into the investigated setting is to look at the dynamics of the average number of photons $|\alpha|^2$ and phase ϕ of the cavity mode α . Such dynamics is given in Fig.5.3 for an adiabatic switch-on of the lattice potential. Without the RPF (solid blue curve), a single prominent burst of light in the probe field is expected for each Bloch oscillation period. However, when the RPF is taken into account (dashed red curve), an increasing in time shift is observed in both the photon number

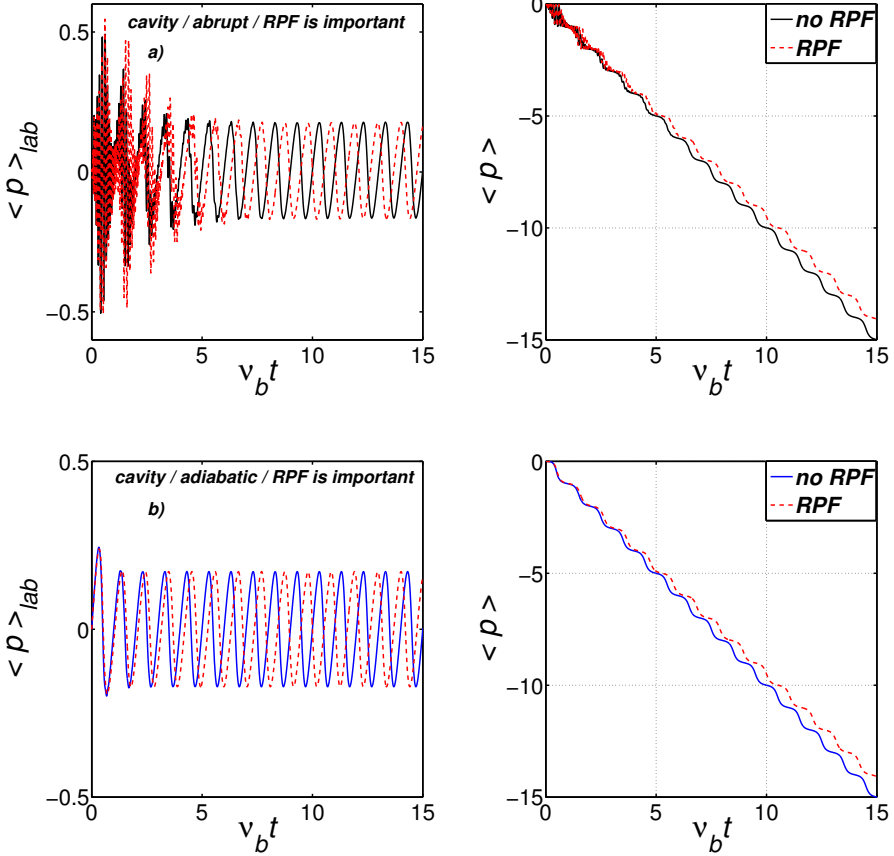


Figure 5.1: Time evolution of the average atomic momentum in the laboratory (left) and accelerated (right) frames in the presence of the cavity for the cases of abrupt and adiabatic switch-on of the optical lattice when the RPF is essentially important. The following parameters are used: $\nu_b = 0.035\omega_r$, $\kappa = 160\omega_r$, $\delta = 0$, $\Gamma = 1600\omega_r$, $\Omega_1 = 54\omega_r$, $\Omega_p = 6240\omega_r$, $N = 2 \cdot 10^4$, $U_0 = 0.04\omega_r$ and $\alpha_0 = 20$ for an abrupt switch-on of the lattice and $\alpha_0(1 - \exp(-\gamma t))$ with $\gamma = 0.1\omega_r$ for an adiabatic switch-on.

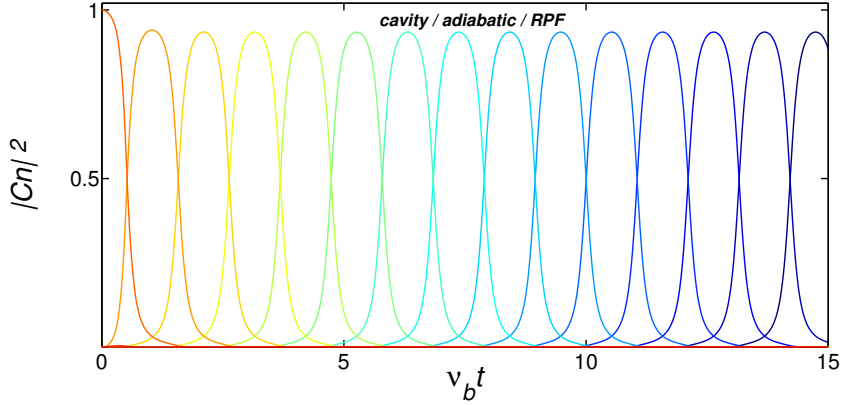


Figure 5.2: Population $|C_n|^2$ of each momentum state given by a different color as a function of $\nu_b t$ in the presence of the cavity and adiabatic switch-on of the lattice potential in the case when the RPF needs to be taken into account. The same parameters as in Fig.5.1 are used.

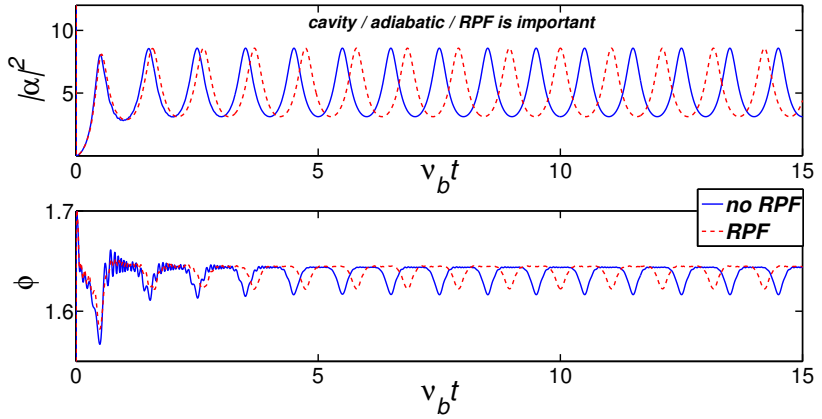


Figure 5.3: Average number of photons $|\alpha|^2$ in the radiation field and phase ϕ of the cavity mode α as functions of scaled time $\nu_b t$ for an adiabatic switch-on of the lattice potential in the presence of the cavity for the cases when the RPF is neglected (blue) and included (red). The same parameters as in Fig.5.1 are used.

and phase dynamics as a result of the Bloch oscillation frequency modification imposed by the RPF. Since, for this choice of parameters, the bursts of light in the radiation field have a periodicity different from the Bloch period, such dynamics cannot be used as a reliable monitor of the atomic motion, and the potential non-destructive measurement of the Bloch oscillation frequency fails.

The control over the RPF is a rather difficult task, so the better way to deal with its negative impact is to make it very small. In order to neglect the RPF effect, the additionally gained term due to the RPF in Eq.(5.8) must be very small compared to the actual Bloch oscillation frequency ν_b , which requires at least $\Delta \geq 1.5 \cdot 10^7 \omega_r$ or $\Delta \geq 35\text{GHz}$. Also, the RPF effect is insignificant when Ω_p is small, i.e. the incident pump laser beam is rather weak. These conditions can be reached by varying, for instance, the pump-probe coupling strength U_0 , photon number $|\alpha_0|^2$ and the number of atoms N , while keeping the rest of the parameters unchanged.

The numerical simulations based on Eqs.(5.8) and (5.9) in the presence of the RPF with the parameters $N = 2 \times 10^6$, $U_0 = 0.004\omega_r$ and $\alpha_0 = 200$ reveal that the selected set of parameters is perfect to get rid of the negative impact of the RPF on the studied system. Such parameters allow to diminish the Bloch oscillation frequency modification to the corresponding value of $5 \times 10^{-4}\nu_b$. As shown in Fig.5.4, both sudden (Fig.5.4(a)) and adiabatic (Fig.5.4(b)) risings of the optical lattice, in configuration with the cavity, demonstrate a large agreement in the average atomic momentum dynamics in the cases with and without the RPF. The only difference observed between the two cases is the transient during the first few Bloch oscillation caused by the non-adiabatic switch-on of the lattice, after which the dynamics stabilizes anyway.

The time evolution of the average number of photons $|\alpha|^2$ in the probe field (see Fig.5.4(c)) also proves, as expected, that the effect of the RPF is negligible for the chosen parameters. In comparison to the previous case when it is essential and important to take into account the RPF, in this case the time-dependent shift is not observed, since the RPF remains insignificantly small, and the light bursts have the correct periodicity again. Moreover, the amount of photons in the radiation field at each Bloch oscillation is perfectly detectable. Thus, this dynamics is reliable and suitable to continuously track the atomic motion.

The impact of the RPF on the considered system can be alternatively decreased to the value of $5 \times 10^{-4}\nu_b$ by keeping the parameters $U_0 = 0.004\omega_r$ and $\alpha_0 = 200$ the same, while reducing the cavity decay width to $\kappa = 16\omega_r$, which in turn allows one to have a smaller amount of atoms, e.g., $N = 2 \times 10^5$. A larger cavity finesse F is required to realize the selected value of κ , since the finesse of the cavity is inversely proportional to the cavity decay width. The

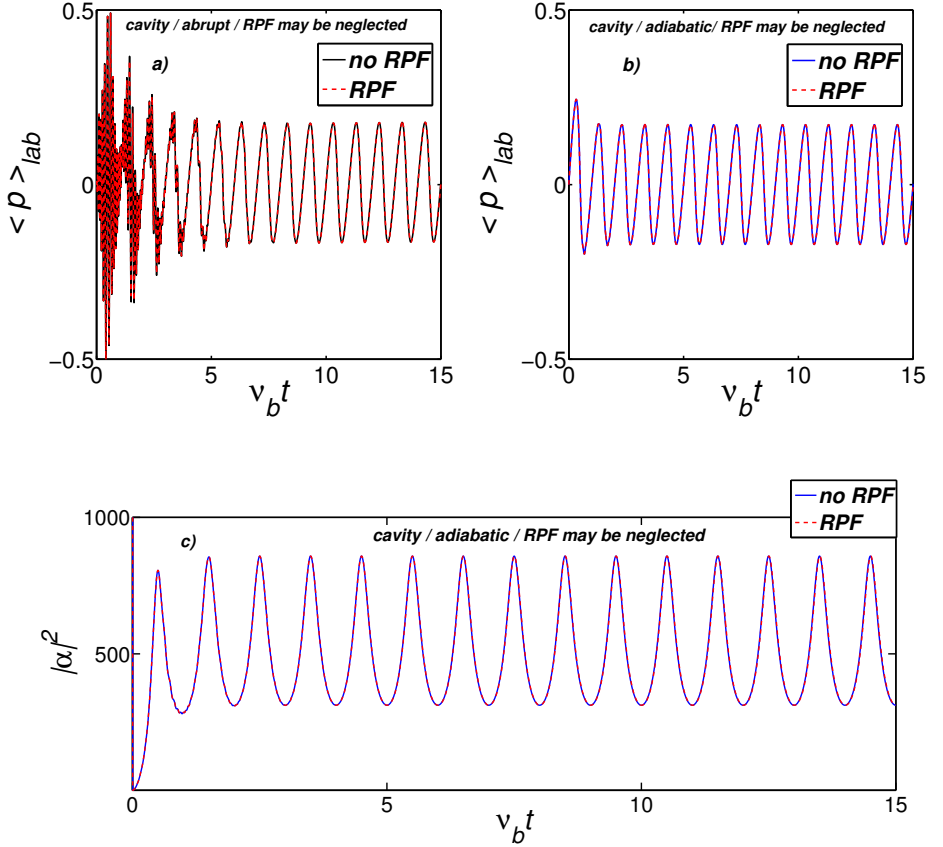


Figure 5.4: Average atomic momentum in the laboratory frame with the cavity as a function of normalized time for a) abrupt and b) adiabatic switch-on of the lattice potential when the RPF is taken into account (dashed curves) and is disregarded (solid curves). c) Time evolution of the average number of photons in the probe field with and without the RPF effect for the case when the lattice is turned on adiabatically. The used parameters are: $\nu_b = 0.035\omega_r$, $\kappa = 160\omega_r$, $\delta = 0$, $\Gamma = 1600\omega_r$, $\Omega_1 = 54\omega_r$, $\Omega_p = 6240\omega_r$, $N = 2 \cdot 10^6$, $U_0 = 0.004\omega_r$ and $\alpha_0 = 200$.

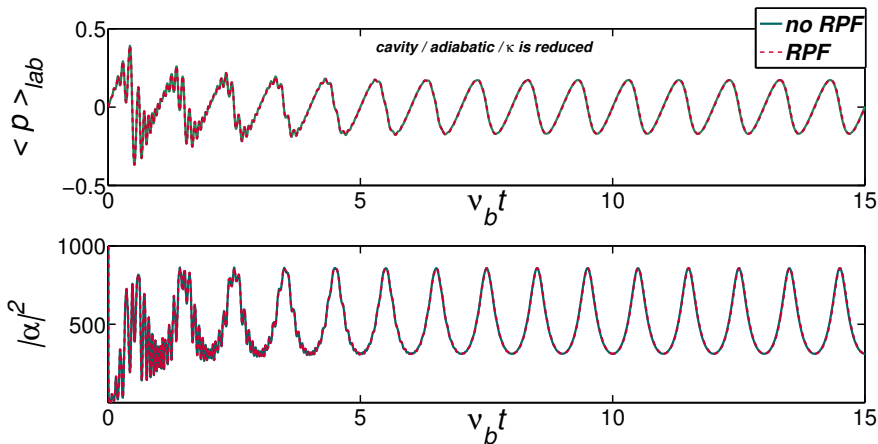


Figure 5.5: Smaller $\kappa = 16\omega_r$ (or equivalently, larger finesse) is selected to perform the dynamics of the average atomic momentum in the laboratory frame (above) and the number of photons $|\alpha|^2$ in the radiation field (below) for an adiabatic switch-on of the lattice potential in the presence of the cavity with (red) and without (navy blue) the RPF impact. The used parameters are: $\nu_b = 0.035\omega_r$, $\delta = 0$, $\Gamma = 1600\omega_r$, $\Omega_1 = 54\omega_r$, $\Omega_p = 6240\omega_r$, $N = 2 \cdot 10^5$, $U_0 = 0.004\omega_r$ and $\alpha_0 = 200$.

cavity finesse corresponding to the chosen set of parameters is $F \simeq 20000$.

The results of the numerical simulations performed using the above parameters are shown in Fig.5.5. It is seen that the average atomic momentum given in the laboratory frame of reference demonstrates identical behavior in both cases, when the effect of the RPF is disregarded (navy blue solid curve) and when it is taken into account (red dashed curve), like for the previous set of parameters. Moreover, the time evolution of the photon number in the radiation field α in the presence of the RPF duplicates the one obtained without the RPF impact. However, a few Bloch periods are required for the bursts of light in the probe field to stabilize in comparison to the previous case. Anyway, the increase of the cavity finesse seems to be an effective way to fight against the undesirable effect especially if one wants to have a smaller amount of atoms in the system to approach real experimental conditions.

Even though the RPF may play a crucial role in the dynamics of the considered system, it is always possible to find a range of parameters that allow one to avoid the unwanted effect. However, to be able to disregard the RPF, high attention to the choice of parameters is required. Note that all other features of the system viewed in this chapter assume the RPF to be negligibly small already.

It should also be noted that in order to perform a high precision gravity measurement using the considered model, the pump laser must be detuned far away from the atomic resonance. Otherwise, the intracavity light field Ω_p may exert a non-negligible constant radiation pressure force acting on the atoms, which in turn may alter the measure of the atomic acceleration and, hence, the frequency of the Bloch oscillations.

5.2 Impact of fluctuations

It is well known that any unintended noise represents a limiting factor for measurements, and the considered scheme is not an exception. That is why it is important to gather information about the noises that may appear in the system and consider their possible effect on the investigated dynamics. This section is dedicated to the study of this specific issue. In particular, the system's response to a technical phase noise perturbing the optical lattice potential formed by the standing wave and amplitude noise in the pump laser beam are discussed.

5.2.1 Phase fluctuations

In order to monitor the atomic dynamics in a non-destructive fashion, the Bloch oscillations are required to be regular and persist for long times. This, however, happens only if the atomic motion is perfectly adiabatic, i.e., there are no negative factors violating the ARP conditions (2.9), so that the interband transitions are prevented. If the lattice potential is subject to, for example, a phase noise, the adiabaticity can be easily broken and the atoms tunnel to the next higher Bloch band resulting in a drift and diffusion of the atomic cloud's momentum. This subsection demonstrates that the cavity induced stability of the Bloch oscillations is a reasonable solution to the problem of the adiabaticity breaking introduced by a mechanical noise.

To learn how stable the system is against a mechanical noise, a few sequential random kicks of different amplitudes are applied to the phase of the optical lattice potential. The noise modeled this way can be accounted for as, for instance, an acoustic noise on the lattice mirrors. In the particular case discussed below three chosen phase fluctuations of various amplitudes $\delta_\phi = 0.16\pi$, 0.37π and 0.46π happen during the evolution at respective times $\tau_a = 3.6\nu_b t$, $\tau_b = 11.9\nu_b t$ and $\tau_c = 22.3\nu_b t$. For all three phase modifications, the presence of the ring cavity is demonstrated to bring back the stability of the system.

The Bloch oscillations appear to be very sensitive to such noise in the absence of the ring cavity as these randomly generated kicks in the lattice phase drive a significant amount of atoms to other momentum states, and the red dashed curve in Fig.5.6 clearly demonstrates this. This effect is also prominently expressed in Fig.5.7(a) where the time evolution of the population of each momentum state is identified by a different color. Since the optical lattice is switched on adiabatically, the dynamics of the system without the cavity at the beginning of the evolution demonstrate the characteristic periodic behavior until the first phase kick takes place. This imposed noise that immediately vi-

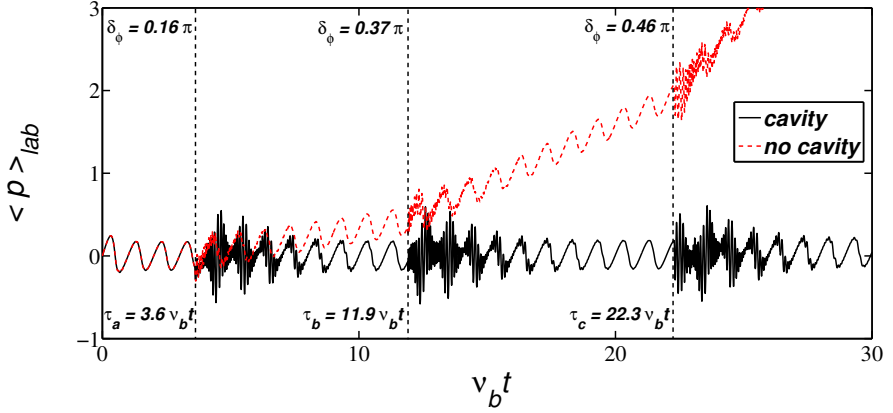


Figure 5.6: Dephasing of the average atomic momentum in the laboratory frame induced by phase fluctuations of the lattice potential in the presence of the cavity (solid black line) and without the cavity (red dashed line) when an adiabatic switch-on of the optical lattice is performed. The simulations are realized using the following parameters: $\nu_b = 0.035\omega_r$, $\kappa = 160\omega_r$, $\delta = 0$, $N = 2 \cdot 10^6$, $U_0 = 0.004\omega_r$ and $\alpha_0 = 200$. During the evolution three phase kicks of amplitudes $\delta_\phi = 0.16\pi$, 0.37π and 0.46π happen at respective times $\tau_a = 3.6\nu_b t$, $\tau_b = 11.9\nu_b t$ and $\tau_c = 22.3\nu_b t$.

olates the adiabaticity of the process is responsible for the steady drift of the atomic momentum and leaves some atoms outside of the Bloch oscillations dynamics. The two subsequent phase kicks prove that the behavior of the system is repeated. Besides, the larger the amplitude of the phase fluctuation, the more atoms become lost from the dynamics since this process is seen by the system as cumulative, i.e., every subsequent phase kick drives even more atoms to higher Bloch bands.

The situation changes significantly in the presence of the ring cavity feedback. In this case, the cavity forces the atoms to stay synchronized and the tunneling to the higher Bloch bands each time a phase fluctuation occurs is surely prevented (see Fig.5.7(b)). This ability of the cavity to keep the whole atomic population in the lowest band makes the Bloch oscillations robust against the phase noise. Indeed, when the cavity is added to the system, the average atomic momentum in the laboratory frame after each random phase kick returns,

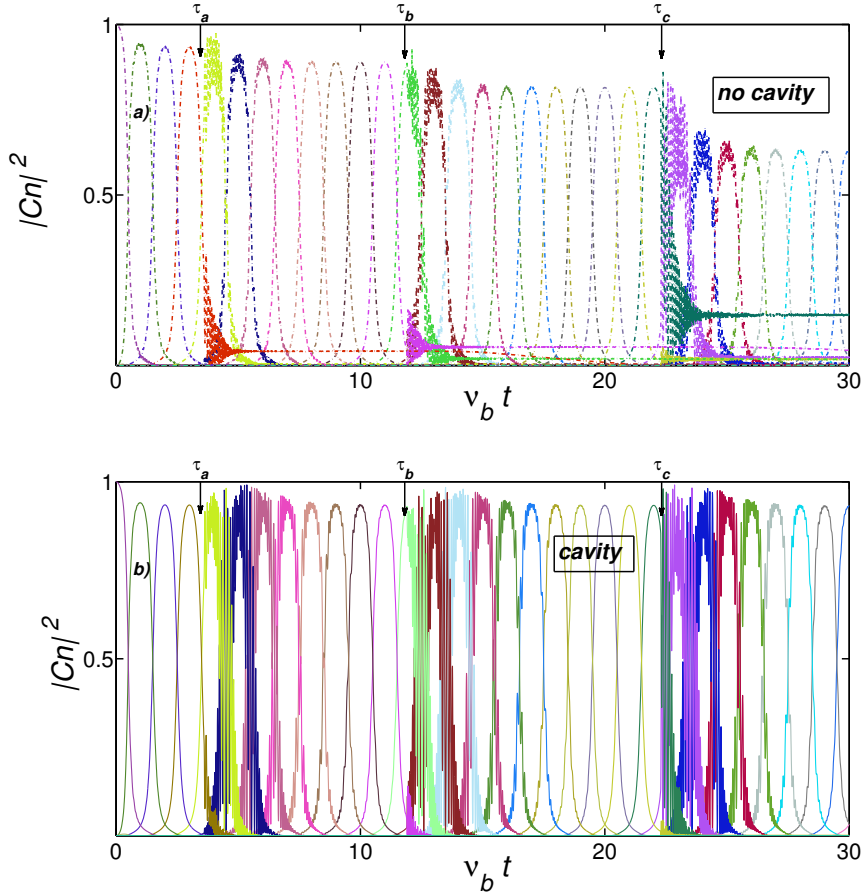


Figure 5.7: Various colors represent the time evolution of the momentum states population $|C_n|^2$ a) in the system without the cavity and b) in the presence of the cavity and adiabatic switch-on of the lattice potential in both cases. Three random phase kicks occur throughout the evolution. The same parameters as in Fig.5.6 are used.

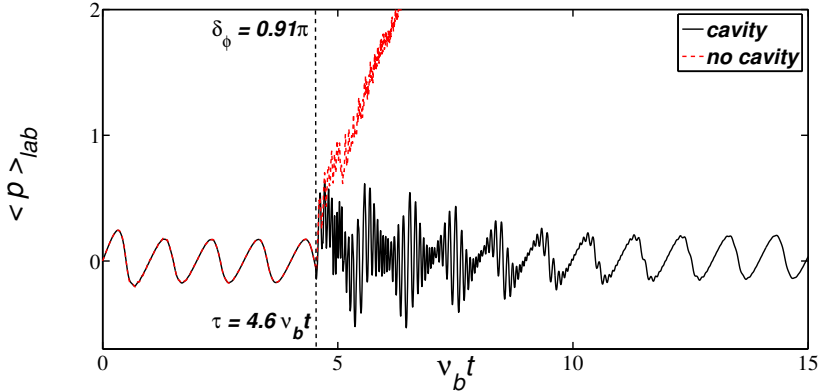


Figure 5.8: Dephasing of the average atomic momentum in the laboratory frame imposed by the large phase fluctuation $\delta_\phi = 0.91\pi$ of the optical lattice happening at $\tau = 4.6\nu_b$ in the presence of the cavity (solid black) and without the cavity (red dashed). The other used parameters are the same as in Fig.5.6.

within a few Bloch oscillation periods, to the very same dynamics it had at the beginning of the evolution (black solid curve in Fig.5.6). This phenomenon can be understood from the fact that the atoms generate the radiation wave that remains in phase with them until it synchronizes again with the optical lattice. The presence of the cavity actually helps to smooth the change of the phase of that wave. Therefore, the cavity is certainly a good tool to remove the negative impact of the applied noise on the dynamics of the system observed in the case without the cavity. Even for a large phase fluctuation, for example, $\delta_\phi = 0.91\pi$, the cavity induced feedback works well (see Fig.5.8) with only a slightly longer time required to stabilize the system in comparison to the kicks of smaller amplitudes shown in Fig.5.6.

Since the dephasing induced by the phase fluctuations of the standing wave forming the optical lattice may be neutralized by the cavity, the non-destructive mechanism to monitor the atomic dynamics is still valid. In fact, Fig.5.9 shows that in the presence of the cavity the bursts of light in the probe field used to control the atomic motion stabilize shortly after each phase kick. This stabilization is certainly a result of the feedback provided by the cavity field on the optical lattice. It brings back the normal behavior of the system characterized

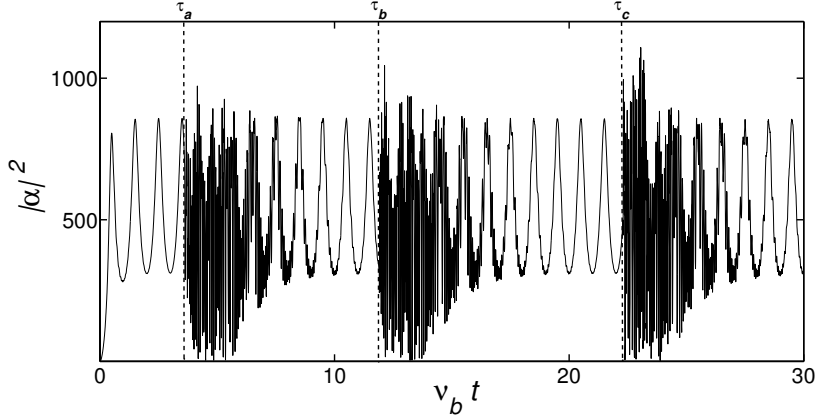


Figure 5.9: Number of photons $|\alpha|^2$ in the probe field as a function of $\nu_b t$ in the presence of the cavity. The present dynamics is a result of a few random fluctuations in the lattice potential phase. The same parameters as in Fig.5.6 are used.

by a single light burst per Bloch oscillation period and maintains the mechanism effective over time for any phase modification $\delta_\phi \in [0, \pi]$.

The model of the system given by Eqs.(2.7) and (2.8) gives rise to another interesting fact. So far the stability of the cavity setup against mechanical noise was tested using random kicks in the optical lattice phase. However, this external lattice potential can be equivalently generated by an additional laser beam pumping the probe mode of the ring cavity and having the same phase and frequency as the pump laser. Thus, the phase fluctuations of the optical lattice can be associated with the phase perturbations in the cavity field. Even though the random phase kicks could be applied to the cavity wave instead of the lattice potential, the system would still demonstrate the same process of stabilization of the Bloch oscillations, since in this case the optical lattice would in turn provide a feedback onto the cavity field, enforcing the synchronization and a large reduction of the imposed noise.

5.2.2 Amplitude fluctuations

In general, most contemporary experimental laboratories have in their possession lasers of great amplitude stability over a wide range of frequencies. However, an unexpected amplitude noise may still affect the studied system that is based on a feedback mechanism. The influence of possible amplitude fluctuations of a laser on the investigated dynamics may even be drastic. To examine the potential impact of the pump laser amplitude modulation on the time evolution of the system with and without the optical ring cavity, two cases are considered.

First of all, to make sure that even a short-term modification of the laser amplitude results in a deviation from the expected dynamics, the case when the amplitude changes spontaneously and then immediately returns to the initial value within a single Bloch period is simulated in Fig.5.10. Fig.5.10(a) represents the average atomic momentum in the laboratory frame as a function of scaled time $\nu_b t$ in the presence of the cavity (solid red curve) and without the cavity (dashed purple curve). For this particular simulation a rather large amplitude kick of 30% is taken to make the difference between the two dynamics more prominent. For a fairly small amplitude modification longer evolution times are required in order to notice the disagreement in the average atomic momentum behavior in the presence of the cavity and without the cavity. As can be seen in Fig.5.10(a), even a single random kick of short duration $\Delta\tau = \tau_b - \tau_a$ (in this case $\Delta\tau = 0.75\nu_b t$ with $\tau_a = 5.1\nu_b t$ and $\tau_b = 5.85\nu_b t$) in the laser amplitude leads, sooner or later, to an atomic momentum drift in the absence of the cavity, while the cavity imposed feedback does not let the drift to occur. Due to the kick in the laser amplitude, the dynamics in the presence of the cavity become slightly distorted for a short while and return to normal within a few Bloch periods. The number of photons $|\alpha|^2$ in the radiation field also demonstrates a regular and stable behavior with only a short-term defect after which the dynamics is restored, see Fig.5.10(b). However, the fact that the system with the cavity is stable against a single amplitude modulation of the pump laser beam does not guarantee the stability in the case when a continuous amplitude noise is applied.

Fluctuations in the laser amplitude are often of continuous nature. Let us now see how the system reacts to such constantly active noise. To perform the simulations related to this case a continuous deviation of the pump laser amplitude is selected such that at each integration step the amplitude becomes modulated randomly by $\pm 1, 5\%$ of its initial value. The results of the numerical simulations are presented in Fig.5.11. For an adiabatic switch-on of the

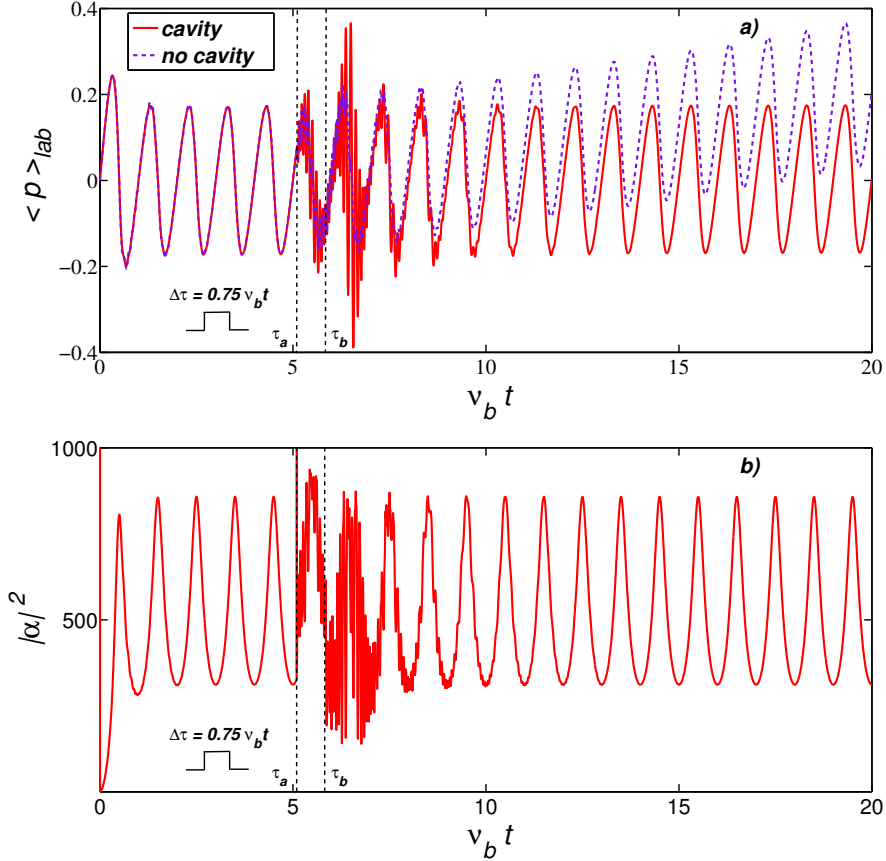


Figure 5.10: a) Time evolution of the average atomic momentum in the laboratory frame in the presence of the cavity (solid red) and without the cavity (dashed purple) for an adiabatic switch-on of the lattice potential. b) Dynamics of the number of photons in the radiation field as a function of time. A 30% kick in the pump laser amplitude of duration $\Delta\tau = 0.75\nu_b t$ ($\tau_a = 5.1\nu_b t$ and $\tau_b = 5.85\nu_b t$) happens throughout the evolution, after which the amplitude is back to the initial value. The following parameters are used to perform the simulations: $\nu_b = 0.035\omega_r$, $\kappa = 160\omega_r$, $\delta = 0$, $N = 2 \cdot 10^6$, $U_0 = 0.004\omega_r$ and $\alpha_0 = 200$.

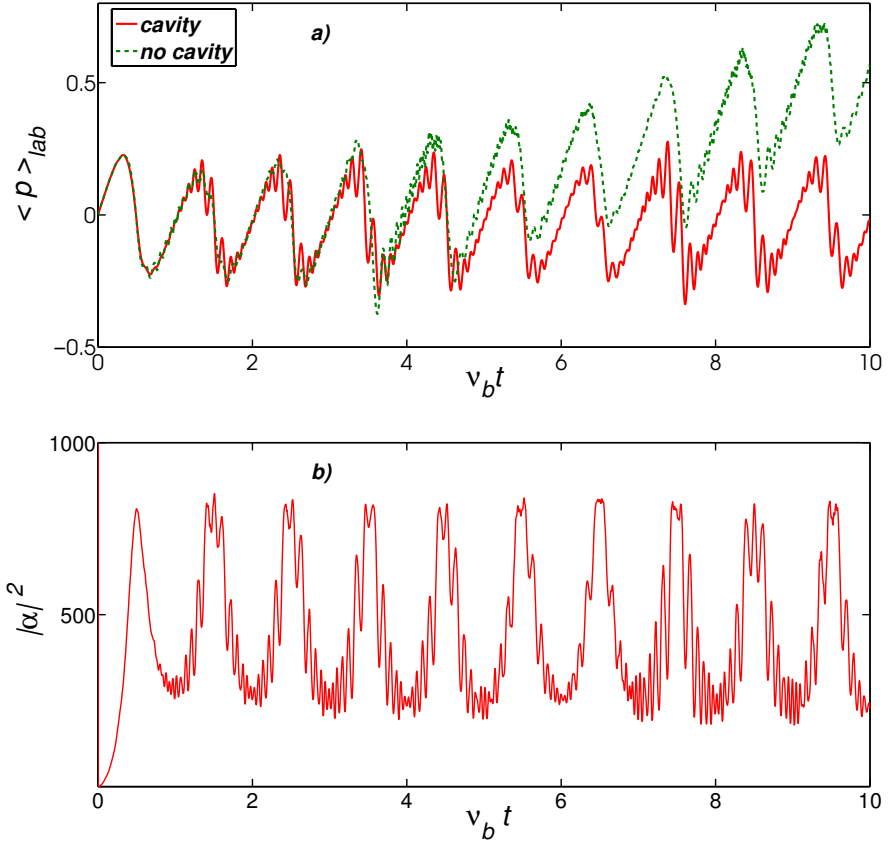


Figure 5.11: a) Average atomic momentum in the laboratory frame with (solid red) and without (dashed green) the cavity, when the optical lattice is turned on adiabatically, and b) photon number $|\alpha|^2$ in the probe field as functions of scaled time $\nu_b t$. An amplitude noise of $\pm 1, 5\%$ is constantly present in the pump laser during the evolution of the system. The same parameters as in Fig.5.10 are used.

optical lattice the average atomic momentum $\langle p \rangle_{lab}$ in the absence of the cavity displays a drift caused by the amplitude noise (see dashed green curve in Fig.5.11(a)). The presence of the cavity instead ensures the same characteristic behavior of the dynamics even with additional noise (see solid red curve in Fig.5.11(a)). Thus, it has been confirmed again that the presence of the cavity influences the dynamics of the system in a positive way, preventing the atoms from tunneling to the excited Bloch bands. Despite the noise in its dynamics, the number of photons $|\alpha|^2$ in the probe field show a characteristic behavior as well, which still demonstrates a prominent burst of light per Bloch period and allows the atomic motion to be traced non-destructively, as before.

Although special care is usually taken to eliminate noise sources such as laser amplitude and phase fluctuations, which may limit the preferred measurement approach, the cavity feedback mechanism provides an additional protection and guarantees the stability of the system against unintended technical noises.

5.3 Clearance of excited Bloch bands

The model under consideration reveals another interesting feature that is very welcomed in real experiments. When an ultracold atomic cloud is created, all atoms are believed to be in a single momentum state associated with the only non-excited Bloch band. However, in reality, an insignificantly small amount of atoms inevitably ends up residing initially in other momentum states. This quantum depletion of the condensate happens due to the interparticle interaction resulting in some atoms being pushed out of the condensate. Therefore, even at zero temperature there is always a fraction of the atoms with nonzero momenta. Even though this is usually the case, the proposed mode-locking mechanism clears up the excited bands, bringing the atoms back to a single momentum state in the presence of the cavity.

To demonstrate this phenomenon the Bloch oscillation dynamics is simulated via Eqs.(2.7) and (2.8) with an initial momentum states distribution for both cases with and without the cavity. The results of the numerical simulations are shown in Fig.5.12(a) and Fig.5.12(b), respectively. The atoms are first distributed over several momentum states, say 75% of the atoms occupy the state n , while the adjacent momentum states $n - 1$ and $n + 1$ contain 12,5% of the total amount of atoms each. The chosen value of 12,5% is clearly too large for an excited state population in comparison to what can actually be realized experimentally, and simply has a demonstrative purpose only. Thus, starting out from that initial atomic distribution, we compare the time-evolution of the populations $|C_n|^2$ of the momentum states for the cases when the cavity is added to the system and without the cavity.

Fig.5.12(a) shows that, if the cavity is not present, the distribution remains unchanged after a few oscillations with only the atoms that initially were in the n th state executing Bloch oscillations within the lowest Bloch band. In the presence of the cavity, the whole population condenses to a single momentum state instead after some wild transients, and the excited bands become depopulated, which is seen in Fig.5.12(b). The population of each momentum state during the evolution is shown by a different color in order to facilitate their visual distinction. Also, the total population represented by the blue line on the top of each picture is verified to stay equal to unity during the evolution, so no atomic loss is observed.

Furthermore, it should be noted that the way the optical lattice containing the atoms is switched on does not really affect this fascinating feature of excited bands clearance. Indeed, the evolution of the momentum states population given in Fig.5.13 for a sudden switch-on of the lattice potential in the presence

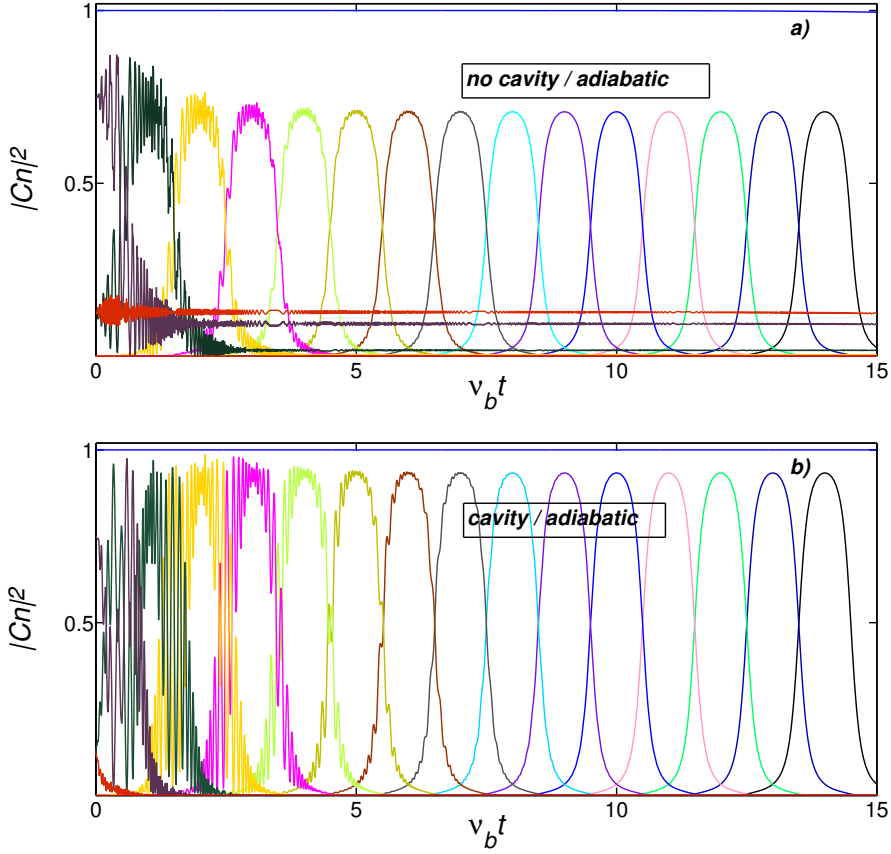


Figure 5.12: Time evolution of the populations $|C_n|^2$ of the momentum states when the atoms are initially distributed over the states $n - 1$, n and $n + 1$ with $|C_{n-1}|^2 = |C_{n+1}|^2 = 0.125$ and $|C_n|^2 = 0.75$ for the case of a) adiabatic switch-on of the optical lattice without the cavity, b) adiabatic rising of the lattice in the presence of the cavity. Various colors representing the population dynamics of each state are taken to ease visual distinction between the curves. The following parameters are used: $N = 2 \cdot 10^6$, $\nu_b = 0.035\omega_r$, $\kappa = 160\omega_r$, $\delta = 0$, $U_0 = 0.004\omega_r$, and the lattice is switched on adiabatically via $\alpha_0(1 - \exp(-\gamma t))$ with $\gamma = 0.1\omega_r$ and $\alpha_0 = 200$.

of the cavity, compared to the dynamics shown in Fig.5.12(b), confirms this statement. Thus, it is possible to undoubtedly conclude that no matter how the lattice is turned on, adiabatically or non-adiabatically, the mode-locking of Bloch oscillations imposed by the cavity leads to a depopulation of the excited Bloch bands adjacent to the non-excited one, forcing the atoms to stay within the lowest Bloch band even though they initially were distributed over several momentum states. Even if an accidental excitation of higher bands happens due to a sudden non-adiabatic switch-on of the optical lattice potential, the mode-locking mechanism is capable for refocusing the whole atomic population in the lowest Bloch band. This might serve as a practical advantage, for instance, to prevent long-term atomic momentum drifts throughout the evolution of the system.

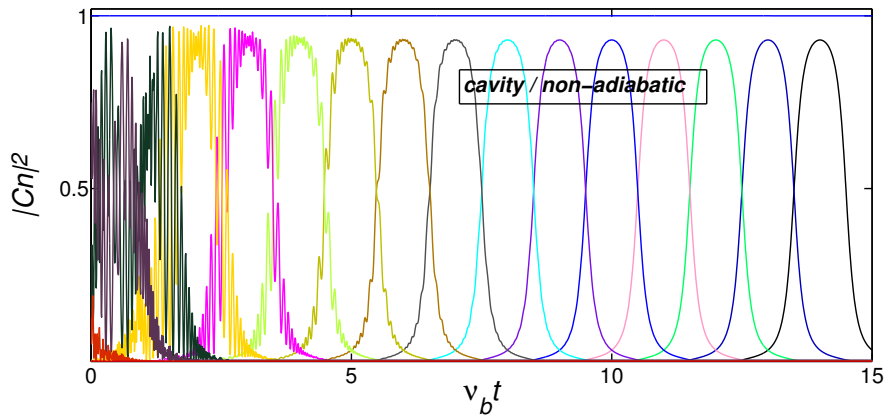


Figure 5.13: The same situation as in Fig.5.12(b) is modeled for an abrupt switch-on of the optical lattice in the presence of the cavity.

5.4 Impact of collisions

In order to maximally approach the experimental conditions, another important effect needs to be taken into consideration. Up until now the interaction between the atoms has been disregarded in sufficiently dilute atomic clouds. However, it is known that the interatomic interaction is always present in a real BEC and it induces a dephasing that negatively affects the dynamics of the system. Thus, if it is impossible to operate in the dilute density limit of a BEC, a way to reduce or even eliminate the impact of interactions should be found. In this section the effect of the atom-atom interactions on the system's evolution is investigated in great detail and an optical ring cavity added to the system is once again proven to be a good stabilizer of the performed dynamics.

To describe the behavior of the system including the interatomic interaction, the basic CARL-BEC model discussed in Chapter 2 needs to be slightly modified. In particular, Eq.(2.7) gains an additional term on its right-hand side, which secures the constant amount of atoms in the system throughout the evolution. This term represents the atom-atom interactions approximated by binary collisions, so that the equations used to simulate the impact of the atomic interaction effect have the following form [114]:

$$i\hbar \frac{\partial \psi}{\partial t} = -\frac{\hbar^2}{2m} \frac{\partial^2 \psi}{\partial x^2} - i\hbar U_0 (\alpha e^{2ikx} - \alpha^* e^{-2ikx}) \psi \quad (5.12)$$

$$- mgx\psi + \hbar \frac{W_0}{2} \sin(2kx)\psi + 2\pi\beta |\psi|^2 \psi,$$

$$\frac{d\alpha}{dt} = NU_0 \int |\psi|^2 e^{-2ikx} d(2kx) + (i\delta - \kappa)\alpha, \quad (5.13)$$

where the interaction strength

$$\beta = \frac{4\hbar k a_s N}{m\Sigma}, \quad (5.14)$$

a_s is the interatomic scattering length and Σ is the atomic cloud cross-section perpendicular to the optical axis x .

After moving into the accelerated frame of reference and expansion of the atomic wave function ψ into plane waves, assuming that the atomic cloud is homogeneous and its size is much longer than the radiation wavelength, Eqs. (5.12) and (5.13) become:

$$\begin{aligned} \frac{\partial C_n}{\partial t} &= -4i\omega_r (n + \nu_b t)^2 C_n + U_0 (\tilde{\alpha}^* C_{n+1} - \tilde{\alpha} C_{n-1}) \\ &\quad - i\beta \sum_{k,l} C_k C_l C_{k+l-n}^*, \end{aligned} \quad (5.15)$$

$$\frac{d\tilde{\alpha}}{dt} = U_0 N \sum_n C_{n-1}^* C_n + (i\delta - \kappa)(\tilde{\alpha} - \alpha_0). \quad (5.16)$$

This set of ordinary differential equations is solved numerically for a moderate interaction strength $\beta \simeq \omega_r$, and the results of the simulations for both cases with and without the cavity and adiabatic switch-on of the lattice potential are shown in Fig.5.14 and Fig.5.15. The time evolution of the average atomic momentum in the laboratory frame (see Fig.5.14(a)) reveals that no drift in the momentum is caused by the atomic collisions in the presence of the cavity (solid red curve) unlike the case without the cavity (dashed blue curve), where the average momentum of the atomic system starts drifting. This interaction induced dephasing of the Bloch oscillations in the absence of the cavity and rapid broadening of the atomic momentum in the first Brillouin zone clearly prevent the non-destructive monitoring of the atomic dynamics limiting the observation to only a few Bloch oscillations in a BEC of typical atomic density. On the other hand, in the presence of the cavity the atom-atom interactions do not drive the atoms to other momentum states and the capability to observe a large number of Bloch oscillations on extended time scales is efficiently restored. The latter can also be seen in Fig.5.14(b), where the number of photons in the probe field is given as a function of time and each prominent light burst corresponds to a Bloch oscillation period, with only a slight noise in the dynamics, which occurs due to the additional non-linear term in Eq.(5.15), which represents the collisions.

Further evidence of the positive impact of the cavity on the system including the effects caused by the interatomic interaction is the dynamics of the populations $|C_n|^2$ of the momentum states, presented in Fig.5.15 by a different color to make the visual distinction between the curves easier. The collisional dephasing in the case without the cavity is responsible for the loss of the atoms from the dynamics. Indeed, the momentum transfer between adjacent momentum states is non-efficient in the absence of the cavity, therefore some atoms remain in the previous states with less and less atoms undergoing Bloch oscillations, see Fig.5.15(a). With the cavity, the induced dephasing is definitely suppressed and all atoms are forced to perform the Bloch oscillations (Fig.5.15(b)).

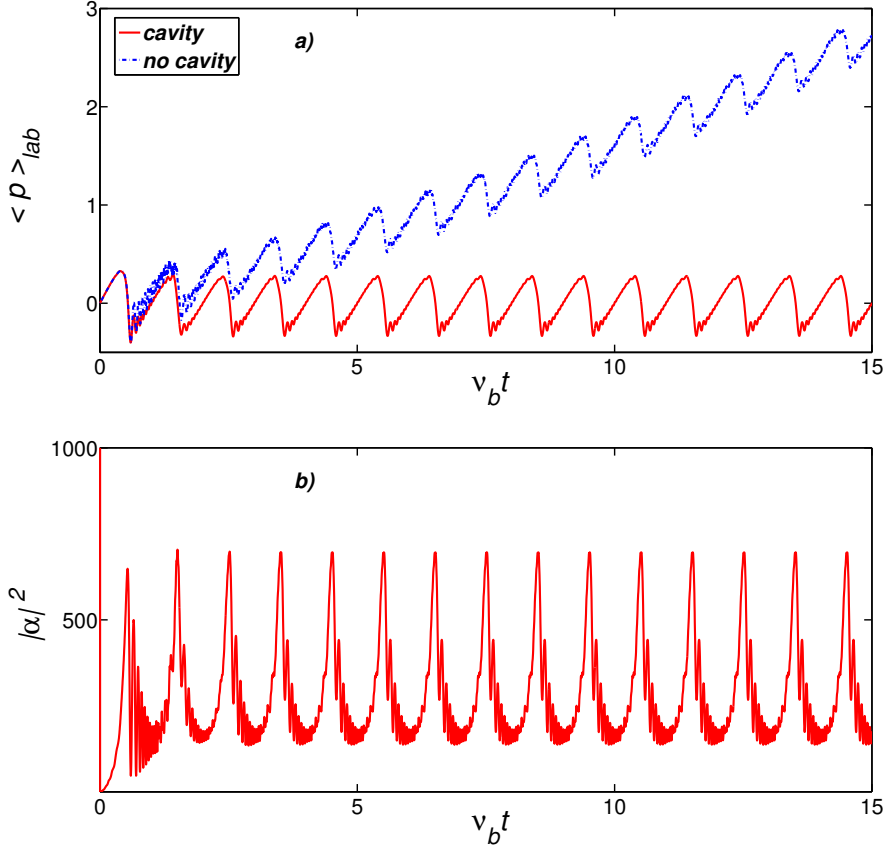


Figure 5.14: Impact of atomic collisions on the time evolution a) of the average atomic momentum in the laboratory frame in the presence of the cavity (red) and without the cavity (blue) and b) number of photons $|\alpha|^2$ in the radiation field, when the optical lattice is turned on adiabatically. The assumed interaction strength $\beta \simeq \omega_r$ corresponds to a typical experimental situation: $a_s = 110a_B$ for ^{87}Rb , where a_B is the Bohr radius, and $\Sigma \simeq 300\mu\text{m}^2$. The rest of the parameters are: $N = 2 \cdot 10^6$, $\nu_b = 0.035\omega_r$, $\kappa = 160\omega_r$, $\delta = 0$, $U_0 = 0.004\omega_r$, and the lattice is switched on adiabatically via $\alpha_0(1 - \exp(-\gamma t))$ with $\gamma = 0.1\omega_r$ and $\alpha_0 = 200$.

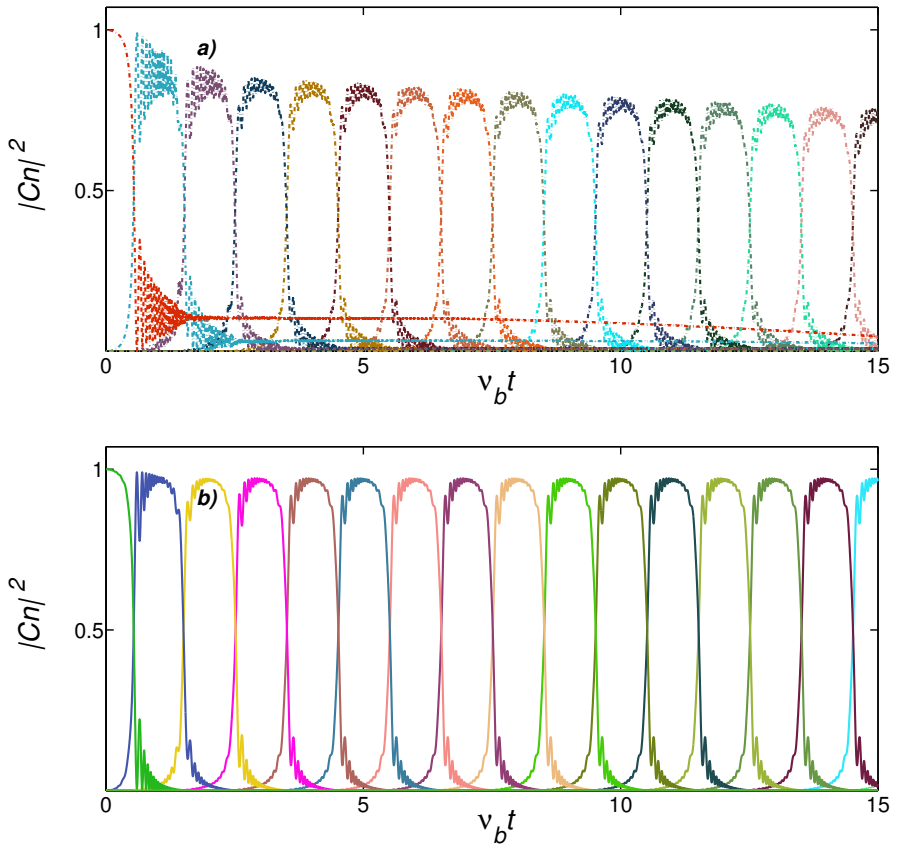


Figure 5.15: Influence of the atom-atom interactions on the time evolution of the populations $|C_n|^2$ of the momentum states when the optical lattice is switched on adiabatically for the cases a) without the cavity and b) in the presence of the cavity. The same parameters as in Fig.5.14 are used to perform the simulations.

Chapter 6

Conclusion

The system considered in this thesis is an ultracold atomic cloud confined in a vertical optical standing wave and undergoing Bloch oscillations under the influence of gravity. After a unidirectionally pumped optical ring cavity is added to the system, the atoms interact not only with the confining lattice potential, but with the two counter-propagating cavity modes too. The atomic motion in such environment is shown to act back onto the intracavity light fields and imprint into their phase and amplitude detectable signatures. In a certain range of parameters, this feedback known as collective atomic recoil lasing (CARL) evolves into a regime where it cooperates with the Bloch oscillations dynamics. Indeed, if the collective atom-field coupling strength is too large ($NU_0/\kappa \gg \alpha_0$), the CARL mechanism takes over and imposes its dynamics on the atoms, dominating the Bloch oscillations. However, for a moderate coupling ($NU_0/\kappa \approx \alpha_0$) both the CARL and Bloch dynamics collaborate to set up a synchronized regime characterized by regular and stable Bloch oscillations. The transition between the competing one another dynamics to the synchronized regime is studied in detail in Chapter 4, and a set of parameters suitable to obtain stabilized Bloch oscillations is found.

The detailed investigation of the system without the ring cavity, provided in Chapter 2, reveals the most crucial condition to be able to observe regular Bloch oscillations for long times. This is only possible if the atomic motion is perfectly adiabatic. However, if the optical lattice is turned on in a non-adiabatic fashion or it is subject to amplitude or phase noise, the adiabatic rapid passage conditions ($\nu_b/8\omega_r \ll (W_0/16\omega_r)^2 \ll 1$) become violated and the atoms can quickly tunnel to the next higher Bloch band, which leads to the average atomic

momentum drifts. To prevent that and keep the momentum transfers upon Bragg reflections fully complete, a careful selection of parameters is absolutely necessary in the case of an adiabatic switch-on ($\alpha_0 = \tilde{\alpha}_0(1 - \exp(-\gamma t))$ with $\gamma \gg \nu_b$) of the lattice potential without the cavity. Another possible way to circumvent this problem is to let the atoms simultaneously interact with an optical ring cavity added to the system.

Chapter 3 shows that the presence of the ring cavity turns out to be surprisingly beneficial. The scattered field in the reverse cavity mode induces a positive feedback on the atomic evolution by efficiently restoring the whole atomic population in the first Brillouin zone after some transient of a few Bloch periods, independently on the way of the lattice potential switching in the initial phase. As a result, the transitions between adjacent momentum states are totally successful and the atomic momentum drifts are surely prevented. Due to the cavity-induced feedback the atomic Bloch oscillations become synchronized through the so-called mode-locking mechanism that enforces the adiabaticity of the system. Even in the presence of adverse effects discussed in Chapter 5 the ring cavity makes the atoms execute synchronous Bloch oscillations.

Since the theoretical work presented in this thesis is based on a real experiment which is currently under construction at the Institute of Physics of São Carlos, University of São Paulo, Brazil, the reality of the laboratory setting is taken into account. For instance, the radiation pressure force (RPF) experienced by the atoms is usually neglected under the assumption that the incident pump laser is tuned far from the atomic resonance ($\Omega_p \ll \Delta, \Delta \gg \Gamma$), even though this effect is always present for all matter-light interactions. It is demonstrated that including the RPF effect imposes a significant (5%) modification on the Bloch oscillation frequency, which is too large to be ignored. However, the undesirable effect can be avoided by careful selection of the correct experimental parameters. It should be noted that another strength of the theoretical model is that it applies to any atomic species which are commonly used in atomic physics experiments, although with specific parameters for each of them. The parameters discussed in this work apply to ^{87}Rb ultracold atoms, however, the experimental setup in Brazil will use an atomic cloud of ^{88}Sr , for which the parameters are the following: $N = 10^4$, $\nu_b = 0.025\omega_r$, $\kappa = 125\omega_r$, $\delta = 0$, $U_0 = 0.1\omega_r$ and $\alpha_0 = 10$.

Another aspect that is considered is the presence of noise in the experimental setup. In particular, a phase noise which perturbs the optical lattice, from, for example, acoustic vibrations on the lattice mirrors, and amplitude noise from natural fluctuations in the laser power are introduced. Modelling both sources of noise as random kicks demonstrates the high sensitivity of the Bloch oscillations

to small perturbations. In the absence of the cavity feedback mechanism, the simulated phase noise drives a significant amount of atoms to other momentum states, resulting in a momentum drift which leaves some atoms outside of the expected dynamics. The presence of the cavity prevents tunnelling to higher Bloch bands and forces the atoms to remain synchronized, leaving the system robust against phase noise. In terms of the amplitude noise, where both single and continuous kicks in the pump laser are simulated, it can be seen that atomic momentum drifts can occur in the absence of the cavity. With the cavity, atoms are prevented from tunnelling to excited Bloch bands and the effect of the noise is greatly suppressed. Thus, although in experimental setups a large amount of care goes into preventing noise from affecting the system, the ring cavity dynamics offer an extra layer of robustness to noise which cannot always be completely isolated.

A further related benefit of the ring cavity is the clearing of excited Bloch bands which may be already populated at a non-adiabatic switch-on of the optical lattice or accidentally happen throughout the evolution affected by noise. The ability of the cavity to recover these atoms back into the non-excited band means that all atoms can participate in the Bloch oscillations, increasing the effectiveness of the measurement. Even in the exaggerated simulation case where only 75% of the atoms start in the lowest Bloch band, the cavity can recover the rest of the atoms back into the dynamics after only a few oscillations with short-lived transient behavior for the first few Bloch periods. Thus, the presence of the cavity provides not only stability in the experimental setup, but also ensures maximum efficiency.

The effect of interatomic interactions is also considered beyond the initial state of the condensate. The effect of the ring cavity on the studied system is seen in the case where the atom-atom interactions are not neglected, which is of particular importance to the real experimental setup where a dilute ultracold atomic cloud might not always be achieved. Here, the interatomic collisions can cause a drift in the atomic momentum as the system evolves, resulting in dephasing of the Bloch oscillations. However, introducing the cavity to the system prevents collisional dephasing of the atomic cloud and ensures that all the atoms continue being available for subsequent Bloch oscillations.

The advantage of the considered scheme is not only to reach the regime of self-stabilized Bloch oscillations persistent for long times, but also continuously monitor their dynamics via the cavity field on the photon counter. Indeed, the radiation field reaches a stationary regime characterized by perfectly detectable periodic bursts of light emitted at each Bloch period, which can serve as reliable signatures of the Bloch oscillations without perturbing their periodicity. Thus,

the observed light bursts in the probe cavity mode provide a non-destructive monitor of the atomic Bloch oscillations. The discussed adverse effects may, however, degrade the ability of the system to reliably track the atomic motion and limit the potential for continuous observation of the Bloch oscillations dynamics. Even though great care is always taken to reduce the impact of the experimental non-ideal effects on Bloch oscillation measurements, in the cases where these cannot be avoided the ring cavity feedback mechanism acts to suppress the negative effects completely. This ensures that even outside of idealized settings the ring cavity allows for non-destructive measurement of the Bloch oscillations, thus showing the practical benefits of the presence of the cavity.

Applying the features studied in this thesis to real atomic gravimeters based on observation of Bloch oscillations would offer great improvements as the gravimetry process can be effectively reduced to making a single non-destructive measurement with just one atomic sample, drastically decreasing the laboriousness of current detection methods. The upcoming experiment is expected to make extensive use of the considered system, being the first experiment of its kind to measure gravity to a high degree of accuracy through multiple Bloch oscillations of a single atomic cloud.

Appendices

Appendix A

Derivation of angle β

In the main body of Chapter 2 the studied model is described. A periodic potential is initially created to trap the atomic cloud in the vertical arm of the ring cavity (see Fig.2.1), so that the atoms execute Bloch oscillations under the action of the applied gravitational force. This optical lattice can be generated by, for example, two far detuned from the atomic resonance external laser beams with wavevectors

$$\mathbf{K}_{1,2} = K \begin{pmatrix} \cos \frac{\beta}{2} \\ \pm \sin \frac{\beta}{2} \\ 0 \end{pmatrix}, \quad (\text{A.1})$$

crossing each other under the angle β at the location of the atoms. Here, the phase of the laser light is generalized to $(\mathbf{K}_{1,2} \cdot \mathbf{r} - \omega t)$ by replacing the wavenumber with a wavevector that specifies the direction of a plane wave in 3D-space, parameterized by the position vector \mathbf{r} .

The external laser beams generate the following optical potential:

$$V_{ext}(\mathbf{r}) = \int [\sin(\mathbf{K}_1 \cdot \mathbf{r} - \omega t) + \sin(\mathbf{K}_2 \cdot \mathbf{r} - \omega t)]^2 dt \quad (\text{A.2})$$

$$= \int 4 \sin^2 \left(\frac{\mathbf{K}_1 + \mathbf{K}_2}{2} \cdot \mathbf{r} - \omega t \right) \cos^2 \left(\frac{\mathbf{K}_1 - \mathbf{K}_2}{2} \cdot \mathbf{r} \right) dt \quad (\text{A.3})$$

$$= 4 \cos^2 \left(\frac{\mathbf{K}_1 - \mathbf{K}_2}{2} \cdot \mathbf{r} \right) = 2 + 2 \cos [(\mathbf{K}_1 - \mathbf{K}_2) \cdot \mathbf{r}] \quad (\text{A.4})$$

$$= 2 + 2 \cos \left(2Ky \sin \frac{\beta}{2} \right). \quad (\text{A.5})$$

Appendix A. Derivation of angle β

This potential should be commensurate with the standing wave potential formed by the cavity modes, $V_{cav} = 2 + 2 \cos(2ky)$, so that the condition

$$K \sin \frac{\beta}{2} = k . \quad (\text{A.6})$$

must be fulfilled. This can be achieved, e.g., using an external laser with wavelength $\lambda_0 = 532$ nm, for which the above condition reads as:

$$\frac{2\pi}{\lambda_0} \sin \frac{\beta}{2} = \frac{2\pi}{\lambda} , \quad (\text{A.7})$$

where $\lambda = 780$ nm corresponds to the rubidium D2 transition. For these parameters, the condition (A.7) results in $\beta = 86^\circ$.

Appendix B

Origin of transient

It is obvious that the ARP approximation is not sufficient enough to describe entirely the evolution of the system during the first few Bloch oscillations. The reason is that other momentum states being populated as well have an impact on the momentum transfer between the states n and $n - 1$. As an example, let us consider only five momentum states: $n + 1, n, n - 1, n - 2$ and $n - 3$.

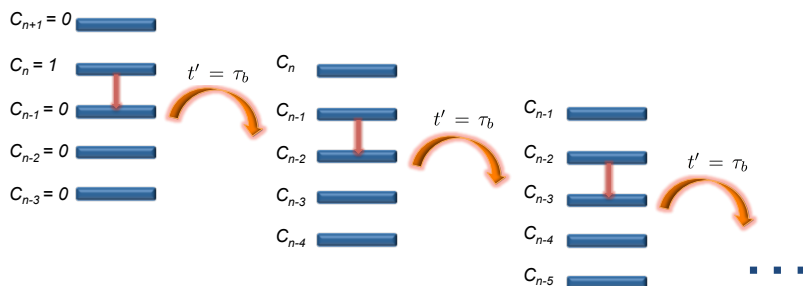


Figure B.1: Five momentum states scheme. All atoms are assumed to be initially in the n th momentum state. Each Bloch period τ_b the system undergoes a transition to a lower momentum state, while the upper state is eliminated due to its expected null population and an additional lower state is introduced instead. The initial conditions for a subsequent Bloch oscillation are taken from the numerical solution of Eqs.(2.7) and (2.8) for the previous transition.

Appendix B. Origin of transient

All atoms initially are in the n th momentum state, so that $C_n(0) = 1$ and $C_{n+1}(0) = C_{n-1}(0) = C_{n-2}(0) = C_{n-3}(0) = 0$. The dynamics of the system is determined by self-consistent Eqs.(2.7) and (2.8) derived in Sec.2.1. The same set of equations can be solved numerically for each transition happening every $t' = \tau_b$, keeping the final atomic distribution after a previous Bloch oscillation as the initial condition for the successive one and the total number of momentum states equal to five (see Fig.B.1).

While the ARP approximation based on the assumption $\tilde{\alpha} \approx \alpha_0$ (no cavity) assumes that only two adjacent momentum states are involved into the system's dynamics during each Bloch period τ_b , and all atoms from the n th state are expected to be transferred to the state $n - 1$ during the first oscillation, other momentum states in reality become populated too. Fig.B.2(a) clearly demonstrates that with no cavity a significant amount of atoms end up in the state $n + 1$ after the first transition, the population of which in the case of ARP

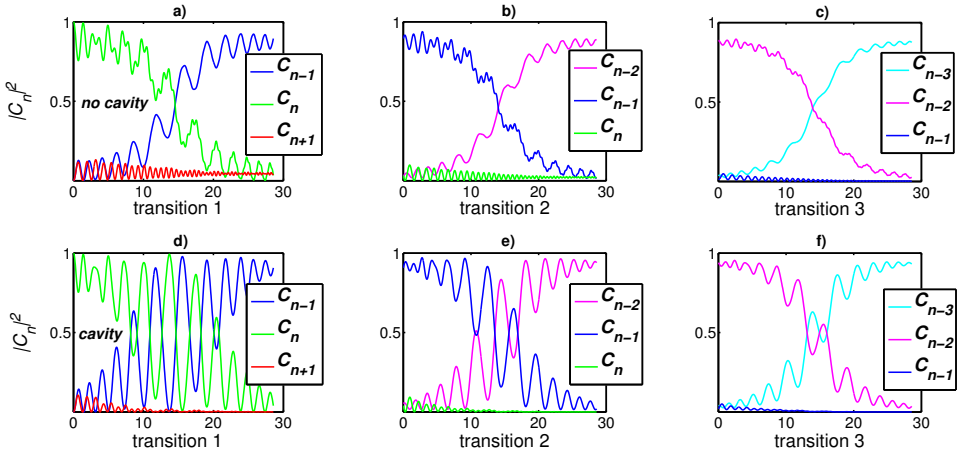


Figure B.2: These pictures show the dynamics of the system during the first three Bloch oscillations in the five states approximation. The upper row of the pictures corresponds to the case without the cavity, where it is clearly seen that the upper momentum state remains populated till the end of the third transition. The lower row of the pictures represents the case when the cavity is present, and the upper state after each transition stays unpopulated. The selected rubidium parameters from Fig.3.2 are used.

approximation is supposed to be zero. Thus, the presence of other momentum states plays an important role in the dynamics of the system. It also explains why ARP fails to describe the transient and can be adopted only for a long-term evolution. When the $(n + 1)$ th state is eliminated due to its assumptive null population after the first transition and the state $n - 4$ is taken into consideration instead ($C_{n-4} = 0$) in order to keep the same amount of momentum states participating in the evolution of the system during the second Bloch period (see Fig.B.1), the dynamics obviously loses some atoms from the removed $(n + 1)$ th state. Note that the atoms can only be lost from the Bloch oscillations dynamics, but not from the system itself, since the considered model is designed in a way that does not let the atoms to escape the system and the total amount of atoms remains constant. Repeating the described above procedure a few more times (Fig.B.2(b) and Fig.B.2(c)), it is possible to observe that the third transition leads to the upper momentum state population to be reduced to zero, and as a consequence the atomic loss from the dynamics is terminated. In the presence of the ring cavity, however, the atoms would not be lost, since the cavity does not allow the atoms to remain in the upper momentum state at the end of each transition, which is shown in Fig.B.2(d)-(f).

To determine the amount of atoms that may be missing from the dynamics after the first few Bloch oscillations if the ARP approximation is adopted in the case without the cavity, ten consecutive transitions are considered and the total momentum states population at the beginning of each of them is plotted in Fig.B.3. Blue circles in Fig.B.3 confirm that the cavity stabilizes the system in such a way that the atomic loss from the dynamics is significantly suppressed by keeping the upper momentum state unpopulated at the end of each oscillation. However, a loss of about 6.5% of the atoms is observed before it is terminated by the dynamics in the case without the cavity, which is shown by red squares in Fig.B.3. The fact that the ARP approximation is missing other momentum states prevents accurate description of the transient in the system's dynamics during the first few Bloch periods. Certainly, more momentum states are taken into consideration, closer to the real evolution of the system and its better understanding one gets. Yet even with the restrictions, the five states approximation allows to demonstrate the necessity to take into account all momentum states and their influence on each transition.

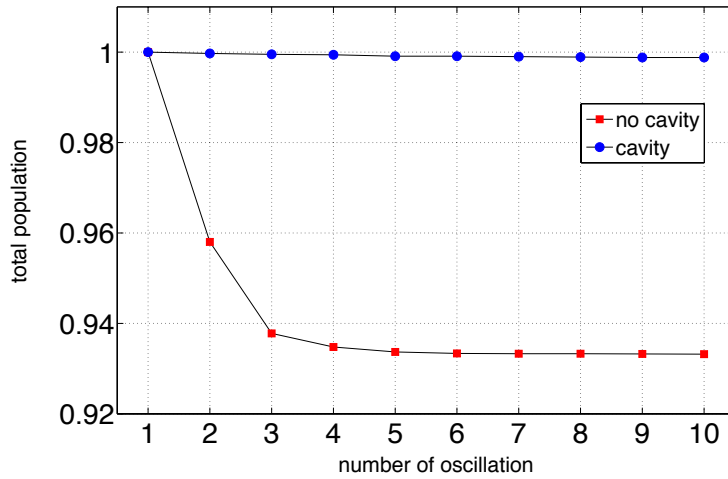


Figure B.3: Total population of the momentum states at the beginning of each transition in the five states approximation in the presence of the cavity (blue circles) and without the cavity (red squares). The cavity constrains greatly the atomic loss from the Bloch oscillations dynamics during the evolution, while without the cavity a loss of about 6.5% of the atoms is experienced during the first three transitions after which the atomic loss is terminated. The same parameters as in Fig.B.2 are used.

Acknowledgements

First of all I would like to sincerely thank my terrific supervisor Dr. Nicola Piovella who has always been there for me, for his valuable support and encouragement. It has been a great pleasure to work with him. He has always willingly shared his knowledge and expertise with me during these years and inspired me to choose this specific research project that resulted in my PhD thesis and a number of impactful papers. I also believe that my theoretical work is potentially useful in atomic physics research and very soon will find its experimental realization.

I have received invaluable feedback from the members of my doctoral committee. I would therefore like to thank them, Ass.Prof. Leonardo Fallani (European Laboratory for Non-Linear Spectroscopy, University of Florence, Italy), Prof. Luca Salasnich (University of Padova, Italy) and Prof. Gian-Luca Oppo (University of Strathclyde, Scotland, UK) for their insight and commentary which have helped me refine the thesis.

Special thanks to my Applied Quantum Mechanics group at the University of Milan. In particular, I thank Prof. Matteo Paris, Dr. Stefano Olivares, Dr. Simone Cialdi, Dr. Fabrizio Castelli and Prof. Marco Giammarchi as well as PostDocs and other PhD students alike, for always keeping a cheerful and kind atmosphere in the group.

I would like to thank Prof. Marco Bersanelli, the director of the PhD School in Physics, Astrophysics and Applied Physics at the University of Milan, for always believing in me and giving me the opportunity to complete my doctoral research program at this university. I wish to also acknowledge the significant support and understanding that I have received from the PhD School secretary Dr. Andrea Zanzani. He has always been available and given me reasonable advice to any problem.

I am very grateful for being a member of the COSCALI program, funded by the Research Executive Agency (Grant No.PIRSES-GA-2010-268717), and would like to thank its node leaders Prof. Robin Kaiser (Nonlinear Institute of Nice, France), Prof. Claus Zimmermann and Dr. Sebastian Slama (University of Tübingen, Germany). I would like to particularly thank Prof. Philippe W. Courteille and Dr. Romain Bachelard (Institute of Physics of São Carlos, Brazil) with whom I extensively collaborated with during these years. I am truly lucky to have the opportunity to be able to work with you all, learn from you and get

to know some of you on a more personal level. Hopefully we will meet again before too long!

I would also like to thank Dr. Gordon Robb (University of Strathclyde, Scotland, UK) for his supervision during my Erasmus Placement Program. My time in Glasgow was very valuable and helped me focus on what would come to be my doctoral research.

Last, but not least, I offer heartfelt thanks to my family and friends for their never-ending love and support. I would like to give special thanks to Valentina Pukhova, Angela Duque and Ksenia Germanovich. We started our doctoral programs together and we complete our PhDs together, well done ladies! I address my special thought to Ruben del Aguila for his patience, support and encouragement as well as reading every single word of this thesis and valuable suggestions. I also thank my non-scientific friends Yulia Zhuldibina, Alexander Kalebin, Olga Litvinova, Svetlana Korzeneva, Roberto Mauri and Christian Stehle. I would call myself lucky to be surrounded by such great people. You all heard me complain, cry and laugh. You cheered me up, helped me celebrate, and kept me sane, and without you this journey would have been a lot more difficult. Thanks!

Bibliography

- [1] F. Bloch, *Z. Phys.* **52**, 555 (1928).
- [2] C. Zener, *Proc. R. Soc. A* **145**, 523 (1934).
- [3] N.W. Ashcroft, and N.D. Mermin, *Solid State Physics*, Saunders College Publishing, Philadelphia (1976).
- [4] J. Feldmann, K. Leo, J. Shah, D. A. B. Miller, J. E. Cunningham, T. Meier, G. von Plessen, A. Schulze, P. Thomas, and S. Schmitt-Rink, *Phys. Rev. B* **46**, 7252 (1992).
- [5] K. Leo, P. Haring Bolivar, F. Brüggemann, R. Schwedler, and K. Köhler, *Solid State Commun.* **84**, 943 (1992).
- [6] C. Waschke, H. Roskos, R. Schwedler, K. Leo, H. Kurz, and K. Köhler, *Phys. Rev. Lett.* **70**, 3319 (1993).
- [7] S.Chu, *Science* **253**, 861 (1991).
- [8] C. Cohen-Tannoudji, in *Fundamental Systems in Quantum Optics*, J. Dalibard, J. M. Raimond, J. Zinn-Justin, eds., Elsevier, Amsterdam (1992).
- [9] M. Ben Dahan, E. Peik, J. Reichel, Y. Castin, and C. Salomon, *Phys. Rev. Lett.* **76**, 4508 (1996).
- [10] S.R. Wilkinson, C.F. Bharucha, K.W. Madison, Q. Niu, M.G. Raizen, *Phys. Rev. Lett.* **76**, 4512 (1996).
- [11] M.G. Raizen, C. Salomon, and Q. Niu, *Phys. Today* **50**, 30 (1997).
- [12] M. Inguscio and L. Fallani, *Atomic Physics: Precise Measurements and Ultracold Matter*, Oxford University Press, New York (2013).

- [13] M. Glück, A.R. Kolovsky, H.J. Korsch, and N. Moiseyev, *Eur. Phys. J. D* **4**, 239 (1998).
- [14] M. Holthaus, *J. Opt. B: Quantum Semiclassical Opt.* **2**, 589 (2000).
- [15] J. Zapata, A.M. Guzmán, M.G. Moore, and P. Meystre, *Phys. Rev. A* **63**, 023607 (2001).
- [16] Q. Thommen, J.C. Garreau, and V. Zehnlé, *Phys. Rev. A* **65**, 053406 (2002).
- [17] T. Hartmann, F. Keck, H.J. Korsch, and S. Mossmann, *New. J. Phys.* **6**, 2 (2004).
- [18] J. Lasson, *Phys. Rev. A* **73**, 013823 (2006).
- [19] W.V. Houston, *Phys. Rev. A* **57**, 184 (1940).
- [20] P. Cladé, E. de Mirandes, M. Cadoret, S. Guellati-Khélifa, C. Schwob, F. Nez, L. Julien, and F. Biraben, *Phys. Rev. Lett.* **96**, 033001 (2006).
- [21] R. Bouchendira, P. Cladé, S. Guellati-Khélifa, F. Nez, and F. Biraben, *Phys. Rev. Lett.* **106**, 080801 (2011).
- [22] V. Ivanov, A. Alberti, M. Schioppo, G. Ferrari, M. Artoni, M.L. Chiofalo, and G.M. Tino, *Phys. Rev. Lett.* **100**, 043602 (2008).
- [23] A. Alberti, G. Ferrari, V. Ivanov, M.L. Chiofalo, and G.M. Tino, *New J. Phys.* **12**, 065037 (2010).
- [24] N. Poli, F.-Y. Wang, M.G. Tarallo, A. Alberti, M. Prevedelli, and G.M. Tino, *Phys. Rev. Lett.* **106**, 038501 (2011).
- [25] M.N. Nabighian, M.E. Ander, V.J.S. Grauch, R.O. Hansen, T.R. LaFehr, Y. Li, W.C. Pearson, J.W. Peirce, J.D. Phillips, and M.E. Ruder, *Geophysics* **70**, 63ND (2005).
- [26] D.A. Chapin, *The Leading Edge* **17**, 100 (1998).
- [27] D.A. Chapin and M.E. Ander, Chapter 15: Applying gravity to petroleum exploration in E.A. Beaumont and N.H. Foster eds., *Treatise of Petroleum Geology: Exploring for Oil and Gas Traps*, American Association of Petroleum Geologists (1999).

- [28] T.R. LaFehr, *Geophysics* **45**, 1634 (1980).
- [29] R.I. Gibson and P.S. Millegan, *Geologic applications of gravity and magnetics: Case Histories*, Society of Exploration Geophysicists and American Association of Petroleum Geologists (1998).
- [30] R.J. Blakery, *Potential theory in gravity and magnetic applications*, Cambridge University Press (1995).
- [31] S.G. Smith, *Journal of Navigation* **39**, 401 (1986).
- [32] D. Titterton and J. Weston, *Strapdown Inertial Navigation Technology*, The Institution of Engineering and Technology (2005).
- [33] A. Wicht, J.M. Hensley, E. Sarajlic, and S. Chu, *Phys. Scr.* **t102**, 82 (2002).
- [34] M. Fattori, G. Lamporesi, T. Petelski, J. Stuhler, and G.M. Tino. *Phys. Lett. A* **318**, 184 (2003).
- [35] J. Stuhler, M. Fattori, T. Petelski, and G.M. Tino, *J. Opt. B* **5**, S75 (2003).
- [36] J.B. Fixler, G.T. Foster, J.M. McGuirk, and M. Kasevich. *Science* **315**, 74 (2007).
- [37] G. Lamporesi, A. Bertoldi, L. Cacciapuoti, M. Prevedelli, and G.M. Tino. *Phys. Rev. Lett.* **100**, 050801 (2007).
- [38] F. Sorrentino, L. Cacciapuoti, Y.-H. Lien, M. Prevedelli, G. Rosi, and G. M. Tino. *New J. Phys.* **12**, 095009 (2010).
- [39] J. Audretsch and K.-P. Marzlin, *Phys. Rev. A* **50**, 2080 (1994).
- [40] S. Fray, C.A. Diez, T.W. Hänsch, and M. Weitz, *Phys. Rev. Lett.* **93**, 240404 (2004).
- [41] S. Dimopoulos, P.W. Graham, J.M. Hogan, and M.A. Kasevich, *Phys. Rev. Lett.* **98**, 111102 (2007).
- [42] G.M. Tino and F. Vetrano. *Class. Quantum Grav.* **24**, 2167 (2007).
- [43] H. Müller, S.-W. Chiow, S. Herrmann, S. Chu, and K.-Y. Chung, *Phys. Rev. Lett.* **100**, 031101 (2008).
- [44] S. Dimopoulos, P.W. Graham, J.M. Hogan, M.A. Kasevich, and S. Rajendran. *Phys. Lett. B* **678**, 37 (2009).

-
- [45] H. Müller, A. Peters, and S. Chu, *Nature* **463**, 926 (2010).
- [46] H.B.G. Casimir and D. Polder, *Phys. Rev.* **73**, 360 (1948).
- [47] I.E. Dzyaloshinskii, E.M. Lifshitz, and L.P. Pitaevskii, *Adv. Phys.* **38**, 165 (1961).
- [48] P. Milonni, *The Quantum Vacuum: An Introduction to Quantum Electrodynamics*, Academic Press, Boston (1994).
- [49] K.A. Milton, *J. Phys. A* **37**, R209 (2004).
- [50] M. Antezza, L.P. Pitaevskii, and S. Stringari, *Phys. Rev. Lett.* **95**, 113202 (2005).
- [51] M. Kasevich and S. Chu, *Appl. Phys. B* **54**, 321 (1992).
- [52] A. Peters, K.Y. Chung, and S. Chu, *Nature* **400**, 849 (1999).
- [53] A. Peters, K.Y. Chung, and S. Chu, *Metrologia* **38**, 25 (2001).
- [54] Z. Lin, X. Zong-Yuan, Y. Wei, T. Biao, P. Wen-Cui, W. Yi-Bo, X. Peng, W. Jin, and Z. Ming-Sheng, *Chin. Phys. Lett.* **28**, 013701 (2011).
- [55] B.P. Anderson and M.A. Kasevich, *Science* **282**, 1686 (1998).
- [56] M. Greiner, I. Bloch, O. Mandel, T.W. Hänsch, and T. Esslinger, *Phys. Rev. Lett.* **87**, 160405 (2001).
- [57] O. Morsch, J.H. Müller, M. Cristiani, D. Ciampini, and E. Arimondo, *Phys. Rev. Lett.* **87**, 140402 (2001).
- [58] G. Ferrari, N. Poli, F. Sorrentino, and G.M. Tino, *Phys. Rev. Lett.* **97**, 060402 (2006).
- [59] P. Cladé, S. Guellati-Khélifa, C. Schwob, F. Nez, L. Julien, and F. Biraben, *Europhys. Lett.* **71**, 730 (2005).
- [60] B.M. Peden, D. Meiser, M.L. Chiofalo, and M.J. Holland, *Phys. Rev. A* **80**, 043803 (2009).
- [61] B. Prasanna Venkatesh, M. Trupke, E.A. Hinds, and D.H.J. O'Dell, *Phys. Rev. A* **80**, 063834 (2009).

- [62] D. Kruse, C. von Cube, C. Zimmermann, and Ph.W. Courteille, *Phys. Rev. Lett.* **91**, 183601 (2003).
- [63] A.T. Black, H.W. Chan, and V. Vuletic, *Phys. Rev. Lett.* **91**, 203001 (2003).
- [64] Th. Elsässer, B. Nagorny, and A. Hemmerich, *Phys. Rev. A* **69**, 033403 (2003).
- [65] M. Samoylova, N. Piovella, D. Hunter, G. Robb, R. Bachelard, Ph.W. Courteille, *Las. Phys. Lett.* **11**, 126005 (2014).
- [66] M. Samoylova, N. Piovella, G. Robb, R. Bachelard, Ph.W. Courteille, arXiv:1503.05616, submitted to *Opt. Express* (2015).
- [67] T. Ido, Y. Isoya, and H. Katori, *Phys. Rev. A* **61**, 061403(R) (2000).
- [68] G. Ferrari, R.E. Drullinger, N.Poli, F. Sorrentino, and G.M. Tino, *Phys. Rev. A* **73**, 023408 (2006).
- [69] J. Goldwin, B. Prasanna Venkatesh, and D.H.J. O'Dell, *Phys. Rev. Lett.* **115**, 073003 (2014).
- [70] R. Bonifacio and L. De Salvo, *Nucl. Instrum. Methods Phys. Res. Sect. A* **341**, 360 (1994).
- [71] S. Slama, S. Bux, G. Krenz, C. Zimmermann, and Ph.W. Courteille, *Phys. Rev. Lett.* **98**, 053603 (2007).
- [72] S. Bux, C. Gnahn, R.A. Maier, C. Zimmermann, and Ph.W. Courteille, *Phys. Rev. Lett.* **106**, 203601 (2011).
- [73] B. Nagorny, Th. Elsässer, and A. Hemmerich, *Phys. Rev. Lett.* **91**, 153003 (2003).
- [74] D. Kruse, M. Ruder, J. Benhelm, C. von Cube, C. Zimmermann, Ph.W. Courteille, B. Nagorny, Th. Elsässer, and A. Hemmerich, *Phys. Rev. A* **67**, 051802(R) (2003).
- [75] N. Piovella, M. Gatelli, and R. Bonifacio, *Opt. Comm.* **194**, 167 (2001).
- [76] N. Piovella, M. Cola, and R. Bonifacio, *J. Mod. Opt.* **15**, 1019 (2004).
- [77] E. Peik, M.B. Dahan, I. Bouchoule, Y. Castin, and C. Salomon, *Phys. Rev. A* **55**, 2989 (1997).

-
- [78] M. Glück, A. R. Kolovsky, and H. Jürgen Korsch, Phys. Rep. **366**, 103 (2002).
- [79] A. Abragam, *The Principles of Nuclear Magnetism*, Oxford University Press, London (1961).
- [80] P. Marte, P. Zoller, and J. L. Hall, Phys. Rev. A **44**, 4118 (1991).
- [81] Y.B. Band, Phys. Rev. A **47**, 4970 (1993).
- [82] S. R. Wilkinson, C.F. Bharucha, M.C. Fischer, K.W. Madison, P.R. Morrow, Q. Niu, B. Sundaram, and M.G. Raizen, Nature **387**, 575 (1997).
- [83] E.B. Treacy, Phys. Lett. A **27**, 421 (1968).
- [84] M.M.T. Loy, Phys. Rev. Lett. **32**, 814 (1974).
- [85] I. Nebenzahl, and A. Szöke, Appl. Phys. Lett. **25**, 327 (1974).
- [86] C. Kittel, *Introduction to Solid State Physics*, 7th Ed., Wiley (1996).
- [87] E. Haller, R. Hart, M.J. Mark, J.G. Danzl, L. Reichsöllner, and H.-C. Nägerl, Phys. Rev. Lett. **104**, 200403 (2010).
- [88] H.A. Haus, IEEE J. Quantum Electron. **12**, 169 (1976).
- [89] F.X. Kärtner, L.R. Brovelli, D. Kopf, M. Kamp, I. Calasso, and U. Keller, Opt. Eng. **34**, 2024 (1995).
- [90] C. Hönninger, R. Paschotta, F. Morier-Genoud, M. Moser, and U. Keller, JOSA B **16**, 46 (1999).
- [91] R. Bonifacio, L. De Salvo, L.M. Narducci, and E.J. D'Angelo, Phys. Rev. A **50**, 1716 (1994).
- [92] R. Bonifacio and L. De Salvo, Appl. Phys. B **60**, S233 (1995).
- [93] R. Bonifacio, C. Pellegrini, and L.M. Narducci, Opt. Comm. **50**, 373 (1984).
- [94] G. Preparata, Phys. Rev. A **38**, 233 (1988).
- [95] M.G. Moore and P. Meystre, Phys. Rev. A **58**, 3248 (1998).
- [96] M.G. Moore, O. Zobay, and P. Meystre, Phys. Rev. A **60**, 1491 (1999).

- [97] N. Piovella, M. Cola, and R. Bonifacio, *Phys. Rev. A* **67**, 013817 (2003).
- [98] R. Bonifacio, F.S. Cataliotti, M. Cola, L. Fallani, C. Fort, N. Piovella, and M. Inguscio, *Opt. Commun.* **233**, 155 (2004).
- [99] J.-Y. Courtois, G. Grynberg, B. Lounis, and P. Verkerk, *Phys. Rev. Lett.* **72**, 3017 (1994).
- [100] G.L. Lippi, G.P. Barozzi, S. Barbay, and J.R. Tredicce, *Phys. Rev. Lett.* **76**, 2452 (1996).
- [101] P.R. Hemmer, N.P. Bigelow, D.P. Katz, M.S. Shahriar, L. De Salvo, and R. Bonifacio, *Phys. Rev. Lett.* **77**, 1468 (1996).
- [102] W.J. Brown, J.R. Gardner, D.J. Gauthier, and R. Vilaseca, *Phys. Rev. A* **56**, 3255 (1997).
- [103] R. Bonifacio and P. Verkerk, *Opt. Commun.* **124**, 469 (1996).
- [104] M. Perrin, G.L. Lippi, and A. Politi, *Phys. Rev. Lett.* **86**, 4520 (2001).
- [105] M. Perrin, Z. Ye, and L.M. Narducci, *Phys. Rev. A* **66**, 043809 (2002).
- [106] M. Perrin, G.L. Lippi, and A. Politi, *J. Mod. Opt.* **49**, 419 (2002).
- [107] P.R. Berman, *Phys. Rev. A* **59**, 585 (1999).
- [108] C. Zimmermann, D. Kruse, C. von Cube, S. Slama, B. Deh, and Ph.W. Courteille, *J. Mod. Opt.* **51**, 957 (2003).
- [109] C. von Cube, S. Slama, D. Kruse, C. Zimmermann, Ph.W. Courteille, G.R.M. Robb, N. Piovella, and R. Bonifacio, *Phys. Rev. Lett.* **93**, 083601 (2004).
- [110] S. Slama, G. Krenz, S. Bux, C. Zimmermann, and Ph.W. Courteille, *Phys. Rev. A* **75**, 063620 (2007).
- [111] S. Bux, H. Tomczyk, D. Schmidt, P. W. Courteille, N. Piovella, and C. Zimmermann, *Phys. Rev. A* **87**, 023607 (2013).
- [112] D. Schmidt, H. Tomczyk, S. Slama, and C. Zimmermann, *Phys. Rev. Lett.* **112**, 115302 (2014).
- [113] G.R.M. Robb, N. Piovella, A. Ferraro, R. Bonifacio, Ph.W. Courteille, and C. Zimmermann, *Phys. Rev. A* **69**, 041403(R)(2004).

- [114] N. Piovella, L. Salasnich, and R. Bonifacio, *Las. Phys.* **14**, 278 (2004).
- [115] M. Cola, M.G.A. Paris, and N. Piovella, *Phys. Rev. A* **70**, 043809 (2004).
- [116] R. Bonifacio, M. M. Cola, N. Piovella, and G. R. M. Robb, *Europhys. Lett.* **69**, 55 (2005).
- [117] R. Bonifacio, N. Piovella, G. R. M. Robb, and M. M. Cola, *Opt. Commun.* **252**, 381 (2005).
- [118] N. Piovella, L. Volpe, M. Cola, and R. Bonifacio, *Las. Phys.* **17**, 174 (2007).
- [119] M. Cola, L. Volpe, and N. Piovella, *Phys. Rev. A* **79**, 013613 (2009).
- [120] N. Piovella, *Eur. Phys. J. Special Topics*, **203**, 127 (2012).
- [121] N. Piovella, R. Bonifacio, B.W.J. McNeil, and G.R.M. Robb, *Opt. Commun.* **187**, 165 (2001).
- [122] S. Inouye, A.P. Chikkatur, D.M. Stamper-Kurn, J. Stenger, D.E. Pritchard, and W. Ketterle, *Science* **285**, 571 (1999).
- [123] M. Kozuma, Y. Suzuki, Y. Torii, T. Sugiura, T. Kuga, E. W. Hagley, and L. Deng, *Science* **286**, 2309 (1999).
- [124] D. Schneble, Y. Torii, M. Boyd, E.W. Streed, D.E. Pritchard, and W. Ketterle, *Science* **300**, 475 (2003).
- [125] L. Fallani, C. Fort, N. Piovella, M. Cola, F.S. Cataliotti, M. Inguscio, and R. Bonifacio, *Phys. Rev. A* **71**, 033612 (2005).
- [126] Y. Yoshikawa, Y. Torii, and T. Kuga, *Phys. Rev. Lett.* **94**, 083602 (2005).
- [127] M. G. Moore and P. Meystre, *Phys. Rev. Lett.* **86**, 4199 (2001).